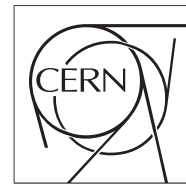




The Compact Muon Solenoid Experiment
Analysis Note

The content of this note is intended for CMS internal use and distribution only



October 31, 2012

Search for Direct Stop Quark Pair Production in the Single Lepton Channel at 8 TeV

L. Bauerdick, K. Burkett, I. Fisk, Y. Gao, O. Gutsche, B. Hooberman, S. Jindariani, J. Linacre, V. Martinez Outschoorn

Fermilab National Accelerator Laboratory, Batavia, USA

C. Campagnari, A. George, F. Golf, D. Kovalevsky, V. Krutelyov

University of California, Santa Barbara, Santa Barbara, USA

G. Cerati, M. D'Alfonso, D. Evans, R. Kelley, I. MacNeill, S. Padhi, Y. Tu, F. Würthwein, V. Welke, A. Yagil, J. Yoo

University of California, San Diego, San Diego, USA

Abstract

This note describes a search for direct stop quark pair production in the single lepton channel using 9.7 fb^{-1} of pp collision data at $\sqrt{s} = 8 \text{ TeV}$ taken with the CMS detector in 2012. A search for an excess of events over the Standard Model prediction is performed in a sample with a single isolated electron or muon, several jets including a b-tagged jet, missing transverse energy, and large transverse mass.

Contents

1	Introduction	3
2	Overview and Strategy for Background Determination	3
2.1	$\ell +$ jets background	4
2.2	Dilepton background	5
2.3	Other backgrounds	5
2.4	Future improvements	6
3	Data Samples	6
4	Event Selection	8
4.1	Single Lepton Selection	8
4.2	Isolated track veto	8
4.3	Signal Region Selection	8
4.4	Control Region Selection	9
4.5	Definition of M_T peak region	10
4.6	Default $t\bar{t}$ MC sample	10
4.7	MC Corrections	10
4.7.1	Corrections to Jets and E_T^{miss}	10
4.8	Lepton Selection Efficiency Measurements	10
4.9	Trigger Efficiency Measurements	16
5	Control Region Studies	18
5.1	W+Jets MC Modelling Validation from CR1	18
5.2	Single Lepton Top MC Modelling Validation from CR2	23
5.3	Dilepton studies in CR4	25
5.3.1	Modeling of Additional Hard Jets in Top Dilepton Events	25
5.3.2	Validation of the “Physics” Modelling of the $t\bar{t} \rightarrow \ell\ell$ MC in CR4	28
5.4	Test of control region with isolated track in CR5	31
6	Other Backgrounds	35
7	Tail-to-Peak ratio for lepton + jets top and W events	35
8	Background Prediction	37
9	Systematic Uncertainties on the Background	41
9.1	Statistical uncertainties on the event counts in the M_T peak regions	41
9.2	Uncertainty from the choice of M_T peak region	41
9.3	Uncertainty on the $W+jets$ cross-section and the rare MC cross-sections	41

9.4	Tail-to-peak ratios for lepton + jets top and W events	41
9.5	Uncertainty on extra jet radiation for dilepton background	42
9.6	Uncertainty from MC statistics	42
9.7	Uncertainty on the $t\bar{t} \rightarrow \ell\ell$ Background	42
9.7.1	Check of the impact of Signal Contamination	44
9.7.2	Check of the uncertainty on the $t\bar{t} \rightarrow \ell\ell$ Background	44
9.8	Uncertainty from the isolated track veto	50
9.8.1	Isolated Track Veto: Tag and Probe Studies	50
9.9	Summary of uncertainties	54
10	Results	56
11	Limits	60
12	Conclusion	69
A	Performance of the Isolation Requirement	70
B	Example BG prediction calculation	72
B.1	Central value of dilepton background	72
B.2	Central value of the $t\bar{t} \rightarrow \ell + \text{jets}$ background	72
B.3	Central value for the $W + \text{jets}$ background	73
B.4	Central value for the rare backgrounds	73
C	Additional CR Data and MC Comparisons	74
D	Control Region Plots Summary	79
D.1	CR4: ≥ 1 b-tag, exactly 2 leptons	79
D.2	CR5: ≥ 1 b-tag, 1 lepton + 1 isolated track	80
D.3	CR1: 0 b-tags, exactly 1 lepton	81
D.4	CR2: 0 b-tags, exactly 2 leptons	82
E	Signal Kinematics	83
F	Model dependence of the signal acceptance	85
G	Glossary of abbreviations	85

1 Introduction

This note presents a search for the production of supersymmetric (SUSY) stop quark pairs in events with a single isolated lepton, several jets, missing transverse energy, and large transverse mass. We use a data sample corresponding to an integrated luminosity of 9.7 fb^{-1} . This search is of theoretical interest because of the critical role played by the stop quark in solving the hierarchy problem in SUSY models. This solution requires that the stop quark be light, less than a few hundred GeV and hence within reach for direct pair production. We focus on two decay modes $\tilde{t} \rightarrow t\chi_1^0$ and $\tilde{t} \rightarrow b\chi_1^+$ which are expected to have large branching fractions if they are kinematically accessible, leading to:

- $pp \rightarrow \tilde{t}\bar{t} \rightarrow t\bar{t}\chi_1^0\chi_1^0$, and
- $pp \rightarrow \tilde{t}\bar{t} \rightarrow b\bar{b}\chi_1^+\chi_1^- \rightarrow b\bar{b}W^+W^-\chi_1^0\chi_1^0$.

Both of these signatures contain high transverse momentum (p_T) jets including two b-jets, and missing transverse energy (E_T^{miss}) due to the invisible χ_1^0 lightest SUSY particles (LSP's). In addition, the presence of two W bosons leads to a large branching fraction to the single lepton final state. Hence we require the presence of exactly one isolated, high p_T electron or muon, which provides significant suppression of several backgrounds that are present in the all-hadronic channel. The largest backgrounds for this signature are semi-leptonic $t\bar{t}$ and $W+\text{jets}$. These backgrounds contain a single leptonically-decaying W boson, and the transverse mass (M_T) of the lepton-neutrino system has a kinematic endpoint requiring $M_T < M_W$. For signal stop quark events, the presence of additional LSP's in the final states allows the M_T to exceed M_W . Hence we search for an excess of events with large M_T . The dominant background in this kinematic region is dilepton $t\bar{t}$ where one of the leptons is not identified, since the presence of two neutrinos from leptonically-decaying W bosons allows the M_T to exceed M_W . Backgrounds are estimated from Monte Carlo (MC) simulation, with careful validation and determination of scale factors (where necessary) and corresponding uncertainties based on data control samples.

The expected stop quark pair production cross section (see Fig. 1) varies between 18 pb for $m_{\tilde{t}} = 200 \text{ GeV}$ and 0.09 pb for $m_{\tilde{t}} = 500 \text{ GeV}$ [1]. The critical challenge of this analysis is due to the fact that for light stop quarks ($m_{\tilde{t}} \approx m_t$), the production cross section is large but the kinematic distributions, in particular M_T , are very similar to SM $t\bar{t}$ production. In this regime it becomes very difficult to distinguish the signal and background. For large stop quark mass the kinematic distributions differ from those in SM $t\bar{t}$ production, but the cross section decreases rapidly, reducing the signal-to-background ratio.

2 Overview and Strategy for Background Determination

We are searching for a $t\bar{t}\chi_1^0\chi_1^0$ or $WbW\bar{b}\chi_1^0\chi_1^0$ final state (after top decay in the first mode, the final states are actually the same). So to first order this is “ $t\bar{t}$ + extra E_T^{miss} ”.

We work in the $\ell+\text{jets}$ final state, where the main background is $t\bar{t}$. We look for E_T^{miss} inconsistent with $W \rightarrow \ell\nu$. We do this by concentrating on the $\ell\nu$ transverse mass (M_T), since except for resolution and W-off-shell effects, $M_T < M_W$ for $W \rightarrow \ell\nu$. Thus, the initial analysis is simply a counting experiment in the tail of the M_T distribution.

The event selection is one-and-only-one high p_T isolated lepton, four or more jets, and an E_T^{miss} cut. At least one of the jets has to be b tagged to reduce $W+\text{jets}$. The event sample is then dominated by $t\bar{t}$, but there are also contributions from $W+\text{jets}$, single top, dibosons, as well as rare SM processes such as ttW .

The $t\bar{t}$ events in the M_T tail can be broken up into two categories: (i) $t\bar{t} \rightarrow \ell+\text{jets}$, and (ii) $t\bar{t} \rightarrow \ell^+\ell^-$ where one of the two leptons is not found by the second-lepton-veto (here the second lepton can be a hadronically decaying τ). For a reasonable M_T cut, say $M_T > 150 \text{ GeV}$, the dilepton background is approximately 70% of the total. This is because in dileptons there are two neutrinos from W decay, thus M_T is not bounded by M_W . This is a very important point: while it is true that we are looking in the tail of M_T , the bulk of the background events end up there not because of some exotic E_T^{miss} reconstruction failure, but because of well understood physics processes. This means that the background estimate can be taken from Monte Carlo (MC) after carefully accounting for possible data/MC differences.

The search is performed in a number of Signal Regions (SRs) defined by minimum requirements on E_T^{miss} and M_T . The SRs are defined in Section 4.3.

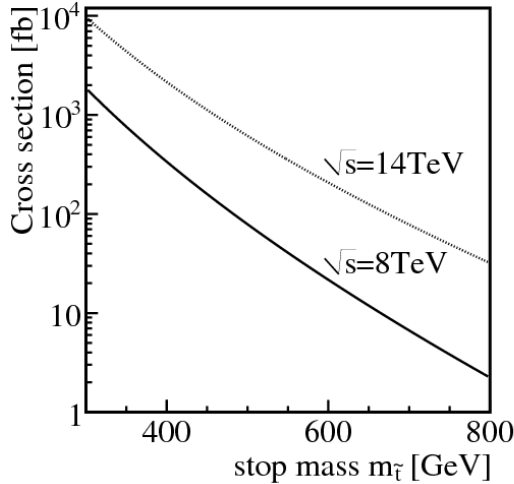


Figure 1: The stop quark pair production cross section as a function of the stop quark mass [2].

- 51 In Section 5 we will describe the analysis of various Control Regions (CRs) that are used to test the
 52 Monte Carlo model and, if necessary, to extract data/MC scale factors. In this section we give a general
 53 description of the procedure. The details of how the final background prediction is assembled are given
 54 in Section 8.
- 55 One general point is that in order to minimize systematic uncertainties, the MC background predictions
 56 are whenever possible normalized to the bulk of the $t\bar{t}$ data, i.e. events passing all of the requirements
 57 but with $M_T \approx 80$ GeV. This (mostly) removes uncertainties due to $\sigma(t\bar{t})$, lepton ID, trigger efficiency,
 58 luminosity, etc.

59 2.1 $\ell +$ jets background

- 60 The $\ell +$ jets background is dominated by $t\bar{t} \rightarrow \ell +$ jets, but also includes some $W +$ jets as well as single
 61 top. The MC input used in the background estimation is the ratio of the number of events with M_T in
 62 the signal region to the number of events with $M_T \approx 80$ GeV. This ratio is (possibly) corrected by a
 63 data/MC scale factor obtained from a study of CRs, as outlined below.
- 64 Note that the ratio described above is actually different for $t\bar{t}$ /single top and $W +$ jets. This is because
 65 in W events there is a significant contribution to the M_T tail from very off-shell W s. This contribution
 66 is much smaller in top events because $M(\ell\nu)$ cannot exceed $M_{top} - M_b$. Therefore the large M_T tail in
 67 $t\bar{t}$ /single top is dominated by jet resolution effects, while for $W +$ jets events the large M_T tail is dominated
 68 by off-shell W production.
- 69 For $W +$ jets the ability of the Monte Carlo to model this ratio (R_{wjet}) is validated in a sample of $\ell +$ jets
 70 enriched in $W +$ jets by the application of a b-veto. The equivalent ratio for top events (R_{top}) is tested
 71 in a sample of well identified $Z \rightarrow \ell\ell$ with one lepton added to the E_T^{miss} calculation. This sample is well
 72 suited to testing the resolution effects on the M_T tail, since off-shell effects are eliminated by the Z -mass
 73 requirement. However, this test is unfortunately statistically limited and its usefulness is limited to event

74 selections with modest E_T^{miss} requirements.

75 Note that the fact that the ratios are different for $t\bar{t}$ /single top and $W +$ jets introduces a systematic
76 uncertainty in the background calculation because one needs to know the relative fractions of these two
77 components in the $M_T \approx 80$ GeV lepton + jets sample.

78 2.2 Dilepton background

79 To suppress dilepton backgrounds, we veto events with an isolated track of $p_T > 10$ GeV (see Sec. 4.2
80 for details). Being the common feature for electron, muon, and one-prong tau decays, this veto is highly
81 efficient for rejecting $t\bar{t}$ to dilepton events. The remaining dilepton background can be classified into the
82 following categories:

- 83 • lepton is out of acceptance ($|\eta| > 2.5$)
- 84 • lepton has $p_T < 10$ GeV, and is inside the acceptance
- 85 • lepton has $p_T > 10$ GeV, is inside the acceptance, but survives the additional isolated track veto

86 The last category includes 1-prong and 3-prong hadronic tau decays, as well as electrons and muons either
87 from direct W decay or via $W \rightarrow \tau \rightarrow \ell$ decay that fail the isolation requirement. We note that at present
88 we do not attempt to veto 3-prong tau decays as they are about 15% of the total dilepton background
89 according to the MC.

90 The high M_T dilepton background predictions come from MC, but their rate is normalized to the $M_T \approx 80$
91 GeV peak. In order to perform this normalization in data, the rare background events in the M_T peak
92 are subtracted off. This also introduces a systematic uncertainty.

93 There are two types of effects that can influence the MC dilepton prediction: physics effects and instru-
94 mental effects. We discuss these next, starting from physics.

95 First of all, many of our $t\bar{t}$ MC samples (e.g. MadGraph) have $\text{BR}(W \rightarrow \ell\nu) = \frac{1}{9} = 0.1111$. PDG says
96 $\text{BR}(W \rightarrow \ell\nu) = 0.1080 \pm 0.0009$. This difference matters, so the $t\bar{t}$ MC must be corrected to account for
97 this.

98 Second, our selection is $\ell + 4$ or more jets. A dilepton event passes the selection only if there are two
99 additional jets from ISR, or one jet from ISR and one jet which is reconstructed from the unidentified
100 lepton, e.g., a three-prong tau. Therefore, all MC dilepton $t\bar{t}$ samples used in the analysis must have
101 their jet multiplicity corrected (if necessary) to agree with what is seen in $t\bar{t}$ data. We use a data control
102 sample of well identified dilepton events with E_T^{miss} and at least one jet (including at least one b-tag) as
103 a template to “adjust” the N_{jet} distribution of the $t\bar{t} \rightarrow$ dileptons MC samples.

104 The final physics effect has to do with the modeling of $t\bar{t}$ production and decay. Different MC models
105 could in principle result in different BG predictions. Therefore we use several different $t\bar{t}$ MC samples
106 using different generators and different parameters, to test the stability of the dilepton BG prediction.
107 All these predictions, **after** corrections for branching ratio and N_{jet} dependence, are compared to each
108 other. The spread is a measure of the systematic uncertainty associated with the $t\bar{t}$ generator modeling.

109 The main instrumental effect is associated with the efficiency of the isolated track veto. We use tag-
110 and-probe to compare the isolated track veto performance in $Z + 4$ jets data and MC. Note that the
111 performance of the isolated track veto is not exactly the same on e/μ and on one prong hadronic tau
112 decays. This is because the pions from one-prong taus are often accompanied by π^0 's that can then
113 result in extra tracks due to photon conversions. We let the simulation take care of that. Note that JES
114 uncertainties are effectively “calibrated away” by the N_{jet} rescaling described above.

115 2.3 Other backgrounds

116 Other backgrounds are tW , ttV , dibosons, tribosons, and Drell Yan. These are small. They are taken
117 from MC with appropriate scale factors for trigger efficiency, and reweighting to match the distribution
118 of reconstructed primary vertices in data.

119 **2.4 Future improvements**

120 Finally, there are possible improvements to this basic analysis strategy that can be added in the future:

- 121 • Move from counting experiment to shape analysis. But first, we need to get the counting experiment
122 under control.
- 123 • Add an explicit three prong tau veto
- 124 • Do something to require that three of the jets in the event be consistent with $t \rightarrow Wb, W \rightarrow q\bar{q}$.
125 This could help reject some of the dilepton BG in the search for $\tilde{t} \rightarrow t\chi^0$, but is not applicable to
126 the $\tilde{t} \rightarrow b\chi^+$ search.
- 127 • Consider the $M(\ell b)$ variable, which is not bounded by M_{top} in $\tilde{t} \rightarrow b\chi^+$

128 **3 Data Samples**

129 The datasets used for this analysis are summarized in Tables 1 (data) and 2 (MC). The total integrated
130 luminosity is 9.7 fb^{-1} after applying the official good run list. The main $t\bar{t}$ Monte Carlo sample is gen-
131 erated with Powheg since this sample has the largest number of events, though samples with alternative
132 generators such as Madgraph are also used for the derivation of systematic uncertainties in the $t\bar{t}$ back-
133 ground prediction. The triggers used to select both the signal and control samples are also summarized
134 in Table 3.

Dataset Name
Single Lepton Samples
/SingleElectron/Run2012A-13Jul2012-v1/AOD
/SingleMu/Run2012A-13Jul2012-v1/AOD
/SingleElectron/Run2012B-13Jul2012-v1/AOD
/SingleMu/Run2012B-13Jul2012-v1/AOD
/SingleElectron/Run2012C-PromptReco-v1/AOD
/SingleMu/Run2012C-PromptReco-v1/AOD
/SingleElectron/Run2012C-PromptReco-v2/AOD
/SingleMu/Run2012C-PromptReco-v2/AOD
Dilepton Samples (only used for dilepton control region)
/DoubleElectron/Run2012A-13Jul2012-v1/AOD
/DoubleMu/Run2012A-13Jul2012-v1/AOD
/MuEG/Run2012A-13Jul2012-v1/AOD
/DoubleElectron/Run2012B-13Jul2012-v1/AOD
/DoubleMu/Run2012B-13Jul2012-v1/AOD
/MuEG/Run2012B-13Jul2012-v1/AOD
/DoubleElectron/Run2012C-PromptReco-v1/AOD
/DoubleMu/Run2012C-PromptReco-v1/AOD
/MuEG/Run2012C-PromptReco-v1/AOD
/DoubleElectron/Run2012C-PromptReco-v2/AOD
/DoubleMu/Run2012C-PromptReco-v2/AOD
/MuEG/Run2012C-PromptReco-v2/AOD

Table 1: Summary of data datasets used.

With Pileup: Processed dataset name is (53) Summer12_DR53X-PU_S10_START53_V7A-v*/AODSIM (52) Summer12-START52_V9_FSIM-v*/AODSIM		
Description	Primary Dataset Name	cross-section [pb]
$t\bar{t}$	/TT_CTE10_TuneZ2Star_8TeV-powheg-tauola (53)	225.2
$W \rightarrow \ell\nu$	/WJetsToLNu_TuneZ2Star_8TeV-madgraph-tauola (53)	37509
$W \rightarrow \ell\nu+3$ jets	/W3JetsToLNu_TuneZ2Star_8TeV-madgraph-tauola (53)	640
$W \rightarrow \ell\nu+\geq 4$ jets	/W4JetsToLNu_TuneZ2Star_8TeV-madgraph-tauola (53)	264
WW	/WWJetsTo2L2Nu_TuneZ2star_8TeV-madgraph-tauola (53)	5.8
WZ	/WZJetsTo3LNu_TuneZ2_8TeV-madgraph-tauola (53)	1.1
ZZ	/WZJetsTo2L2Q_TuneZ2star_8TeV-madgraph-tauola (53)	1.1
	/ZZJetsTo2L2Nu_TuneZ2star_8TeV-madgraph-tauola (53)	0.4
	/ZZJetsTo4L_TuneZ2star_8TeV-madgraph-tauola (53)	0.2
	/ZZJetsTo2L2Q_TuneZ2star_8TeV-madgraph-tauola (53)	2.4
t (s -chan)	/T_TuneZ2Star_s-channel_8TeV-powheg-tauola (53)	3.9
\bar{t} (s -chan)	/Tbar_TuneZ2Star_s-channel_8TeV-powheg-tauola (53)	1.8
t (t -chan)	/T_TuneZ2Star_t-channel_8TeV-powheg-tauola (53)	55.5
\bar{t} (t -chan)	/Tbar_TuneZ2Star_t-channel_8TeV-powheg-tauola (53)	30.0
tW	/T_TuneZ2Star_tW-channel-DR_8TeV-powheg-tauola (53)	11.2
$t\bar{W}$	/Tbar_TuneZ2Star_tW-channel-DR_8TeV-powheg-tauola (53)	11.2
$Z/\gamma^* \rightarrow \ell\ell$	/DYJetsToLL_TuneZ2Star_M-50_8TeV-madgraph-tarball (53)	3532.8
$Z/\gamma^* \rightarrow \ell\ell+\geq 4$ jets	/DY4JetsToLL_TuneZ2Star_M-50_8TeV-madgraph-tarball (53)	27.6
$t\bar{t}W$	/TTW_TuneZ2Star_8TeV-madgraph (53)	0.23
$t\bar{t}Z$	/TTZ_TuneZ2Star_8TeV-madgraph (53)	0.21
$t\bar{t}\gamma$	/TTGJets_TuneZ2Star_8TeV-madgraph (53)	0.65
WWW	/WWWW_TuneZ2Star_8TeV-madgraph (53)	0.082
WWZ	/WWZNoGstar_TuneZ2Star_8TeV-madgraph (53)	0.063
WZZ	/WZZNoGstar_TuneZ2Star_8TeV-madgraph (53)	0.019
ZZZ	/ZZZNoGstar_TuneZ2Star_8TeV-madgraph (53)	0.019
$\tilde{t}\tilde{t} \rightarrow t\bar{t}\chi_1^0\chi_1^0$	/SMS-T2tt_FineBin_Mstop-225to1200_mLSP-0to1000_8TeV-Pythia6Z (52)	scan
$\tilde{t}\tilde{t} \rightarrow b\bar{b}\chi_1^+\chi_1^-$	/SMS-T2bw_FineBin_Mstop-100to600_mLSP-0to500_8TeV-Pythia6Z (52)	scan
<hr/>		
$t\bar{t}$	/TTJets_MassiveBinDECAY_TuneZ2Star_8TeV-madgraph-tauola (53)	225.2
$t\bar{t}$ ($Q^2 \times 2$)	/TTjets_TuneZ2Star_scaleup_8TeV-madgraph-tauola (53)	225.2
$t\bar{t}$ ($Q^2 \times 0.5$)	/TTjets_TuneZ2Star_scaledown_8TeV-madgraph-tauola (53)	225.2
$t\bar{t}$ ($x_q > 40$ GeV)	/TTjets_TuneZ2Star_matchingup_8TeV-madgraph-tauola (53)	225.2
$t\bar{t}$ ($x_q > 10$ GeV)	/TTjets_TuneZ2Star_matchingdown_8TeV-madgraph-tauola (53)	225.2
$t\bar{t}$ ($m_{top} = 178.5$ GeV)	/TTJets_TuneZ2Star_mass178.5_8TeV-madgraph-tauola (53)	225.2
$t\bar{t}$ ($m_{top} = 166.5$ GeV)	/TTJets_TuneZ2Star_mass166.5_8TeV-madgraph-tauola (53)	225.2

Table 2: Summary of Monte Carlo datasets used.

Triggers
Single Muon Sample
HLT_IsoMu24_v*
HLT_IsoMu24_eta2p1_v*
Single Electron Sample
HLT_Ele27_WP80_v*
Dilepton Sample (only used for dilepton control regions)
HLT_Mu17_Mu8_v*
HLT_Mu17_Ele8_CaloIdT_CaloIsoVL_TrkIdVL_TrkIsoVL_v*
HLT_Mu8_Ele17_CaloIdT_CaloIsoVL_TrkIdVL_TrkIsoVL_v*
HLT_Ele17_CaloIdT_CaloIsoVL_TrkIdVL_TrkIsoVL_Ele8_CaloIdT_CaloIsoVL_TrkIdVL_TrkIsoVL_v*

Table 3: Summary of triggers used.

135 4 Event Selection

136 Here we define the selections of leptons, jets, and E_T^{miss} . We also describe our measurements of the lepton
137 and trigger efficiency. The analysis uses several different Control Regions (CRs) in addition to the Signal
138 Regions (SRs). All of these different regions are defined in this section. This section also includes some
139 information on the basic MC corrections that we apply.

140 4.1 Single Lepton Selection

141 The single lepton selection is based on the following criteria, starting from the requirements described on
142 https://twiki.cern.ch/twiki/bin/viewauth/CMS/SUSYstop#SINGLE_LEPTON_CHANNEL (re-
143 vision r20)

- 144 • satisfy the trigger requirement (see Table 3). Note that the analysis triggers are inclusive single
145 lepton triggers. Dilepton triggers are used only for the dilepton control region.

- 146 • select events with one high p_T electron or muon, requiring

- 147 – $p_T > 30 \text{ GeV}/c$ and $|\eta| < 1.4442(2.1)$ for electrons (muons). The restriction to the barrel for
148 electrons is motivated by an observed excess of events with large M_T with endcap electrons
149 in the b-veto control region, and does not significantly reduce the signal acceptance since the
150 leptons tend to be central.
- 151 – muon ID criteria is based on the 2012 POG recommended tight working point
- 152 – electron ID criteria is based on the 2012 POG recommended medium working point
- 153 – PF-based isolation ($\Delta R < 0.3$) relative isolation < 0.15 and absolute isolation $< 5 \text{ GeV}$. PU
154 corrections are performed with the $\Delta\beta$ scheme for muons and effective-area fastjet rho scheme
155 for electrons (as recommended by the relevant POGs).
- 156 – $|p_T(\text{PF}_{\text{lep}}) - p_T(\text{RECO}_{\text{lep}})| < 10 \text{ GeV}$
- 157 – $E/p_{\text{in}} < 4$ (electrons only)
- 158 – We remove electron events with $E_T^{\text{miss}} > 50 \text{ GeV}$ and $M_T > 100 \text{ GeV}$ with at least one crystal
159 in the supercluster with laser correction > 2 .¹⁾

- 160 • require at least 4 PF jets in the event with $p_T > 30 \text{ GeV}$ within $|\eta| < 2.5$ out of which at least 1
161 satisfies the CSV medium working point b-tagging requirement

- 162 • require moderate $E_T^{\text{miss}} > 50 \text{ GeV}$ (type1-corrected pfmet with ϕ corrections applied as described
163 in Sec. 4.7.1).

- 164 • Isolated track veto, see Section 4.2

165 4.2 Isolated track veto

166 The isolated track veto is intended to remove top dilepton events. Looking for an isolated track is an
167 effective way of identifying $W \rightarrow e$, $W \rightarrow \mu$, $W \rightarrow \tau \rightarrow \ell$, and $W \rightarrow \tau \rightarrow h^\pm + n\pi^0$. The requirements
168 on the track are

- 169 • $P_T > 10 \text{ GeV}$
- 170 • Relative track isolation $< 10\%$ computed from charged PF candidates with $d_Z < 0.05 \text{ cm}$ from the
171 primary vertex.

172 4.3 Signal Region Selection

173 The signal regions (SRs) are selected to improve the sensitivity for the single lepton requirements and
174 cover a range of scalar top scenarios. The M_T and E_T^{miss} variables are used to define the signal regions
175 and the requirements are listed in Table 4.

¹⁾ This is an ad-hoc removal based on run-event numbers, since the problem was found very recently and the filter was not available when we processed the events.

Signal Region	Minimum M_T [GeV]	Minimum E_T^{miss} [GeV]
SRA	150	100
SRB	120	150
SRC	120	200
SRD	120	250
SRE	120	300
SRF	120	350
SRG	120	400

Table 4: Signal region definitions based on M_T and E_T^{miss} requirements. These requirements are applied in addition to the baseline single lepton selection.

Table 5 shows the expected number of SM background yields for the SRs. A few stop signal yields for four values of the parameters are also shown for comparison. The signal regions with looser requirements are sensitive to lower stop masses $M(\tilde{t})$, while those with tighter requirements are more sensitive to higher $M(\tilde{t})$. Kinematic distributions for a few sample signal points can be found in Appendix E.

Sample	SRA	SRB	SRC	SRD	SRE	SRF	SRG
$t\bar{t} \rightarrow \ell\ell$	619 ± 9	366 ± 7	127 ± 4	44 ± 2	17 ± 1	7 ± 1	4 ± 1
$t\bar{t} \rightarrow \ell + \text{jets} \& \text{single top } (1\ell)$	95 ± 3	67 ± 3	15 ± 1	6 ± 1	2 ± 1	1 ± 1	1 ± 0
$W + \text{jets}$	29 ± 2	15 ± 2	6 ± 1	3 ± 1	1 ± 0	0 ± 0	0 ± 0
Rare	59 ± 3	38 ± 3	16 ± 2	8 ± 1	4 ± 1	2 ± 0	1 ± 0
Total	802 ± 10	486 ± 8	164 ± 5	62 ± 3	23 ± 2	10 ± 1	6 ± 1
Yield UL (optimistic)	147 (10%)	94 (10%)	47 (15%)	25 (20%)	14 (25%)	8.6 (30%)	7.5 (50%)
Yield UL (pessimistic)	200 (15%)	152 (20%)	64 (25%)	30 (30%)	15 (35%)	9.7 (50%)	8.2 (100%)
$T2tt$ $m(\text{stop}) = 250$ $m(\chi^0) = 0$	315 ± 18	193 ± 14	53 ± 8	13 ± 4	2 ± 2	0 ± 0	0 ± 0
$T2tt$ $m(\text{stop}) = 300$ $m(\chi^0) = 50$	296 ± 11	236 ± 10	88 ± 6	28 ± 3	10 ± 2	2 ± 1	0 ± 0
$T2tt$ $m(\text{stop}) = 300$ $m(\chi^0) = 100$	128 ± 7	93 ± 6	29 ± 3	10 ± 2	5 ± 1	2 ± 1	1 ± 1
$T2tt$ $m(\text{stop}) = 350$ $m(\chi^0) = 0$	224 ± 6	206 ± 6	119 ± 4	52 ± 3	20 ± 2	8 ± 1	3 ± 1
$T2tt$ $m(\text{stop}) = 450$ $m(\chi^0) = 0$	71 ± 2	71 ± 2	53 ± 1	36 ± 1	21 ± 1	11 ± 1	5 ± 0

Table 5: Expected SM background contributions and signal yields for a few sample points, including both muon and electron channels. This is “dead reckoning” MC with no correction. It is meant only as a general guide. The uncertainties are statistical only. The signal yield expected upper limits are also shown for two values of the total background systematic uncertainty, indicated in parentheses.

4.4 Control Region Selection

Control regions (CRs) are used to validate the background estimation procedure and derive systematic uncertainties for some contributions. The CRs are selected to have similar kinematics to the SRs, but have a different requirement in terms of number of b-tags and number of leptons, thus enhancing them in different SM contributions. The four CRs used in this analysis are summarized in Table 6.

Selection Criteria	exactly 1 lepton	exactly 2 leptons	1 lepton + isolated track
0 b-tags	CR1) W+Jets dominated: Validate W+Jets M_T tail	CR2) apply Z-mass constraint \rightarrow Z+Jets dominated: Validate $t\bar{t} \rightarrow \ell + \text{jets}$ M_T tail comparing data vs. MC “pseudo- M_T ”	CR3) not used
≥ 1 b-tags	SIGNAL REGION	CR4) Apply Z-mass veto \rightarrow $t\bar{t} \rightarrow \ell\ell$ dominated: Validate “physics” modelling of $t\bar{t} \rightarrow \ell\ell$	CR5) $t\bar{t} \rightarrow \ell\ell$, $t\bar{t} \rightarrow \ell\tau$ and $t\bar{t} \rightarrow \ell\text{fake}$ dominated: Validate τ and fake lepton modeling/detector effects in $t\bar{t} \rightarrow \ell\ell$

Table 6: Summary of signal and control regions.

185 **4.5 Definition of M_T peak region**

186 This region is defined as $50 < M_T < 80$ GeV.

187 **4.6 Default $t\bar{t}$ MC sample**

188 Our default $t\bar{t}$ MC sample is Powheg.

189 **4.7 MC Corrections**

190 All MC samples are corrected for trigger efficiency. In the case of single lepton selections, we apply the
191 p_T and η -dependent scale factors that we measure ourselves, see Section 4.9. In the case of dilepton
192 selections that require the dilepton triggers, we apply overall scale factors of 0.95, 0.88, and 0.92 for ee ,
193 $\mu\mu$, and $e\mu$ respectively [3].

194 The leptonic branching fraction used in some of the $t\bar{t}$ MC samples differs from the value listed in the
195 PDG (10.80 ± 0.09)%. Table 7 summarizes the branching fractions used in the generation of the various
196 $t\bar{t}$ MC samples. For $t\bar{t}$ samples with the incorrect leptonic branching fraction, event weights are applied
197 based on the number of true leptons and the ratio of the corrected and incorrect branching fractions.

$t\bar{t}$ Sample - Event Generator	Leptonic Branching Fraction
Madgraph	0.111
MC@NLO	0.111
Pythia	0.108
Powheg	0.108

Table 7: Leptonic branching fractions for the various $t\bar{t}$ samples used in the analysis. The $t\bar{t}$ MC samples produced with Madgraph and MC@NLO has a branching fraction that is almost 3% higher than the PDG value.

198 All $t\bar{t}$ dilepton samples are corrected (when needed and appropriate) in order to have the correct jet
199 multiplicity distribution. This correction procedure is described in Section 5.3.1.

200 **4.7.1 Corrections to Jets and E_T^{miss}**

201 The official recommendations from the Jet/MET group are used for the data and MC samples. In
202 particular, the jet energy corrections (JEC) are updated using the official recipe. L1FastL2L3Residual
203 (L1FastL2L3) corrections are applied for data (MC), based on the global tags GR.R_52_V9 (START52_V9B)
204 for data (MC). In addition, these jet energy corrections are propagated to the E_T^{miss} calculation, following
205 the official prescription for deriving the Type I corrections.

206 Events with anomalous “rho” pile-up corrections are excluded from the sample since these can correspond
207 to events with unphysically large E_T^{miss} and M_T . In addition, the recommended MET filters are applied.
208 A correction to remove the ϕ modulation in E_T^{miss} is also applied to the data.

209 **4.8 Lepton Selection Efficiency Measurements**

210 In this section we measure the identification and isolation efficiencies for muons and electrons in data
211 and MC using tag-and-probe studies. The tag is required to pass the full offline analysis selection and
212 have $p_T > 30$ GeV, $|\eta| < 2.1$, and be matched to the single lepton trigger, HLT_IsoMu24(_eta2p1) for
213 muons and HLT_Ele27_WP80 for electrons. The probe is required to have $|\eta| < 2.1$ and $p_T > 20$ GeV. To
214 measure the identification efficiency we require the probe to pass the isolation requirement, to measure
215 the isolation efficiency we require the probe to pass the identification requirement.

216 The tag-probe pair is required to have opposite-sign and an invariant mass in the range 76–106 GeV.
217 In order to suppress lepton pairs from sources other than Z boson decays, we require the event to have
218 $E_T^{\text{miss}} < 30$ GeV and no b-tagged jets (CSV loose working point).

219 The muon efficiencies are summarized in Table 8 for inclusive events (i.e. no jet requirements). These
220 efficiencies are displayed in Fig. 2 for several different jet multiplicity requirements. We currently observe

221 good agreement for muons with p_T up to about 300 GeV. For high p_T muons we observe a source of
222 background in the data with large impact parameters, which we suppress by requiring muon $d_0 < 0.02$ cm
223 and $d_Z < 0.5$ cm. The electron efficiencies are summarized in Table 9 for inclusive events (i.e. no jet
224 requirements). These efficiencies are displayed in Fig. 3 for several different jet multiplicity requirements.
225 In general we observe good agreement between the data and MC identification and isolation efficiencies.
226 We do not correct the MC for differences in lepton efficiency. In the background calculation, we do
227 not take any systematics due to lepton selection efficiency uncertainties. This is because all backgrounds
228 except the rare MC background are normalized to the M_T peak, thus the lepton identification uncertainty
229 cancels out. For the rare MC these uncertainties are negligible compared to the assumed cross-section
230 uncertainty (Section 6).

Table 8: Summary of the data and MC muon identification and isolation efficiencies measured with tag-and-probe studies.

MC ID p_T range [GeV]	$ \eta < 0.8$	$0.8 < \eta < 1.5$	$1.5 < \eta < 2.1$
20 - 30	0.9672 \pm 0.0005	0.9640 \pm 0.0006	0.9471 \pm 0.0008
30 - 40	0.9684 \pm 0.0002	0.9657 \pm 0.0003	0.9446 \pm 0.0004
40 - 50	0.9704 \pm 0.0002	0.9687 \pm 0.0002	0.9432 \pm 0.0004
50 - 60	0.9684 \pm 0.0005	0.9640 \pm 0.0005	0.9414 \pm 0.0009
60 - 80	0.9678 \pm 0.0009	0.9640 \pm 0.0010	0.9354 \pm 0.0018
80 - 100	0.9709 \pm 0.0021	0.9642 \pm 0.0027	0.9234 \pm 0.0051
100 - 150	0.9679 \pm 0.0029	0.9654 \pm 0.0035	0.9261 \pm 0.0069
150 - 200	0.9643 \pm 0.0069	0.9568 \pm 0.0088	0.9045 \pm 0.0198
200 - 300	0.9647 \pm 0.0116	0.9388 \pm 0.0171	0.8906 \pm 0.0390
300 - 10000	1.0000 \pm 0.0000	1.0000 \pm 0.0000	1.0000 \pm 0.0000

MC ISO p_T range [GeV]	$ \eta < 0.8$	$0.8 < \eta < 1.5$	$1.5 < \eta < 2.1$
20 - 30	0.8966 \pm 0.0007	0.9153 \pm 0.0008	0.9298 \pm 0.0009
30 - 40	0.9610 \pm 0.0002	0.9632 \pm 0.0003	0.9707 \pm 0.0003
40 - 50	0.9876 \pm 0.0001	0.9897 \pm 0.0001	0.9912 \pm 0.0002
50 - 60	0.9921 \pm 0.0002	0.9927 \pm 0.0003	0.9939 \pm 0.0003
60 - 80	0.9927 \pm 0.0004	0.9937 \pm 0.0004	0.9947 \pm 0.0005
80 - 100	0.9920 \pm 0.0012	0.9921 \pm 0.0013	0.9932 \pm 0.0016
100 - 150	0.9898 \pm 0.0017	0.9923 \pm 0.0017	0.9933 \pm 0.0022
150 - 200	0.9901 \pm 0.0037	0.9922 \pm 0.0039	0.9950 \pm 0.0050
200 - 300	0.9919 \pm 0.0057	1.0000 \pm 0.0000	0.9828 \pm 0.0171
300 - 10000	1.0000 \pm 0.0000	1.0000 \pm 0.0000	1.0000 \pm 0.0000

DATA ID p_T range [GeV]	$ \eta < 0.8$	$0.8 < \eta < 1.5$	$1.5 < \eta < 2.1$
20 - 30	0.9530 \pm 0.0005	0.9517 \pm 0.0006	0.9369 \pm 0.0008
30 - 40	0.9556 \pm 0.0003	0.9519 \pm 0.0003	0.9362 \pm 0.0005
40 - 50	0.9584 \pm 0.0002	0.9558 \pm 0.0003	0.9355 \pm 0.0004
50 - 60	0.9540 \pm 0.0005	0.9487 \pm 0.0006	0.9314 \pm 0.0010
60 - 80	0.9536 \pm 0.0010	0.9466 \pm 0.0012	0.9307 \pm 0.0019
80 - 100	0.9505 \pm 0.0028	0.9414 \pm 0.0035	0.9289 \pm 0.0053
100 - 150	0.9472 \pm 0.0038	0.9454 \pm 0.0045	0.9149 \pm 0.0079
150 - 200	0.9628 \pm 0.0073	0.9675 \pm 0.0089	0.8950 \pm 0.0217
200 - 300	0.9463 \pm 0.0157	0.9290 \pm 0.0206	0.8889 \pm 0.0468
300 - 10000	0.9412 \pm 0.0404	1.0000 \pm 0.0000	0.4000 \pm 0.2191

DATA ISO p_T range [GeV]	$ \eta < 0.8$	$0.8 < \eta < 1.5$	$1.5 < \eta < 2.1$
20 - 30	0.8939 \pm 0.0007	0.9144 \pm 0.0008	0.9361 \pm 0.0008
30 - 40	0.9598 \pm 0.0002	0.9646 \pm 0.0003	0.9744 \pm 0.0003
40 - 50	0.9870 \pm 0.0001	0.9901 \pm 0.0001	0.9920 \pm 0.0002
50 - 60	0.9912 \pm 0.0002	0.9933 \pm 0.0002	0.9953 \pm 0.0003
60 - 80	0.9920 \pm 0.0004	0.9934 \pm 0.0005	0.9956 \pm 0.0005
80 - 100	0.9926 \pm 0.0011	0.9933 \pm 0.0013	0.9955 \pm 0.0014
100 - 150	0.9913 \pm 0.0016	0.9949 \pm 0.0015	0.9965 \pm 0.0017
150 - 200	0.9969 \pm 0.0022	0.9974 \pm 0.0026	0.9944 \pm 0.0055
200 - 300	1.0000 \pm 0.0000	1.0000 \pm 0.0000	1.0000 \pm 0.0000
300 - 10000	1.0000 \pm 0.0000	1.0000 \pm 0.0000	1.0000 \pm 0.0000

Scale Factor ID p_T range [GeV]	$ \eta < 0.8$	$0.8 < \eta < 1.5$	$1.5 < \eta < 2.1$
20 - 30	0.9853 \pm 0.0007	0.9872 \pm 0.0009	0.9893 \pm 0.0012
30 - 40	0.9868 \pm 0.0003	0.9857 \pm 0.0005	0.9911 \pm 0.0007
40 - 50	0.9877 \pm 0.0003	0.9866 \pm 0.0004	0.9918 \pm 0.0006
50 - 60	0.9851 \pm 0.0007	0.9841 \pm 0.0009	0.9894 \pm 0.0014
60 - 80	0.9853 \pm 0.0014	0.9820 \pm 0.0017	0.9949 \pm 0.0028
80 - 100	0.9790 \pm 0.0036	0.9763 \pm 0.0046	1.0059 \pm 0.0080
100 - 150	0.9786 \pm 0.0049	0.9793 \pm 0.0059	0.9879 \pm 0.0113
150 - 200	0.9984 \pm 0.0104	1.0112 \pm 0.0131	0.9894 \pm 0.0323
200 - 300	0.9810 \pm 0.0201	0.9896 \pm 0.0284	0.9981 \pm 0.0684
300 - 10000	0.9412 \pm 0.0404	1.0000 \pm 0.0000	0.4000 \pm 0.2191

Scale Factor ISO p_T range [GeV]	$ \eta < 0.8$	$0.8 < \eta < 1.5$	$1.5 < \eta < 2.1$
20 - 30	0.9970 \pm 0.0012	0.9989 \pm 0.0012	1.0068 \pm 0.0013
30 - 40	0.9987 \pm 0.0004	1.0014 \pm 0.0004	1.0038 \pm 0.0005
40 - 50	0.9994 \pm 0.0002	1.0004 \pm 0.0002	1.0008 \pm 0.0002
50 - 60	0.9991 \pm 0.0003	1.0006 \pm 0.0003	1.0013 \pm 0.0004
60 - 80	0.9993 \pm 0.0006	0.9997 \pm 0.0006	1.0009 \pm 0.0008
80 - 100	1.0006 \pm 0.0016	1.0012 \pm 0.0018	1.0023 \pm 0.0022
100 - 150	1.0015 \pm 0.0023	1.0027 \pm 0.0023	1.0032 \pm 0.0028
150 - 200	1.0068 \pm 0.0044	1.0053 \pm 0.0047	0.9994 \pm 0.0075
200 - 300	1.0081 \pm 0.0058	1.0000 \pm 0.0000	1.0175 \pm 0.0177
300 - 10000	1.0000 \pm 0.0000	1.0000 \pm 0.0000	1.0000 \pm 0.0000

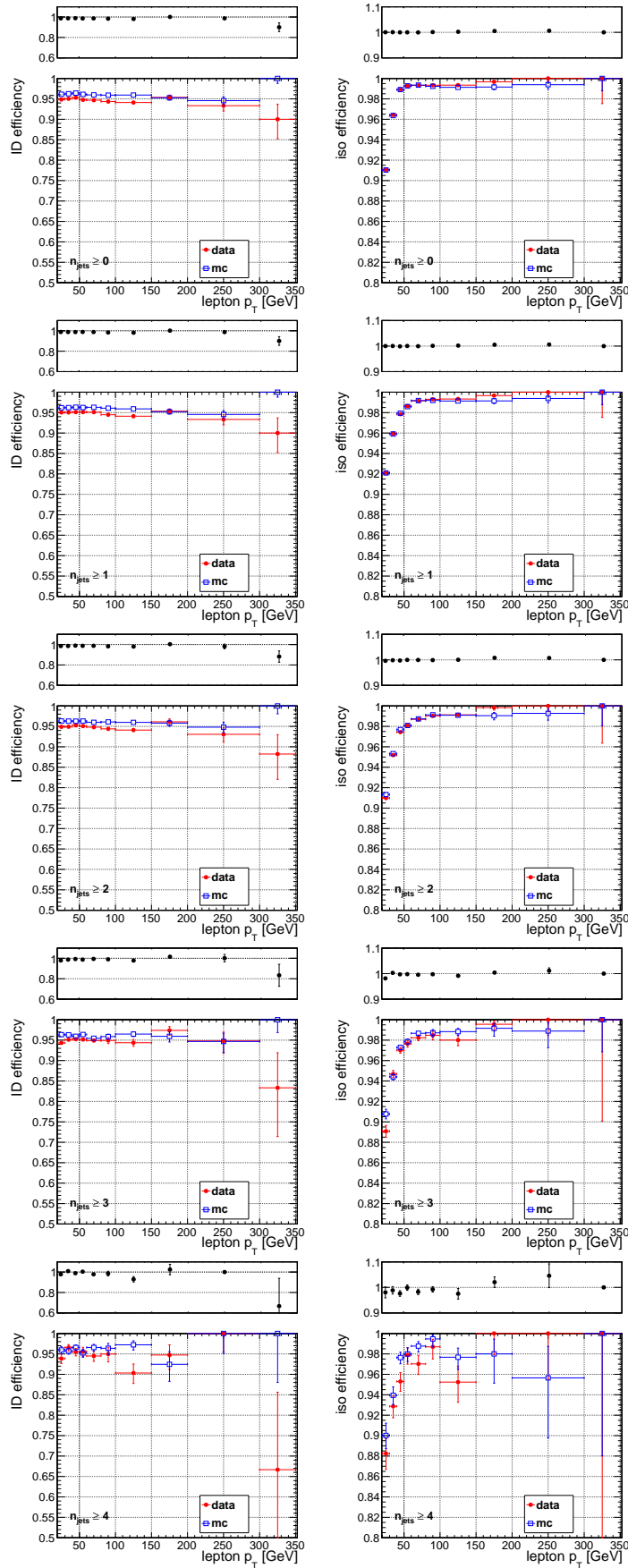


Figure 2: Comparison of the muon identification and isolation efficiencies in data and MC for various jet multiplicity requirements.

Table 9: Summary of the data and MC electron identification and isolation efficiencies measured with tag-and-probe studies.

MC ID p_T range [GeV]	$ \eta < 1.5$	$1.5 < \eta < 2.1$
20 - 30	0.8156 \pm 0.0008	0.6565 \pm 0.0019
30 - 40	0.8670 \pm 0.0004	0.7450 \pm 0.0010
40 - 50	0.8922 \pm 0.0003	0.7847 \pm 0.0008
50 - 60	0.9023 \pm 0.0006	0.7956 \pm 0.0018
60 - 80	0.9097 \pm 0.0011	0.8166 \pm 0.0034
80 - 100	0.9203 \pm 0.0028	0.8196 \pm 0.0090
100 - 150	0.9162 \pm 0.0037	0.8378 \pm 0.0117
150 - 200	0.9106 \pm 0.0087	0.8111 \pm 0.0292
200 - 300	0.9304 \pm 0.0119	0.9153 \pm 0.0363
300 - 10000	0.8684 \pm 0.0388	0.8000 \pm 0.1789
MC ISO p_T range [GeV]	$ \eta < 1.5$	$1.5 < \eta < 2.1$
20 - 30	0.9245 \pm 0.0006	0.9466 \pm 0.0011
30 - 40	0.9682 \pm 0.0002	0.9741 \pm 0.0004
40 - 50	0.9876 \pm 0.0001	0.9883 \pm 0.0002
50 - 60	0.9909 \pm 0.0002	0.9912 \pm 0.0005
60 - 80	0.9916 \pm 0.0004	0.9930 \pm 0.0008
80 - 100	0.9915 \pm 0.0010	0.9908 \pm 0.0025
100 - 150	0.9929 \pm 0.0012	0.9894 \pm 0.0035
150 - 200	0.9919 \pm 0.0029	0.9932 \pm 0.0068
200 - 300	0.9953 \pm 0.0033	1.0000 \pm 0.0000
300 - 10000	1.0000 \pm 0.0000	1.0000 \pm 0.0000
DATA ID p_T range [GeV]	$ \eta < 1.5$	$1.5 < \eta < 2.1$
20 - 30	0.8145 \pm 0.0008	0.6528 \pm 0.0018
30 - 40	0.8676 \pm 0.0004	0.7462 \pm 0.0010
40 - 50	0.8955 \pm 0.0003	0.7922 \pm 0.0008
50 - 60	0.9049 \pm 0.0006	0.8072 \pm 0.0018
60 - 80	0.9110 \pm 0.0011	0.8212 \pm 0.0035
80 - 100	0.9156 \pm 0.0028	0.8358 \pm 0.0091
100 - 150	0.9257 \pm 0.0036	0.8507 \pm 0.0116
150 - 200	0.9186 \pm 0.0084	0.8929 \pm 0.0292
200 - 300	0.9106 \pm 0.0149	0.7576 \pm 0.0746
300 - 10000	0.9400 \pm 0.0336	1.0000 \pm 0.0000
DATA ISO p_T range [GeV]	$ \eta < 1.5$	$1.5 < \eta < 2.1$
20 - 30	0.9201 \pm 0.0006	0.9419 \pm 0.0011
30 - 40	0.9667 \pm 0.0002	0.9734 \pm 0.0004
40 - 50	0.9872 \pm 0.0001	0.9892 \pm 0.0002
50 - 60	0.9904 \pm 0.0002	0.9922 \pm 0.0004
60 - 80	0.9923 \pm 0.0004	0.9916 \pm 0.0009
80 - 100	0.9914 \pm 0.0010	0.9921 \pm 0.0024
100 - 150	0.9945 \pm 0.0011	1.0000 \pm 0.0000
150 - 200	0.9908 \pm 0.0031	1.0000 \pm 0.0000
200 - 300	0.9941 \pm 0.0042	1.0000 \pm 0.0000
300 - 10000	0.9792 \pm 0.0206	1.0000 \pm 0.0000
Scale Factor ID p_T range [GeV]	$ \eta < 1.5$	$1.5 < \eta < 2.1$
20 - 30	0.9987 \pm 0.0014	0.9944 \pm 0.0040
30 - 40	1.0007 \pm 0.0006	1.0015 \pm 0.0019
40 - 50	1.0036 \pm 0.0005	1.0096 \pm 0.0015
50 - 60	1.0029 \pm 0.0010	1.0146 \pm 0.0031
60 - 80	1.0014 \pm 0.0018	1.0057 \pm 0.0060
80 - 100	0.9949 \pm 0.0043	1.0197 \pm 0.0158
100 - 150	1.0104 \pm 0.0057	1.0154 \pm 0.0198
150 - 200	1.0087 \pm 0.0134	1.1008 \pm 0.0535
200 - 300	0.9786 \pm 0.0203	0.8277 \pm 0.0879
300 - 10000	1.0824 \pm 0.0619	1.2500 \pm 0.2795
Scale Factor ISO p_T range [GeV]	$ \eta < 1.5$	$1.5 < \eta < 2.1$
20 - 30	0.9952 \pm 0.0009	0.9950 \pm 0.0016
30 - 40	0.9984 \pm 0.0003	0.9992 \pm 0.0006
40 - 50	0.9996 \pm 0.0002	1.0009 \pm 0.0003
50 - 60	0.9995 \pm 0.0003	1.0009 \pm 0.0006
60 - 80	1.0006 \pm 0.0005	0.9985 \pm 0.0012
80 - 100	0.9999 \pm 0.0014	1.0013 \pm 0.0035
100 - 150	1.0016 \pm 0.0016	1.0108 \pm 0.0036
150 - 200	0.9989 \pm 0.0042	1.0068 \pm 0.0069
200 - 300	0.9987 \pm 0.0053	1.0000 \pm 0.0000
300 - 10000	0.9792 \pm 0.0206	1.0000 \pm 0.0000

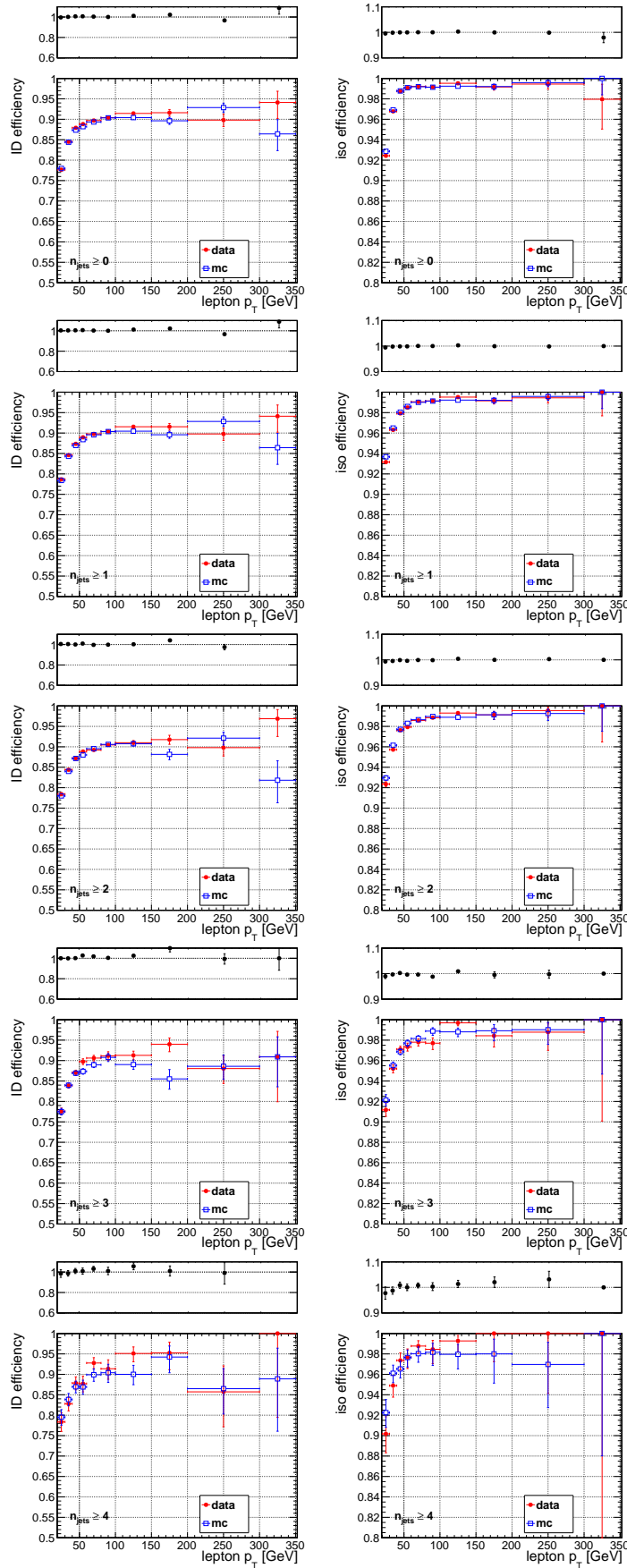


Figure 3: Comparison of the electron identification and isolation efficiencies in data and MC for various jet multiplicity requirements.

231 4.9 Trigger Efficiency Measurements

- 232 In this section we measure the efficiencies of the single lepton triggers, HLT_IsoMu24(_eta2p1) for muons
 233 and HLT_Ele27_WP80 for electrons, using a tag-and-probe approach. The tag is required to pass the
 234 full offline analysis selection and have $p_T > 30$ GeV, $|\eta| < 2.1$, and be matched to the single lepton
 235 trigger. The probe is also required to pass the full offline analysis selection and have $|\eta| < 2.1$, but the
 236 p_T requirement is relaxed to 20 GeV in order to measure the p_T turn-on curve. The tag-probe pair is
 237 required to have opposite-sign and an invariant mass in the range 76–106 GeV.
- 238 The measured trigger efficiencies are displayed in Fig. 4 and summarized in Table 10 (muons) and Table 11
 239 (electrons). These trigger efficiencies are applied to the MC when used to predict data yields selected by
 240 single lepton triggers.

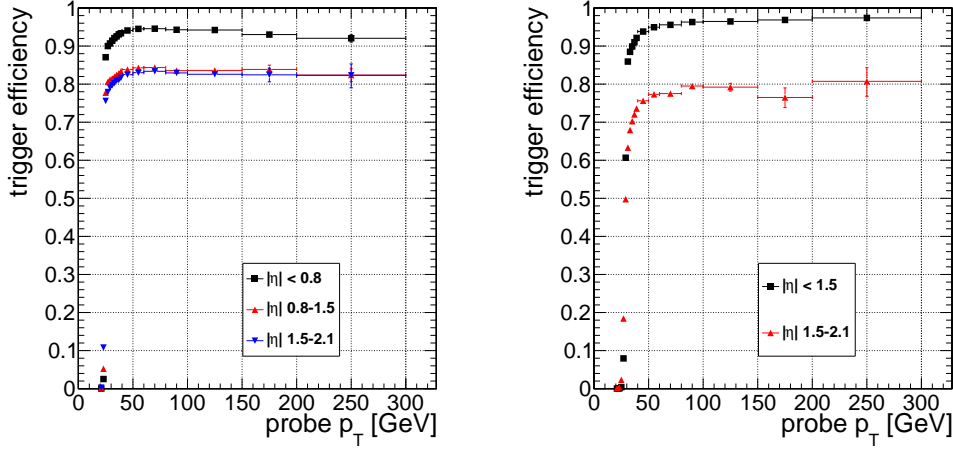


Figure 4: Efficiency for the single muon trigger HLT_IsoMu24(_eta2p1) (left) and single electron trigger HLT_Ele27_WP80 (right) as a function of lepton p_T , for several bins in lepton $|\eta|$.

Table 10: Summary of the single muon trigger efficiency HLT_IsoMu24(_eta2p1). Uncertainties are statistical.

p_T range [GeV]	$ \eta < 0.8$	$0.8 < \eta < 1.5$	$1.5 < \eta < 2.1$
20 - 22	0.00 ± 0.000	0.00 ± 0.000	0.00 ± 0.000
22 - 24	0.03 ± 0.001	0.05 ± 0.001	0.11 ± 0.002
24 - 26	0.87 ± 0.002	0.78 ± 0.002	0.76 ± 0.003
26 - 28	0.90 ± 0.001	0.81 ± 0.002	0.78 ± 0.002
28 - 30	0.91 ± 0.001	0.81 ± 0.002	0.79 ± 0.002
30 - 32	0.91 ± 0.001	0.81 ± 0.001	0.80 ± 0.002
32 - 34	0.92 ± 0.001	0.82 ± 0.001	0.80 ± 0.002
34 - 36	0.93 ± 0.001	0.82 ± 0.001	0.81 ± 0.001
36 - 38	0.93 ± 0.001	0.83 ± 0.001	0.81 ± 0.001
38 - 40	0.93 ± 0.001	0.83 ± 0.001	0.82 ± 0.001
40 - 50	0.94 ± 0.000	0.84 ± 0.000	0.82 ± 0.001
50 - 60	0.95 ± 0.000	0.84 ± 0.001	0.83 ± 0.001
60 - 80	0.95 ± 0.001	0.84 ± 0.002	0.83 ± 0.002
80 - 100	0.94 ± 0.002	0.84 ± 0.004	0.83 ± 0.006
100 - 150	0.94 ± 0.003	0.84 ± 0.005	0.83 ± 0.008
150 - 200	0.93 ± 0.006	0.84 ± 0.011	0.82 ± 0.018
>200	0.92 ± 0.010	0.82 ± 0.017	0.82 ± 0.031

Table 11: Summary of the single electron trigger efficiency HLT_Ele27_WP80. Uncertainties are statistical.

p_T range [GeV]	$ \eta < 1.5$	$1.5 < \eta < 2.1$
20 - 22	0.00 ± 0.000	0.00 ± 0.000
22 - 24	0.00 ± 0.000	0.00 ± 0.001
24 - 26	0.00 ± 0.000	0.02 ± 0.001
26 - 28	0.08 ± 0.001	0.18 ± 0.003
28 - 30	0.61 ± 0.002	0.50 ± 0.004
30 - 32	0.86 ± 0.001	0.63 ± 0.003
32 - 34	0.88 ± 0.001	0.68 ± 0.003
34 - 36	0.90 ± 0.001	0.70 ± 0.002
36 - 38	0.91 ± 0.001	0.72 ± 0.002
38 - 40	0.92 ± 0.001	0.74 ± 0.002
40 - 50	0.94 ± 0.000	0.76 ± 0.001
50 - 60	0.95 ± 0.000	0.77 ± 0.002
60 - 80	0.96 ± 0.001	0.78 ± 0.003
80 - 100	0.96 ± 0.002	0.80 ± 0.008
100 - 150	0.96 ± 0.002	0.79 ± 0.010
150 - 200	0.97 ± 0.004	0.76 ± 0.026
>200	0.97 ± 0.005	0.81 ± 0.038

241 5 Control Region Studies

242 The CR studies described in this Section are key to validating the background predictions. The CRs are
 243 defined in Section 4.4.

244 CR1 and CR2 are designed to test the M_T tail in $W+$ jets and $t\bar{t}$ respectively. Note that, as explained
 245 in Section 2.1, these tails are different in the two samples because the off-shell effects are much more
 246 pronounced for $W+$ jets (the s- and t-channel single top have the same M_T tail as $t\bar{t}$). To put things in
 247 perspective, keep in mind that these backgrounds are only about 15% of the total, see Table 5.

248 CR4 and CR5 address the dominant $t\bar{t}$ dilepton background. In CR4 we test the M_T tail in well identified
 249 dilepton events. In CR5 we test the same quantity, but in events where the second lepton is identified as
 250 an isolated track. Clearly CR4 and CR5 overlap.

251 5.1 $W+$ -Jets MC Modelling Validation from CR1

252 The estimate of the uncertainty on this background is based on CR1, defined by applying the full signal
 253 selection, including the isolated track veto, but requiring 0 b-tags (CSV medium working point as de-
 254 scribed in Sec. 4). The sample is dominated by $W+$ -jets and is thus used to validate the MC modelling
 255 of this background.

256 In Table 12 we show the amount that we need to scale the $W+$ -jets MC by in order to have agreement
 257 between data and Monte Carlo in the M_T peak region, defined as $50 < M_T < 80$ GeV, for the different
 258 signal regions. (Recall, the signal regions have different E_T^{miss} requirements). These scale factors are not
 259 terribly important, but it is reassuring that they are not too different from 1.

Sample	CR1PRESEL	CR1A	CR1B	CR1C	CR1D	CR1E	CR1F	CR1G
μM_T -SF	0.92 ± 0.02	0.97 ± 0.03	0.90 ± 0.04	0.91 ± 0.06	0.93 ± 0.09	0.98 ± 0.13	0.94 ± 0.18	0.96 ± 0.25
$e M_T$ -SF	0.94 ± 0.02	0.90 ± 0.04	0.84 ± 0.05	0.80 ± 0.07	0.83 ± 0.10	0.77 ± 0.13	0.86 ± 0.20	0.87 ± 0.29

Table 12: M_T peak Data/MC scale factors applied to $W+$ -jets samples. No scaling is made for back-
 grounds from other processes. CR1PRESEL refers to a sample with $E_T^{\text{miss}} > 50$ GeV. The uncertainties
 are statistical only.

260 Next, in Fig 41, 6, and 7, we show plots of E_T^{miss} and then M_T for different E_T^{miss} requirements corre-
 261 sponding to those defining our signal regions. It is clear that there are more events in the M_T tail than
 262 predicted from MC. This implies that we need to rescale the MC $W+$ -jets background in the tail region.

263 The rescaling is explored in Table 13, where we compare the data and MC yields in the M_T signal regions
 264 and in a looser control region. Note that the MC is normalized in the M_T peak region by rescaling the
 265 $W+$ -jets component according to Table 12.

266 We also derive data/MC scale factors. As shown in Table 13, these are derived in two different ways,
 267 separately for muons and electrons and then combined, as follows:

- 268 • For the first three sets of scale factors, above the triple horizontal line, we calculate the scale factor
 269 as the amount by which we would need to rescale **all** MC ($W+$ -jets, $t\bar{t}$, single top, rare) in order
 270 to have data-MC agreement in the M_T tail.
- 271 • For the next three set of scale factors, below the triple horizontal line, we calculate the scale factor
 272 as the amount by which we would need to scale $W+$ -jets keeping all other components fixed in order
 273 to have data-MC agreement in the tail.

274 The true $W+$ -jets scale factor is somewhere in between these two extremes. We also note that there is no
 275 statistically significant difference between the electron and muon samples. We use these data to extract
 276 a data/MC scale factor for $W+$ -jets which will be used to rescale the $W+$ -jets MC tail. This scale factor
 277 is listed in the last line of the Table, and is called SFR_{w+jets} . It is calculated as follows.

- 278 • Separately for each signal region
- 279 • As the average of the two methods described above

Sample	CR1PRESEL	CR1A	CR1B	CR1C	CR1D	CR1E	CR1F	CR1G
μ MC	480 ± 22	173 ± 5	114 ± 4	40 ± 2	16 ± 1	8 ± 1	4 ± 1	2 ± 1
μ Data	629	238	139	45	12	8	3	2
μ Data/MC	1.31 ± 0.08	1.37 ± 0.10	1.22 ± 0.11	1.12 ± 0.18	0.75 ± 0.23	0.99 ± 0.37	0.75 ± 0.45	0.96 ± 0.72
e MC	330 ± 8	118 ± 4	79 ± 3	29 ± 2	13 ± 1	5 ± 1	3 ± 1	2 ± 0
e Data	473	174	100	36	16	5	5	2
e Data/MC	1.43 ± 0.07	1.47 ± 0.12	1.27 ± 0.14	1.23 ± 0.22	1.26 ± 0.34	1.07 ± 0.51	1.80 ± 0.91	1.26 ± 0.97
$\mu + e$ MC	810 ± 23	291 ± 7	192 ± 5	69 ± 3	29 ± 2	13 ± 1	7 ± 1	4 ± 1
$\mu + e$ Data	1102	412	239	81	28	13	8	4
$\mu + e$ Data/MC	1.36 ± 0.08	1.42 ± 0.13	1.24 ± 0.15	1.17 ± 0.23	0.97 ± 0.31	1.02 ± 0.51	1.18 ± 0.69	1.09 ± 0.96
μ W MC	300 ± 23	84 ± 5	52 ± 4	20 ± 2	9 ± 2	5 ± 1	3 ± 1	1 ± 1
μ W Data	449 ± 26	149 ± 16	78 ± 12	25 ± 7	5 ± 4	5 ± 3	2 ± 2	1 ± 1
μ W Data/MC	1.50 ± 0.14	1.77 ± 0.21	1.49 ± 0.26	1.25 ± 0.38	0.56 ± 0.39	0.98 ± 0.62	0.60 ± 0.73	0.94 ± 1.14
e W MC	192 ± 8	55 ± 4	36 ± 3	14 ± 2	6 ± 1	3 ± 1	2 ± 1	1 ± 0
e W Data	335 ± 22	111 ± 13	58 ± 10	20 ± 6	10 ± 4	3 ± 2	4 ± 2	1 ± 1
e W Data/MC	1.74 ± 0.14	2.02 ± 0.29	1.58 ± 0.32	1.49 ± 0.50	1.50 ± 0.70	1.10 ± 0.80	2.27 ± 1.55	1.51 ± 1.96
$\mu + e$ W MC	493 ± 24	139 ± 6	89 ± 5	33 ± 3	16 ± 2	8 ± 1	4 ± 1	2 ± 1
$\mu + e$ W Data	785 ± 59	260 ± 37	135 ± 28	45 ± 16	15 ± 9	8 ± 7	6 ± 5	3 ± 3
$\mu + e$ W Data/MC	1.59 ± 0.14	1.87 ± 0.28	1.53 ± 0.33	1.35 ± 0.50	0.95 ± 0.58	1.03 ± 0.83	1.29 ± 1.13	1.16 ± 1.65
SFR_{wjet}	1.48 ± 0.26	1.64 ± 0.38	1.38 ± 0.30	1.26 ± 0.39	0.96 ± 0.45	1.02 ± 0.67	1.23 ± 0.92	1.12 ± 1.31

Table 13: Yields in M_T tail comparing the MC prediction (after applying SFs) to data. CR1PRESEL refers to a sample with $E_T^{\text{miss}} > 50$ GeV and $M_T > 150$ GeV. See text for details.

280

- Including the statistical uncertainty
- Adding in quadrature to the uncertainty one-half of the deviation from 1.0

281

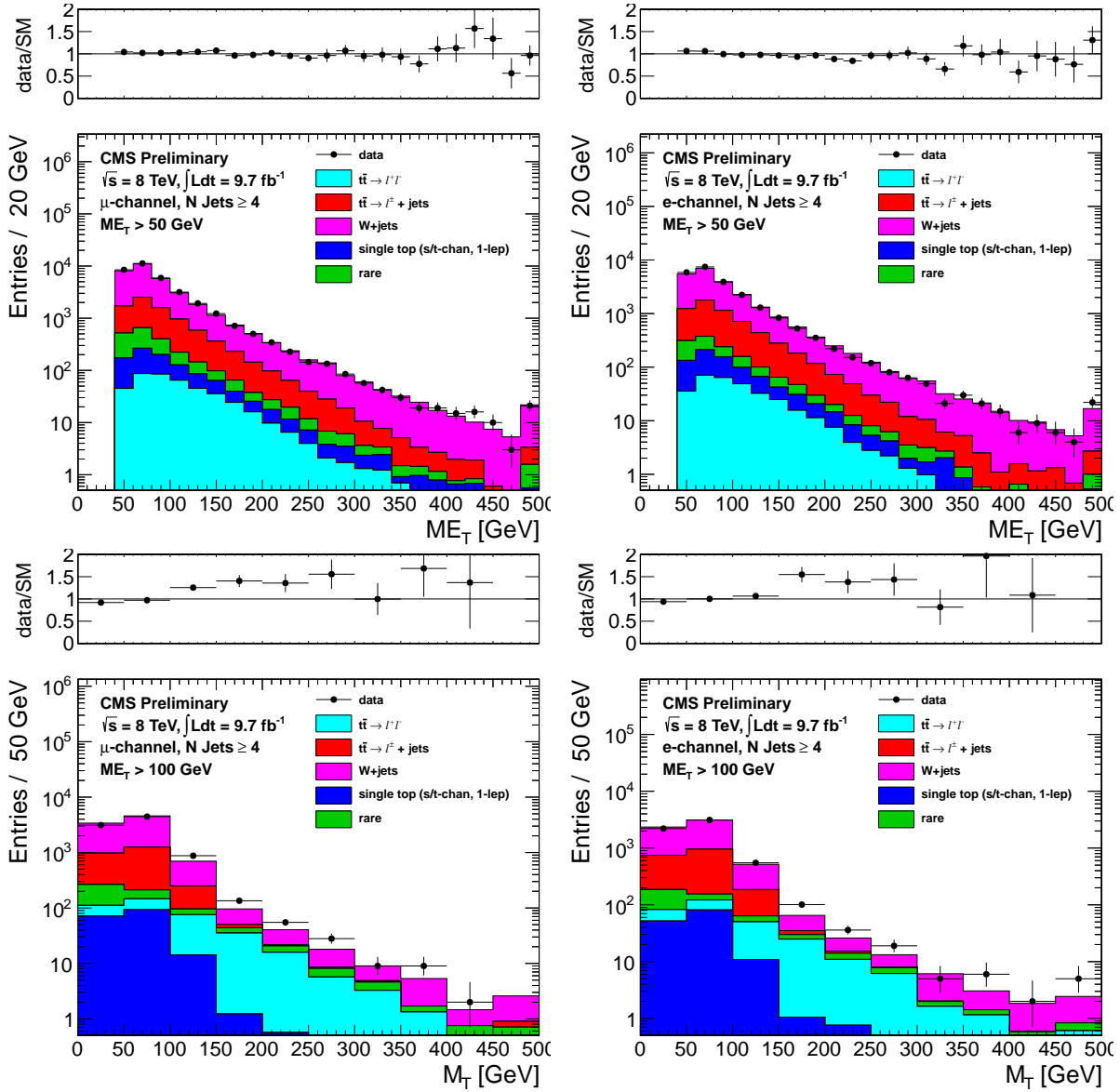


Figure 5: Comparison of the E_T^{miss} (top) and M_T for $E_T^{\text{miss}} > 100$ (bottom) distributions in data vs. MC for events with a leading muon (left) and leading electron (right) satisfying the requirements of CR1.

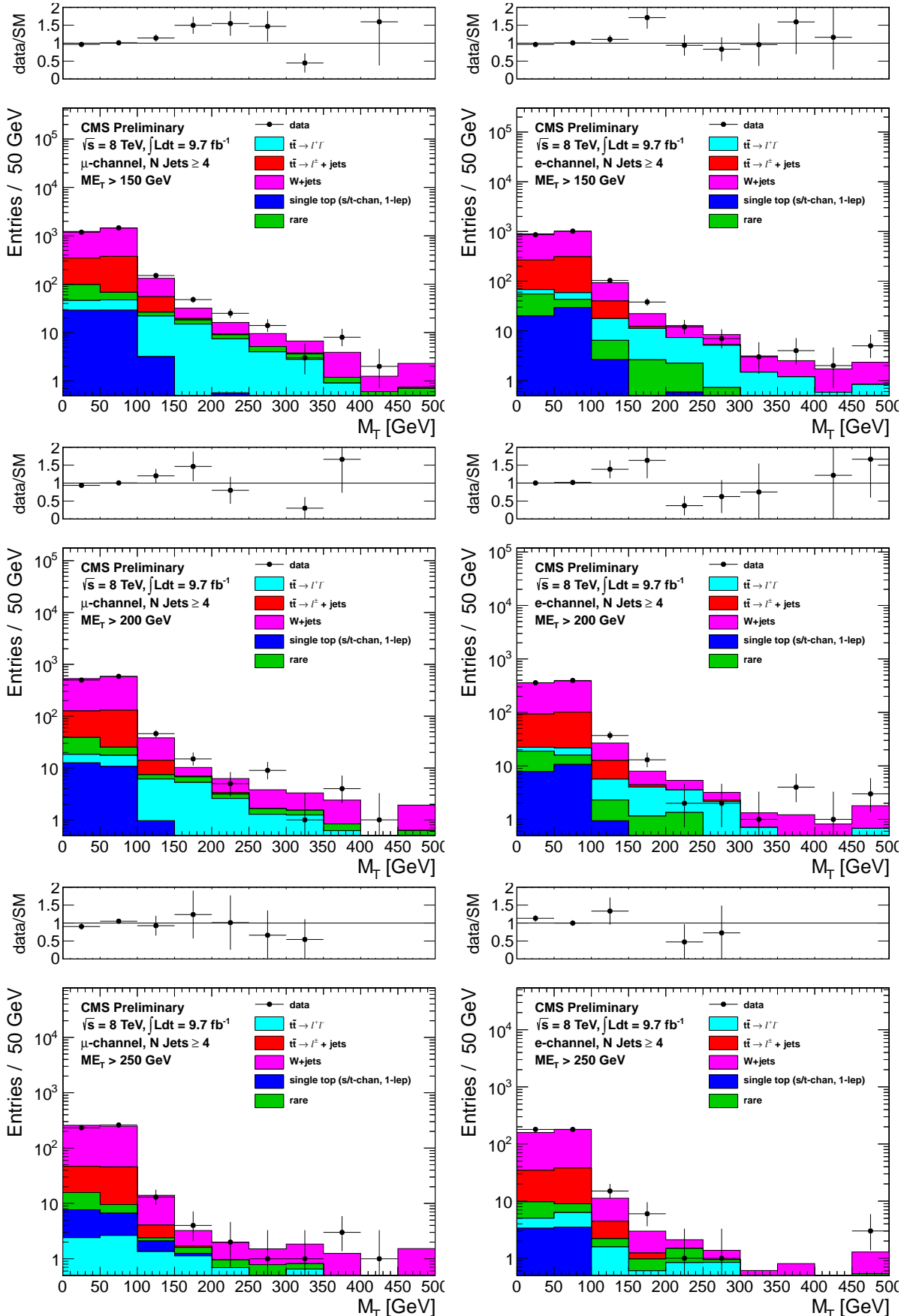


Figure 6: Comparison of the M_T distribution in data vs. MC for events with a leading muon (left) and leading electron (right) satisfying the requirements of CR1. The E_T^{miss} requirements used are 150 GeV (top), 200 GeV (middle) and 250 GeV (bottom).

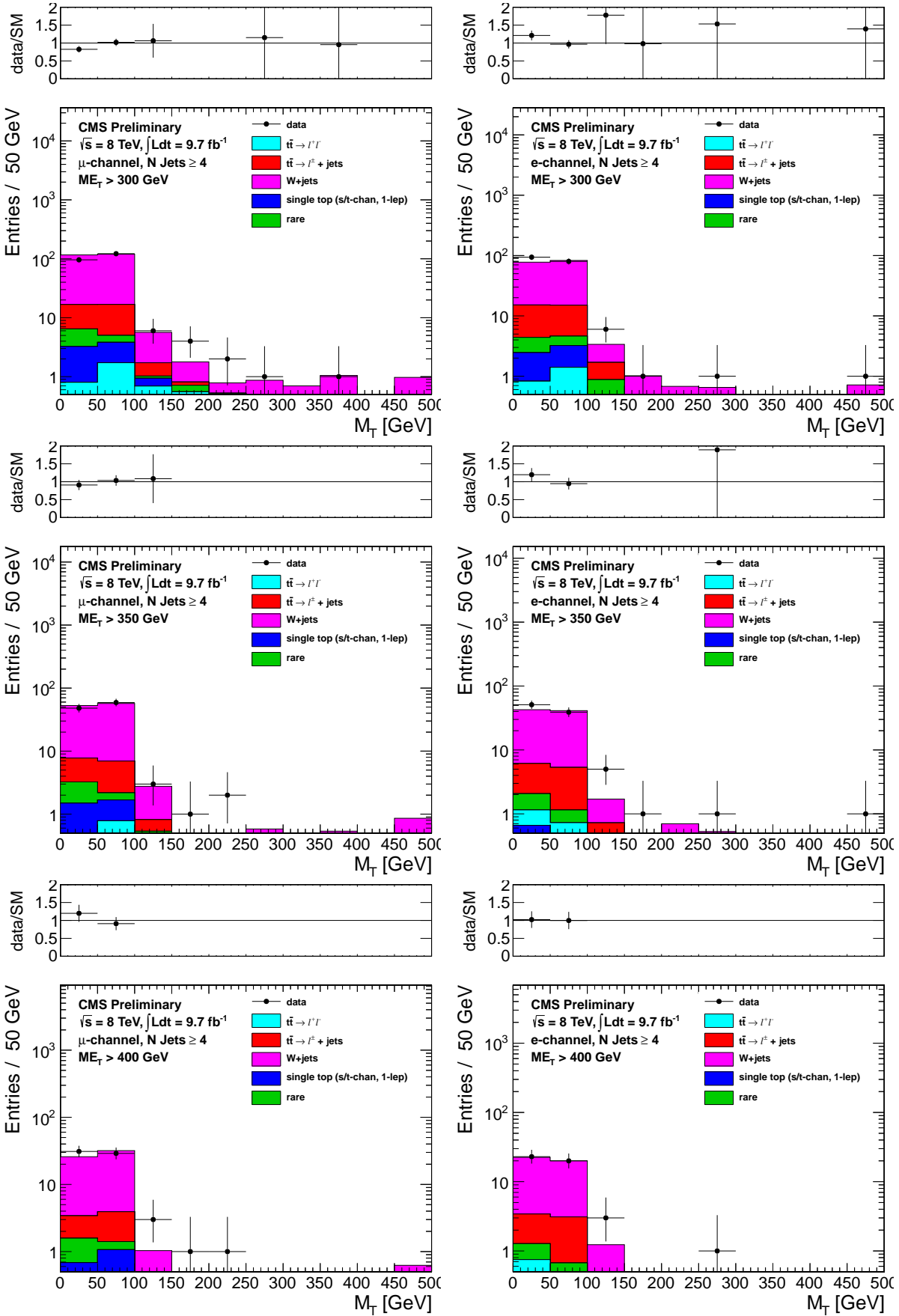


Figure 7: Comparison of the M_T distribution in data vs. MC for events with a leading muon (left) and leading electron (right) satisfying the requirements of CR1. The E_T^{miss} requirements used are 300 GeV (top), 350 GeV (middle) and 400 GeV (bottom).

282 5.2 Single Lepton Top MC Modelling Validation from CR2

283 The M_T tail for single-lepton top events ($t\bar{t} \rightarrow \ell + \text{jets}$ and single top) is dominated by jet resolution
 284 effects. The W cannot be far off-shell because $M_W < M_{\text{top}}$. The modeling of the M_T tail from jet
 285 resolution effects can be studied using $Z+\text{jets}$ data and MC samples. However, as we will show below,
 286 this test is statistically limited and can only be performed for the E_T^{miss} requirements corresponding to
 287 SRA and SRB.

288 Z events are selected by requiring exactly 2 good leptons (satisfying ID and isolation requirements) and
 289 requiring the $M_{\ell\ell}$ to be in the range $81 - 101$ GeV. Events with additional isolated tracks are vetoed, as
 290 in Section 4.2. To reduce $t\bar{t}$ backgrounds, events with a CSV tag are removed. The positive lepton is
 291 treated as a neutrino and so is added to the MET: $E_T^{\text{miss}} \rightarrow p_T(\ell^+) + E_T^{\text{miss}}$, and the M_T is recalculated
 292 with the negative lepton: $M_T(\ell^-, E_T^{\text{miss}})$. The resulting “pseudo- M_T ” is dominated by jet resolution
 293 effects, since no off-shell Z production enters the sample due to the $M_{\ell\ell}$ requirement. This section
 294 describes how well the MC predicts the tail of “pseudo- M_T ”.

295 The underlying distributions are shown in Fig. 42. We then perform the exact same type of Data/MC
 296 comparison and analysis as described for CR1 in Section D.3. For CR1 we collected the data/MC tail
 297 information in Table 13; the equivalent for CR2 is Table 14 (for CR2 the statistics are not sufficient to
 298 split electrons and muons). The last line of Table 14 gives the data/MC scale factors for the $t\bar{t}$ lepton
 299 + jets M_T tail (SFR_{top}). This is calculated in the same way as SFR_{wjets} of Table 13. Just as in CR1,
 300 there is an excess of data in the tails, as reflected in the values of SFR_{top} . There are insufficient events
 301 to derive scale factors for $E_T^{\text{miss}} > 150$ GeV. As a result, the scale factors derived from CR2 are not
 302 used for the central prediction of the single-lepton top background. They serve as a valuable cross check
 303 of the predictions described in Section 7. The single lepton top predictions obtained for SRA and SRB
 304 using the SFR_{top} values described here are consistent with the default predictions.

Sample	CR2PRESEL0	CR2PRESEL1	CR2A	CR2B
MC	32 ± 2	28 ± 2	10 ± 1	10 ± 1
Data	50	45	17	17
Data/MC	1.56 ± 0.24	1.63 ± 0.27	1.68 ± 0.45	1.74 ± 0.48
DY MC	25 ± 2	20 ± 2	5 ± 1	5 ± 1
DY Data	42 ± 7	38 ± 7	12 ± 4	12 ± 4
DY Data/MC	1.73 ± 0.32	1.85 ± 0.37	2.37 ± 0.96	2.58 ± 1.16
SFR_{top}	1.64 ± 0.40	1.74 ± 0.46	2.02 ± 0.68	2.16 ± 0.75

Table 14: Yields in M_T tail comparing the $Z+\text{jets}$ MC prediction (after applying SFs) to data without subtracting the non- $Z+\text{jets}$ components (top table) and with subtracting the non- $Z+\text{jets}$ components (bottom table). CR2PRESEL refers to a sample with $E_T^{\text{miss}} > 50$ GeV and $M_T > 150$ GeV.

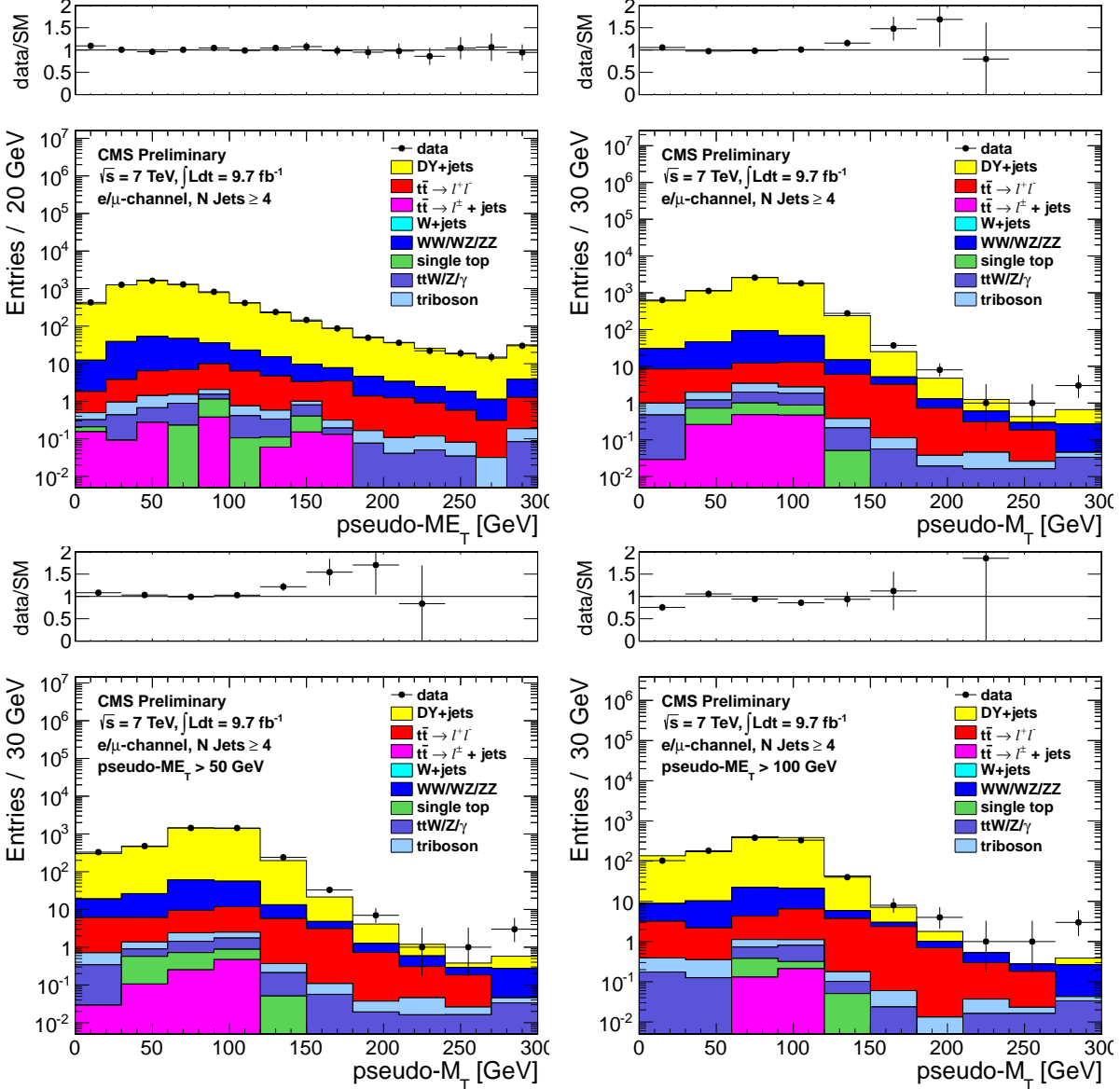


Figure 8: Comparison of the pseudo- E_T^{miss} (top, left), pseudo- M_T (top, right and bottom) distributions in data vs. MC for events satisfying the requirements of CR2, combining both the muon and electron channels. The pseudo- M_T distributions are shown before any additional requirements (top, right) and after requiring pseudo- $E_T^{\text{miss}} > 50$ GeV (bottom, left) and pseudo- $E_T^{\text{miss}} > 100$ GeV (bottom, right).

305 **5.3 Dilepton studies in CR4**

306 **5.3.1 Modeling of Additional Hard Jets in Top Dilepton Events**

307 Dilepton $t\bar{t}$ events have 2 jets from the top decays, so additional jets from radiation or higher order
 308 contributions are required to enter the signal sample. In this Section we develop an algorithm to be
 309 applied to all $t\bar{t} \rightarrow \ell\ell$ MC samples to ensure that the distribution of extra jets is properly modelled.

310 The modeling of additional jets in $t\bar{t}$ events is checked in a $t\bar{t} \rightarrow \ell\ell$ control sample, selected by requiring

- 311 • exactly 2 electrons or muons with $p_T > 20$ GeV
- 312 • $E_T^{\text{miss}} > 50$ GeV
- 313 • ≥ 1 b-tagged jet
- 314 • Z-veto ($|m_{\ell\ell} - 91| > 15$ GeV)

315 Figure 9 shows a comparison of the jet multiplicity distribution in data and MC for this two-lepton
 316 control sample. After requiring at least 1 b-tagged jet, most of the events have 2 jets, as expected from
 317 the dominant process $t\bar{t} \rightarrow \ell\ell$. There is also a significant fraction of events with additional jets. The
 318 3-jet sample is mainly comprised of $t\bar{t}$ events with 1 additional emission and similarly the ≥ 4 -jet sample
 319 contains primarily $t\bar{t} + \geq 2$ jet events.

320 It should be noted that in the case of $t\bar{t} \rightarrow \ell\ell$ events with a single reconstructed lepton, the other lepton
 321 may be mis-reconstructed as a jet. For example, a hadronic tau may be misidentified as a jet (since no
 322 τ identification is used). In this case only 1 additional jet from radiation may suffice for a $t\bar{t} \rightarrow \ell\ell$ event
 323 to enter the signal sample. As a result, both the samples with $t\bar{t} + 1$ jet and $t\bar{t} + \geq 2$ jets are relevant for
 324 estimating the top dilepton background in the signal region.

325 Table 15 shows scale factors (K_3 and K_4) used to correct the fraction of events with additional jets in
 326 MC to the observed fraction in data. These scale factors are calculated from Fig. 9 as follows:

- 327 • N_2 = data yield minus non-dilepton $t\bar{t}$ MC yield for $N_{\text{jets}} = 1$ or 2.
- 328 • N_3 = data yield minus non-dilepton $t\bar{t}$ MC yield for $N_{\text{jets}} = 3$
- 329 • N_4 = data yield minus non-dilepton $t\bar{t}$ MC yield for $N_{\text{jets}} \geq 4$
- 330 • M_2 = dilepton $t\bar{t}$ MC yield for $N_{\text{jets}} = 1$ or 2
- 331 • M_3 = dilepton $t\bar{t}$ MC yield for $N_{\text{jets}} = 3$
- 332 • M_4 = dilepton $t\bar{t}$ MC yield for $N_{\text{jets}} \geq 4$

333 then

- 334 • $SF_2 = N_2/M_2$
- 335 • $SF_3 = N_3/M_3$
- 336 • $SF_4 = N_4/M_4$
- 337 • $K_3 = SF_3/SF_2$
- 338 • $K_4 = SF_4/SF_2$

339 This insures that $K_3 M_3 / (M_2 + K_3 M_3 + K_4 M_4) = N_3 / (N_2 + N_3 + N_4)$ and similarly for the ≥ 4 jet bin.

340 Table 15 also shows the values of K_3 and K_4 for different values of the E_T^{miss} cut in the control sample
 341 definition. This demonstrates that there is no statistically significant dependence of K_3 and K_4 on the
 342 E_T^{miss} cut.

343 The factors K_3 and K_4 (derived with the 100 GeV E_T^{miss} cut) are applied to the $t\bar{t} \rightarrow \ell\ell$ MC throughout
 344 the entire analysis, i.e. whenever $t\bar{t} \rightarrow \ell\ell$ MC is used to estimate or subtract a yield or distribution.

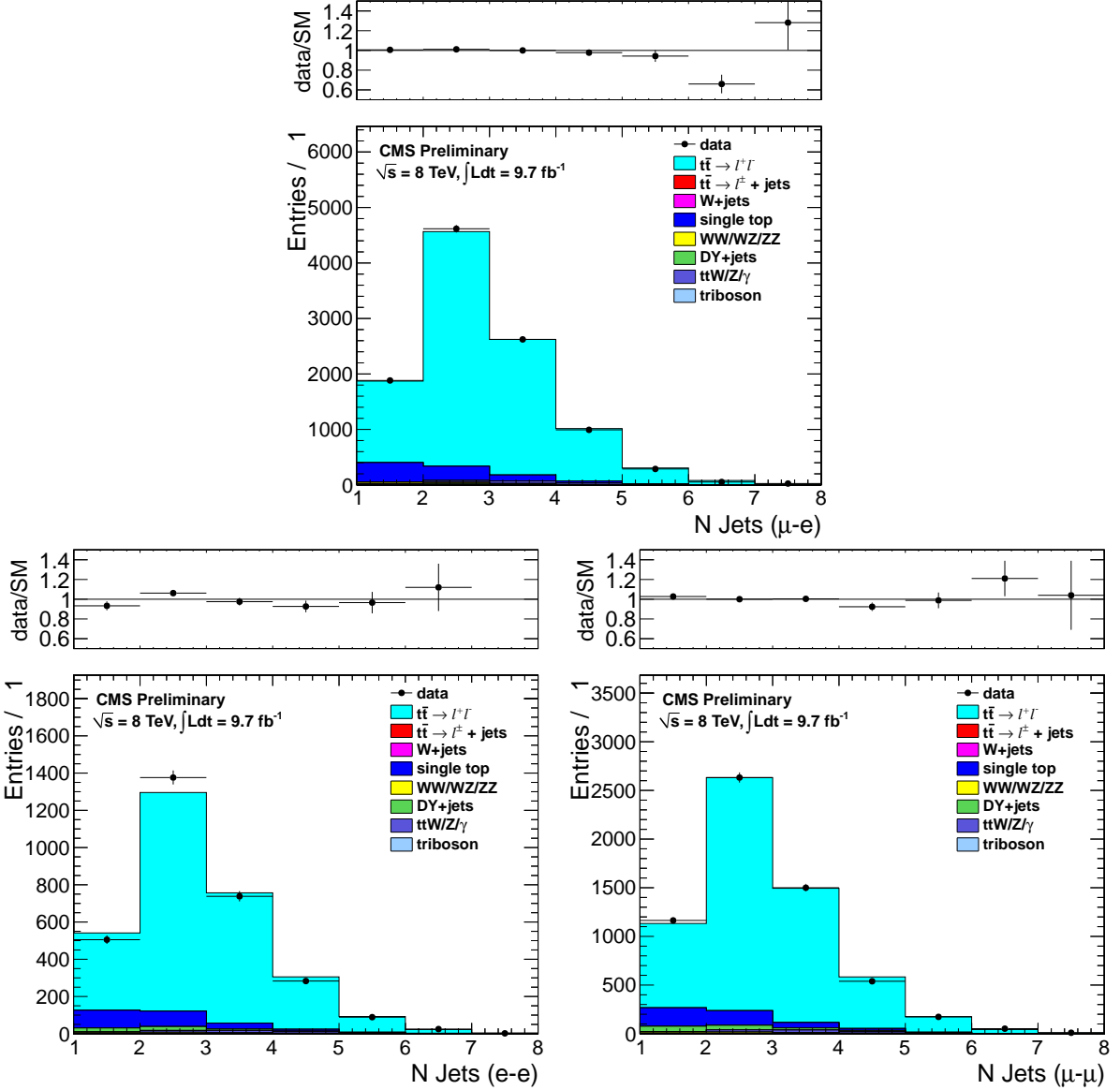


Figure 9: Comparison of the jet multiplicity distribution in data and MC for dilepton events in the $e-\mu$ (top), $e-e$ (bottom left) and $\mu-\mu$ (bottom right) channels.

345 To be explicit, whenever Powheg is used, the Powheg K_3 and K_4 are used; whenever default MadGraph
 346 is used, the MadGraph K_3 and K_4 are used, etc. In order to do so, it is first necessary to count the
 347 number of additional jets from radiation and exclude leptons misidentified as jets. A jet is considered a
 348 misidentified lepton if it is matched to a generator-level second lepton with sufficient energy to satisfy
 349 the jet p_T requirement ($p_T > 30$ GeV). Then $t\bar{t} \rightarrow ll$ events that need two radiation jets to enter our
 350 selection are scaled by K_4 , while those that only need one radiation jet are scaled by K_3 .

Sample	E_T^{miss} cut for data/MC scale factors					
	50 GeV	100 GeV	150 GeV	200 GeV	250 GeV	300 GeV
N jets = 3	$K_3 = 0.98 \pm 0.02$	$K_3 = 1.01 \pm 0.03$	$K_3 = 1.00 \pm 0.08$	$K_3 = 1.03 \pm 0.18$	$K_3 = 1.29 \pm 0.51$	$K_3 = 1.58 \pm 1.23$
N jets ≥ 4	$K_4 = 0.94 \pm 0.02$	$K_4 = 0.93 \pm 0.04$	$K_4 = 1.00 \pm 0.08$	$K_4 = 1.07 \pm 0.18$	$K_4 = 1.30 \pm 0.48$	$K_4 = 1.65 \pm 1.19$

Table 15: Data/MC scale factors used to account for differences in the fraction of events with additional hard jets from radiation in $t\bar{t} \rightarrow \ell\ell$ events. The N jets = 3 scale factor, K_3 , is sensitive to $t\bar{t} + 1$ extra jet from radiation, while the N jets ≥ 4 scale factor, K_4 , is sensitive to $t\bar{t} + \geq 2$ extra jets from radiation. The values derived with the 100 GeV E_T^{miss} cut are applied to the $t\bar{t} \rightarrow \ell\ell$ MC throughout the analysis.

351 **5.3.2 Validation of the “Physics” Modelling of the $t\bar{t} \rightarrow \ell\ell$ MC in CR4**

- 352 As mentioned above, $t\bar{t} \rightarrow$ dileptons where one of the leptons is somehow lost constitutes the main
 353 background. The object of this test is to validate the M_T distribution of this background by looking at
 354 the M_T distribution of well identified dilepton events. We construct a transverse mass variable from the
 355 leading lepton and the E_T^{miss} . We distinguish between events with leading electrons and leading muons.
 356 The $t\bar{t}$ MC is corrected using the K_3 and K_4 factors from Section 5.3.1. It is also normalized to the
 357 total data yield separately for the E_T^{miss} requirements of the various signal regions. These normalization
 358 factors are listed in Table 16 and are close to unity.
 359 The underlying E_T^{miss} and M_T distributions are shown in Figures 39 and 11. The data-MC agreement is
 360 quite good. Quantitatively, this is also shown in Table 17. This is a **very** important Table. It shows that
 361 for well identified $t\bar{t} \rightarrow \ell\ell$, the MC can predict the M_T tail. Since the main background is also $t\bar{t} \rightarrow \ell\ell$
 362 except with one “missed” lepton, this is a key test.

Sample	CR4PRESEL	CR4A	CR4B	CR4C	CR4D	CR4E	CR4F
μ Data/MC-SF	1.01 ± 0.03	0.96 ± 0.04	0.99 ± 0.07	1.05 ± 0.13	0.91 ± 0.20	1.10 ± 0.34	1.50 ± 0.67
e Data/MC-SF	0.99 ± 0.03	0.99 ± 0.05	0.91 ± 0.08	0.84 ± 0.13	0.70 ± 0.18	0.73 ± 0.29	0.63 ± 0.38

Table 16: Data/MC scale factors for total yields, applied to compare the shapes of the distributions. The uncertainties are statistical only.

Sample	CR4PRESEL	CR4A	CR4B	CR4C	CR4D	CR4E	CR4F
μ MC	256 ± 14	152 ± 11	91 ± 9	26 ± 5	6 ± 2	4 ± 2	2 ± 1
μ Data	251	156	98	27	8	6	4
μ Data/MC SF	0.98 ± 0.08	1.02 ± 0.11	1.08 ± 0.16	1.04 ± 0.28	1.29 ± 0.65	1.35 ± 0.80	2.10 ± 1.72
e MC	227 ± 13	139 ± 11	73 ± 8	21 ± 4	5 ± 2	2 ± 1	1 ± 1
e Data	219	136	72	19	2	1	1
e Data/MC SF	0.96 ± 0.09	0.98 ± 0.11	0.99 ± 0.16	0.92 ± 0.29	0.41 ± 0.33	0.53 ± 0.62	0.76 ± 0.96
$\mu+e$ MC	483 ± 19	291 ± 16	164 ± 13	47 ± 7	11 ± 3	6 ± 2	3 ± 2
$\mu+e$ Data	470	292	170	46	10	7	5
$\mu+e$ Data/MC SF	0.97 ± 0.06	1.00 ± 0.08	1.04 ± 0.11	0.99 ± 0.20	0.90 ± 0.37	1.11 ± 0.57	1.55 ± 1.04

Table 17: Yields in M_T tail comparing the MC prediction (after applying SFs) to data. The uncertainties are statistical only.

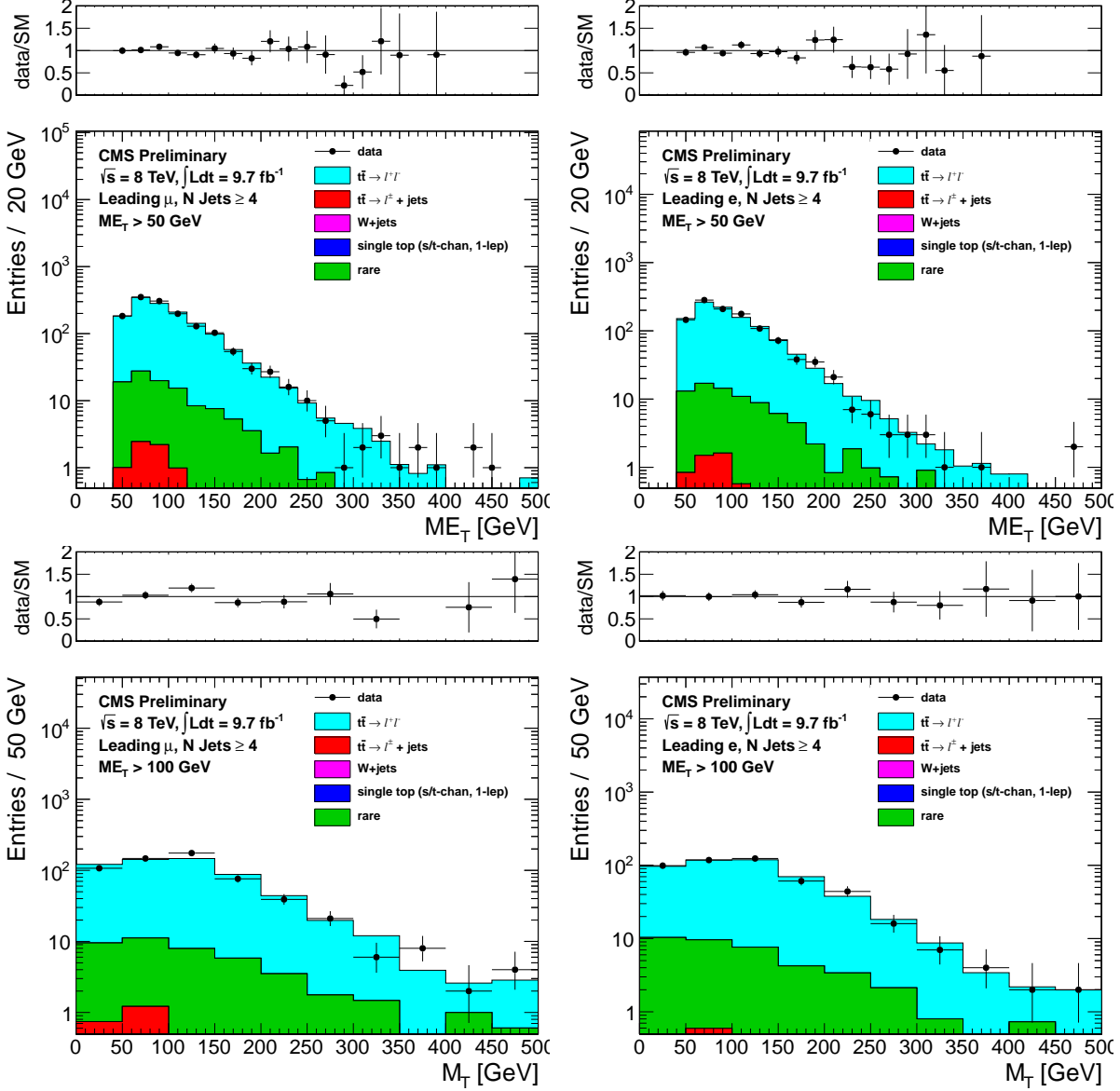


Figure 10: Comparison of the E_T^{miss} (top) and M_T for $E_T^{\text{miss}} > 100$ (bottom) distributions in data vs. MC for events with a leading muon (left) and leading electron (right) satisfying the requirements of CR4.

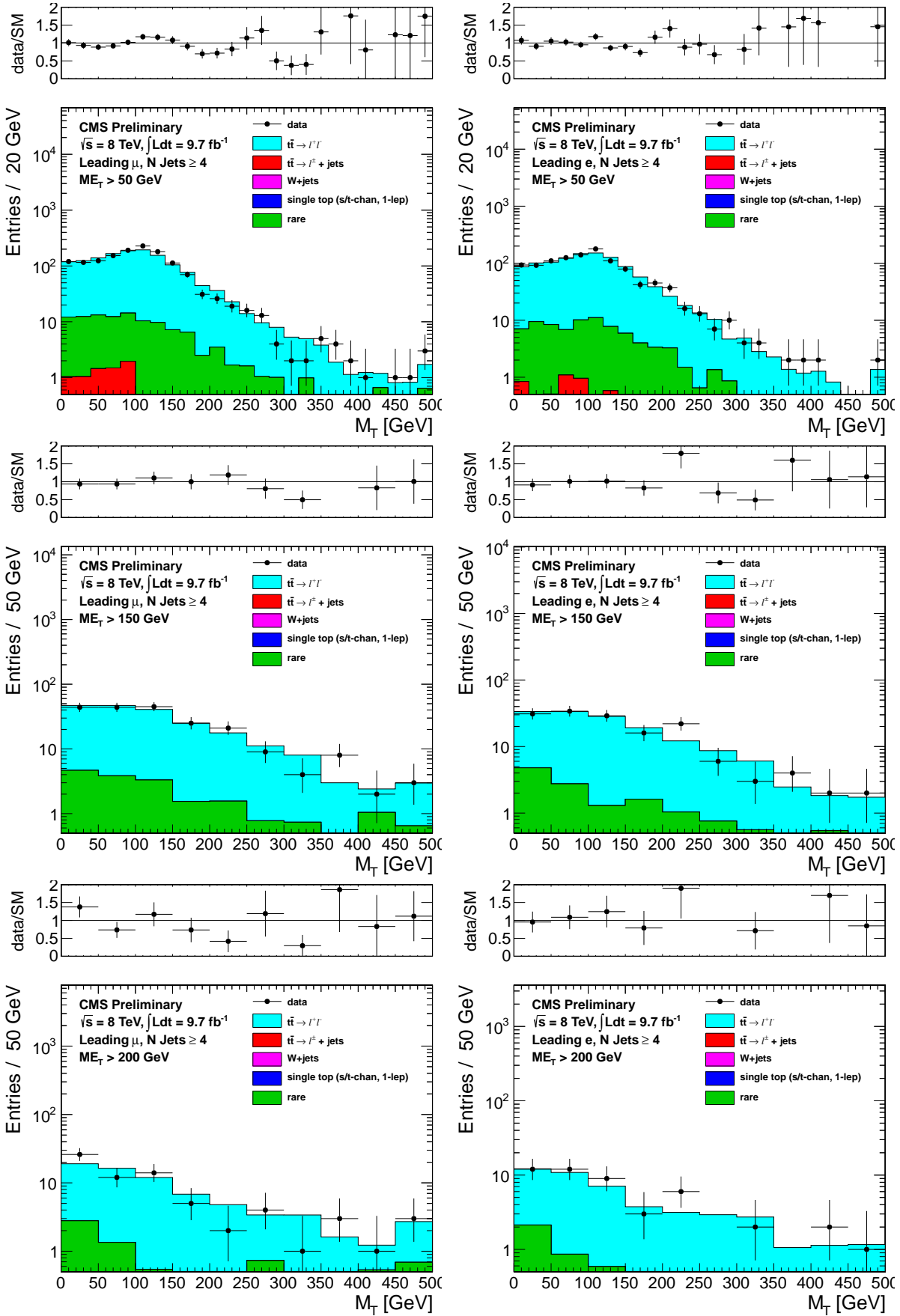


Figure 11: Comparison of the M_T distribution in data vs. MC for events with a leading muon (left) and leading electron (right) satisfying the requirements of CR4. The E_T^{miss} requirements used are 50 GeV (top), 200 GeV (middle) and 250 GeV (bottom).

363 5.4 Test of control region with isolated track in CR5

364 This CR consists of events that pass all cuts but fail the isolated track veto cut. These events (especially
 365 in the tail of M_T) are predominantly $t\bar{t}$ dileptons. Thus the test in this control region is similar to that
 366 performed in CR4 and described in Section 5.3.2. There is some non-trivial complementarity because
 367 CR5 also includes events with taus and events with electrons or muons below the threshold of the CR4
 368 selection. Also, this test is somewhat sensitive to the simulation of the track isolation requirement, since
 369 the number of dilepton events in CR5 depends on the (in)efficiency of that cut.

370 In CR5 there is also a significant component of $t\bar{t} \rightarrow \ell + \text{jets}$, where one of the jets fluctuates to an isolated
 371 track. This component dominates at low M_T and is not necessarily well reproduced quantitatively by
 372 the simulation. This makes the normalization of the top MC a little bit tricky. We define a “pre-veto”
 373 sample as the sample of events that pass all cuts without any isolated track requirements. This sample
 374 is dominated by $t\bar{t} \rightarrow \ell + \text{jets}$. We normalize the dilepton component of the top MC to that sample. This
 375 is done by normalizing the total $t\bar{t}$ MC to the M_T peak region, $50 < M_T < 80$ GeV in this sample.

376 Next we define a “post-veto” sample as the events that have an isolated track (note that we use the
 377 term “post-veto” to refer to the application of the isolated track cut of the sample, which in this case
 378 is an isolated track requirement). The $t\bar{t} \rightarrow \ell + \text{jets}$ component is normalized in this sample, again by
 379 normalizing to the M_T peak region. These normalization factors are summarized in Table 18.

380 The post-veto $t\bar{t} \rightarrow \ell\ell$ is taken from MC, but with scale factor obtained by the normalization of the
 381 “pre-veto” sample.

382 The underlying E_T^{miss} and M_T distributions are shown in Figures 40 and 13. The data-MC agreement
 383 is quite good. Quantitatively, this is also shown in Table 19. This is the second key test of the $t\bar{t} \rightarrow \ell\ell$
 384 modeling

Sample	CR5PRESEL	CR5A	CR5B	CR5C	CR5D	CR5E	CR5F	CR5G
μ pre-veto M_T -SF	1.05 ± 0.01	1.02 ± 0.02	0.95 ± 0.03	0.90 ± 0.05	0.98 ± 0.08	0.97 ± 0.13	0.85 ± 0.18	0.92 ± 0.31
μ post-veto M_T -SF	1.25 ± 0.04	1.17 ± 0.07	1.05 ± 0.12	0.85 ± 0.19	0.84 ± 0.30	1.07 ± 0.54	1.38 ± 1.14	0.68 ± 2.05
e pre-veto M_T -SF	1.01 ± 0.01	0.95 ± 0.02	0.95 ± 0.03	0.94 ± 0.06	0.85 ± 0.09	0.84 ± 0.13	1.05 ± 0.23	1.04 ± 0.33
e post-veto M_T -SF	1.21 ± 0.04	1.12 ± 0.07	1.25 ± 0.14	1.17 ± 0.27	2.01 ± 0.64	1.71 ± 0.99	2.79 ± 2.04	0.81 ± 1.58

Table 18: M_T peak Data/MC scale factors. The pre-veto SFs are applied to the $t\bar{t} \rightarrow \ell\ell$ sample, while
 the post-veto SFs are applied to the single lepton samples. The raw MC is used for backgrounds from
 rare processes. The uncertainties are statistical only.

Sample	CR5PRESEL	CR5A	CR5B	CR5C	CR5D	CR5E	CR5F	CR5G
μ MC	490 ± 9	299 ± 7	155 ± 6	49 ± 3	19 ± 2	7 ± 1	3 ± 1	2 ± 1
μ Data	514	311	167	57	12	4	2	1
μ Data/MC SF	1.05 ± 0.05	1.04 ± 0.06	1.08 ± 0.09	1.17 ± 0.17	0.64 ± 0.20	0.54 ± 0.29	0.66 ± 0.49	0.58 ± 0.62
e MC	405 ± 8	239 ± 7	130 ± 5	43 ± 3	16 ± 2	8 ± 1	6 ± 2	3 ± 1
e Data	427	248	120	38	14	4	3	2
e Data/MC SF	1.06 ± 0.06	1.04 ± 0.07	0.93 ± 0.09	0.89 ± 0.16	0.86 ± 0.25	0.52 ± 0.28	0.54 ± 0.35	0.76 ± 0.60
$\mu+e$ MC	894 ± 12	538 ± 10	284 ± 8	92 ± 4	35 ± 3	15 ± 2	9 ± 2	4 ± 1
$\mu+e$ Data	941	559	287	95	26	8	5	3
$\mu+e$ Data/MC SF	1.05 ± 0.04	1.04 ± 0.05	1.01 ± 0.07	1.04 ± 0.12	0.74 ± 0.16	0.53 ± 0.20	0.58 ± 0.29	0.69 ± 0.43

Table 19: Yields in M_T tail comparing the MC prediction (after applying SFs) to data. The uncertainties
 are statistical only.

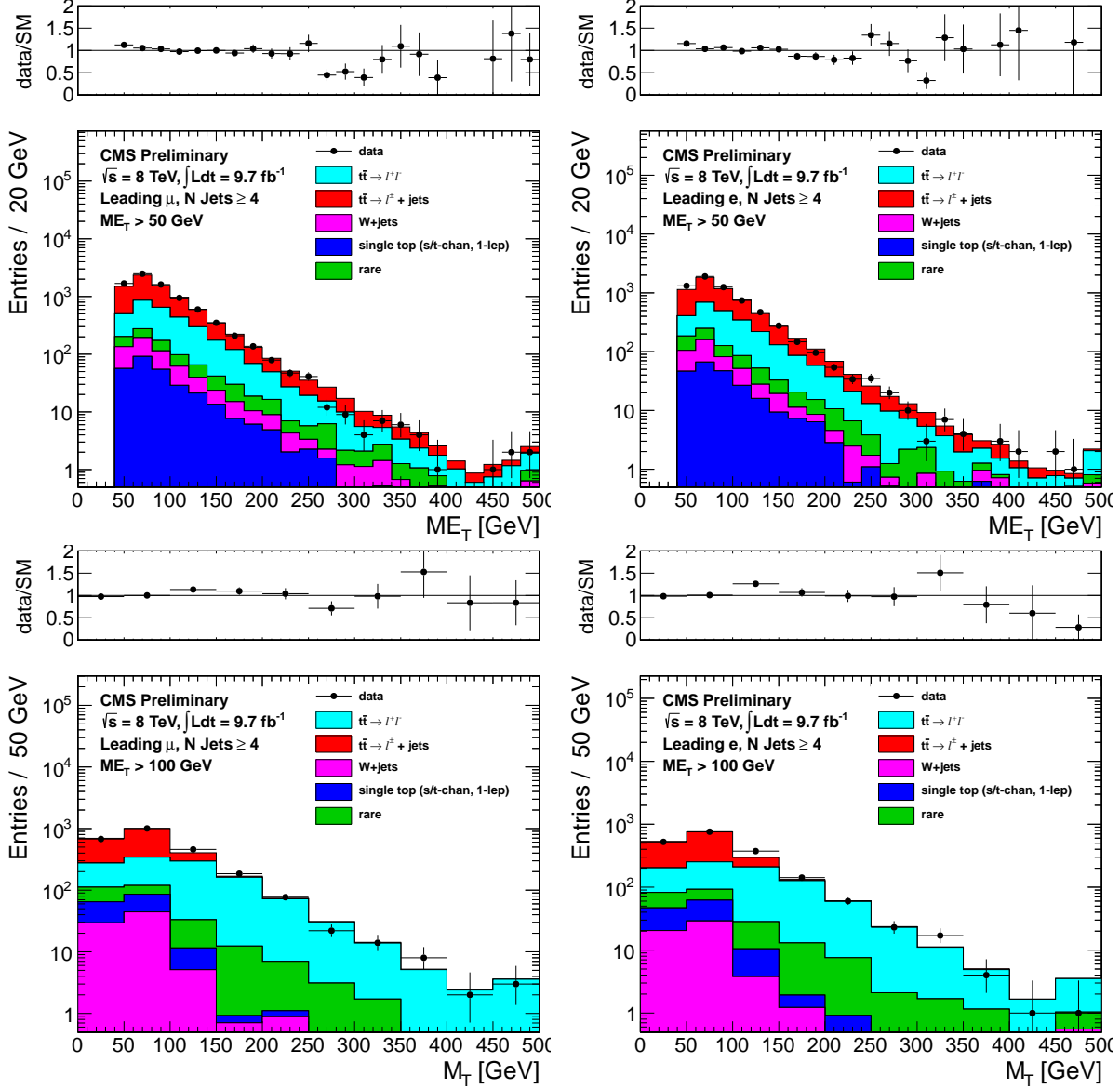


Figure 12: Comparison of the E_T^{miss} (top) and M_T for $E_T^{\text{miss}} > 100$ (bottom) distributions in data vs. MC for events with a leading muon (left) and leading electron (right) satisfying the requirements of CR5.

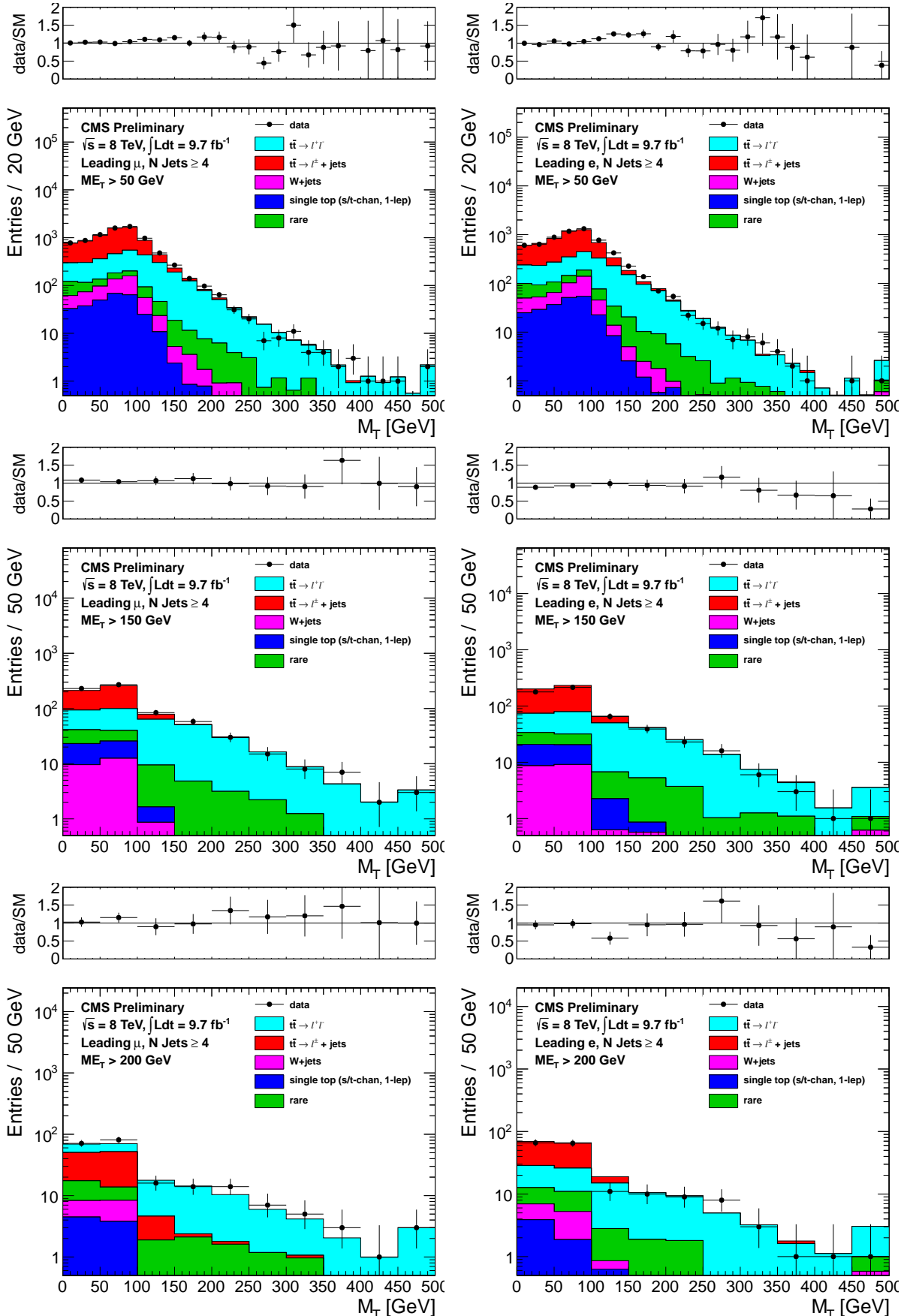


Figure 13: Comparison of the M_T distribution in data vs. MC for events with a leading muon (left) and leading electron (right) satisfying the requirements of CR5. The E_T^{miss} requirements used are 50 GeV (top), 150 GeV (middle) and 200 GeV (bottom).

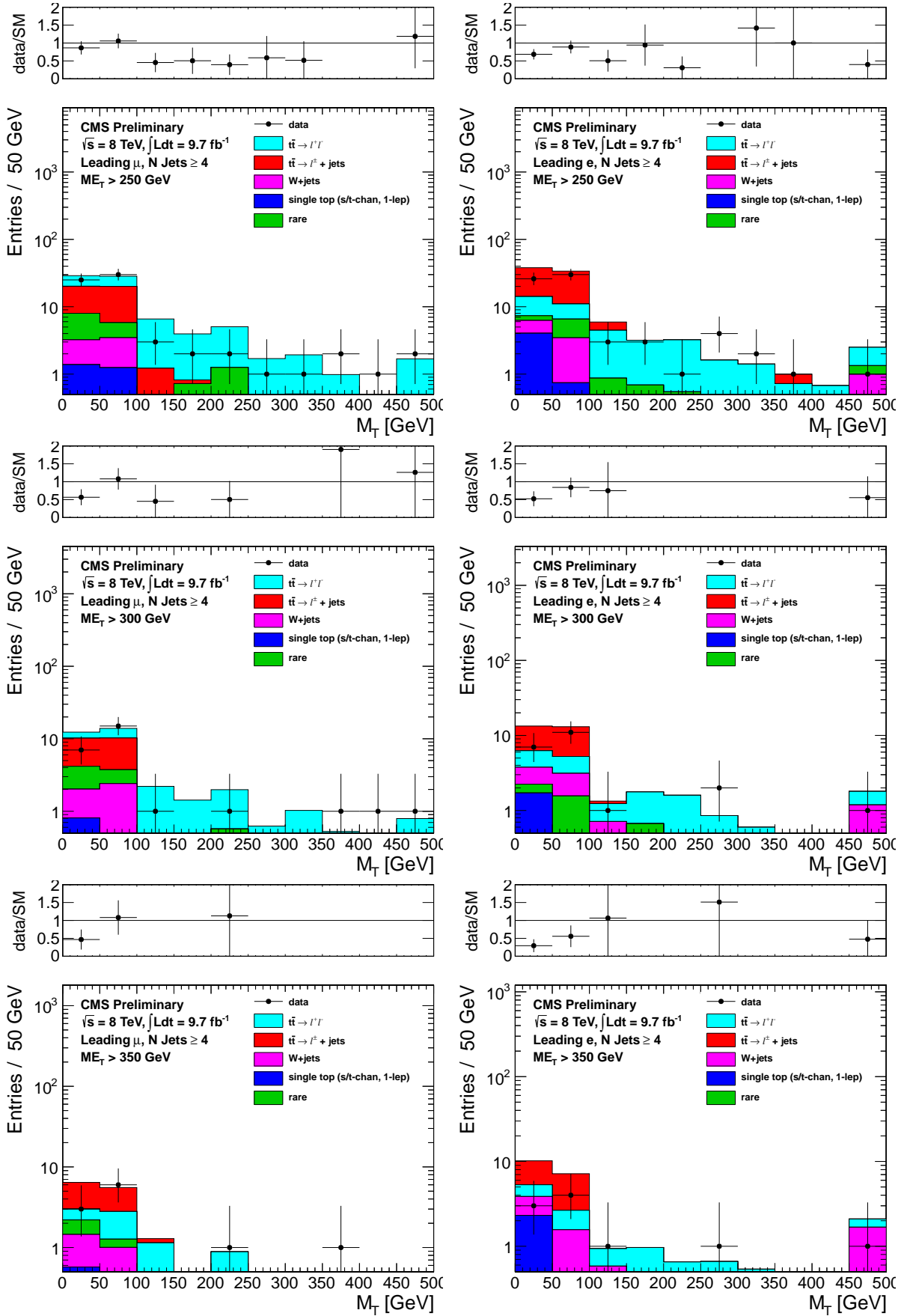


Figure 14: Comparison of the M_T distribution in data vs. MC for events with a leading muon (left) and leading electron (right) satisfying the requirements of CR5. The E_T^{miss} requirements used are 250 GeV (top), 300 GeV (middle) and 350 GeV (bottom).

385 6 Other Backgrounds

386 Additional background contributions from rare processes include

- 387 • $t\bar{t}$ in association with a boson, $t\bar{t} + WZ/\gamma^*$

388

- 389 • $Z/\gamma^* + \text{Jets}$

390

- 391 • diboson, $WW/WZ/ZZ$

392

- 393 • triboson, $WWW/WWZ/WZZ/ZZZ$

394

- 395 • dilepton single top, tW .

396

397 These backgrounds are small, contributing at the $\sim 5\%$ level and their predictions are taken from MC,
 398 normalized to the corresponding cross sections. A 50% systematic uncertainty is assigned for all these
 399 backgrounds. Note that these backgrounds are not double-counted because the contribution to the M_T
 400 peak region is subtracted off when deriving the M_T peak data/MC scale factors.

401 Backgrounds from QCD are expected to be small in the signal regions with large M_T and E_T^{miss} .

402 7 Tail-to-Peak ratio for lepton + jets top and W events

403 An important component of the background calculation is the ratio of the number of events with M_T in
 404 the signal region to the number of events with $50 < M_T < 80$ GeV. As discussed in Section 2.1, these
 405 ratios are different for $W+\text{jets}$ and top events.

Sample	SRA	SRB	SRC	SRD	SRE	SRF	SRG
Muons							
R_{top}^{MC}	0.015 ± 0.001	0.035 ± 0.002	0.021 ± 0.002	0.021 ± 0.004	0.025 ± 0.007	0.015 ± 0.009	0.021 ± 0.015
R_{wjet}^{MC}	0.040 ± 0.001	0.071 ± 0.003	0.062 ± 0.004	0.064 ± 0.006	0.065 ± 0.009	0.067 ± 0.012	0.065 ± 0.016
Electrons							
R_{top}^{MC}	0.015 ± 0.001	0.031 ± 0.002	0.026 ± 0.003	0.025 ± 0.005	0.009 ± 0.005	0.021 ± 0.012	0.034 ± 0.024
R_{wjet}^{MC}	0.040 ± 0.002	0.075 ± 0.004	0.067 ± 0.005	0.063 ± 0.007	0.061 ± 0.010	0.067 ± 0.015	0.070 ± 0.021

Table 20: Ratio of MC events in the M_T -tail over events in the M_T -peak for $t\bar{t} \rightarrow \ell + \text{jets}$ (also used for 1-lepton single top) and $W+\text{jets}$. These are derived before applying the b-tagging requirement.

406 The MC values of these ratios are shown in Table 20. The e and μ channel results are averaged before
 407 corrections are made.

408 The MC value of R_{wjet}^{MC} is corrected based on the studies of CR1 (Section D.3), which lead to the data/MC
 409 scale factor SFR_{wjet} (Table 13). The corrected R_{wjet} is thus given by $R_{wjet}^{MC} \times SFR_{wjet}$.

410 There is no similar scale factor to correct the MC value of R_{top}^{MC} due to the lack of events in CR2
 411 (Section 5.2). We must therefore use a different procedure to derive a corrected value of R_{top} .

412 We start by defining optimistic (too small) and pessimistic (too large) predictions for R_{top} .

413 For the pessimistic prediction, we use the $W+\text{jets}$ MC tail-to-peak ratio and data/MC scale factor, R_{wjet}^{MC}
 414 and SFR_{wjet} (i.e. the pessimistic prediction is the same as R_{wjet}). This prediction is too large because
 415 in $W+\text{jets}$ events the M_T tail comes from off-shell Ws and resolution effects, while in top events to first
 416 order only resolution effects matter.

417 For the optimistic prediction, we use the $t\bar{t} \rightarrow \ell + \text{jets}$ MC tail-to-peak ratio R_{top}^{MC} , but take the $W+\text{jets}$
 418 data/MC scale factor SFR_{wjet} . This prediction is too small because the true top scale factor is to first

- order the same as for on-shell Ws, while SFR_{wjet} is a weighted average of the scale factor for on-shell Ws (which is > 1) and the scale factor for off-shell Ws (which is close to 1 as it is well modeled by MC).
The final prediction for R_{top} is given by the average of the optimistic and pessimistic predictions, and the systematic uncertainty is given by half the difference between the two.
The corrected values of R_{wjet} and R_{top} and their uncertainties are given in Table 21.

Sample	SRA	SRB	SRC	SRD	SRE	SRF	SRG
R_{top}	0.045 ± 0.023	0.074 ± 0.031	0.055 ± 0.031	0.042 ± 0.028	0.041 ± 0.036	0.052 ± 0.049	0.053 ± 0.066
R_{wjet}	0.066 ± 0.015	0.101 ± 0.022	0.081 ± 0.025	0.061 ± 0.029	0.064 ± 0.042	0.082 ± 0.062	0.075 ± 0.088

Table 21: Corrected values of R_{wjet} and R_{top} . Both statistical and systematic uncertainties are included.

424 8 Background Prediction

425 Here we give the details of how we arrive at the background prediction in a given signal region. We con-
 426 centrate on the method used to arrive at the central value of the background prediction. The systematic
 427 uncertainties will be discussed in Section 9. The actual results for the BG prediction will be given in
 428 Section 10.

429 As mentioned in Section 2, we normalize the main $t\bar{t}$ background to the M_T peak. This is actually a
 430 bit tricky because we want to minimize the effect of the isolated track veto on lepton + jets events,
 431 which may not be terribly well reproduced. Thus, we define two normalization region in the M_T peak
 432 ($50 < M_T < 80$ GeV), one before and one after the application of the isolated track veto.

433 The event counts in pre-veto and post-veto normalization regions are given in Tables 22 and 23. The
 434 data-MC agreement in these two tables is quite good, and this is certainly a good thing.

Sample	SRA	SRB	SRC	SRD	SRE	SRF	SRG
Muon							
$t\bar{t} \rightarrow \ell\ell$	371 ± 6	120 ± 4	43 ± 2	17 ± 1	8 ± 1	4 ± 1	1 ± 0
$t\bar{t} \rightarrow \ell + \text{jets} \& \text{single top } (1\ell)$	3666 ± 21	1088 ± 12	355 ± 7	127 ± 4	50 ± 3	22 ± 2	8 ± 1
$W+\text{jets}$	316 ± 8	113 ± 5	46 ± 3	21 ± 2	11 ± 1	5 ± 1	2 ± 1
Rare	117 ± 5	48 ± 3	16 ± 2	6 ± 1	2 ± 1	1 ± 0	1 ± 0
Total	4470 ± 24	1369 ± 13	461 ± 8	171 ± 5	71 ± 3	33 ± 2	13 ± 1
Data	4538	1304	418	168	69	28	12
Electron							
$t\bar{t} \rightarrow \ell\ell$	290 ± 6	98 ± 3	35 ± 2	13 ± 1	6 ± 1	3 ± 1	1 ± 0
$t\bar{t} \rightarrow \ell + \text{jets} \& \text{single top } (1\ell)$	2899 ± 19	861 ± 10	282 ± 6	104 ± 4	42 ± 2	16 ± 2	8 ± 1
$W+\text{jets}$	252 ± 28	87 ± 4	35 ± 3	18 ± 2	8 ± 1	4 ± 1	2 ± 1
Rare	89 ± 5	34 ± 3	15 ± 2	7 ± 1	3 ± 1	0 ± 0	0 ± 0
Total	3530 ± 35	1079 ± 12	367 ± 7	142 ± 5	60 ± 3	24 ± 2	11 ± 1
Data	3358	1022	346	122	51	25	12
Muon+Electron Combined							
$t\bar{t} \rightarrow \ell\ell$	661 ± 9	218 ± 5	78 ± 3	30 ± 2	14 ± 1	7 ± 1	3 ± 1
$t\bar{t} \rightarrow \ell + \text{jets} \& \text{single top } (1\ell)$	6565 ± 28	1949 ± 16	637 ± 9	231 ± 5	92 ± 4	39 ± 2	16 ± 2
$W+\text{jets}$	568 ± 29	199 ± 6	81 ± 4	38 ± 3	19 ± 2	9 ± 1	4 ± 1
Rare	206 ± 7	82 ± 4	31 ± 3	14 ± 2	5 ± 1	2 ± 0	1 ± 0
Total	8000 ± 42	2448 ± 18	828 ± 11	314 ± 7	131 ± 4	56 ± 3	24 ± 2
Data	7896	2326	764	290	120	53	24

Table 22: Preveto MC and data yields in M_T peak region. The n-jets k-factors have been applied to the $t\bar{t} \rightarrow \ell\ell$. The uncertainties are statistical only. These MC and data yields are used to derive data/MC SFs, the pre-veto M_T -SFs, shown in Table 24.

Sample	SRA	SRB	SRC	SRD	SRE	SRF	SRG
Muon							
$t\bar{t} \rightarrow \ell\ell$	139 ± 4	46 ± 2	16 ± 1	7 ± 1	3 ± 1	1 ± 0	1 ± 0
$t\bar{t} \rightarrow \ell + \text{jets} \& \text{single top } (1\ell)$	3273 ± 20	974 ± 11	321 ± 6	113 ± 4	45 ± 2	21 ± 2	8 ± 1
$W + \text{jets}$	294 ± 8	105 ± 5	42 ± 3	19 ± 2	10 ± 1	5 ± 1	2 ± 1
Rare	83 ± 4	34 ± 3	11 ± 1	4 ± 1	2 ± 1	1 ± 0	1 ± 0
Total	3789 ± 22	1160 ± 12	391 ± 7	143 ± 4	60 ± 3	28 ± 2	11 ± 1
Data	3790	1098	358	143	59	24	11
Electron							
$t\bar{t} \rightarrow \ell\ell$	116 ± 4	40 ± 2	14 ± 1	5 ± 1	2 ± 0	1 ± 0	1 ± 0
$t\bar{t} \rightarrow \ell + \text{jets} \& \text{single top } (1\ell)$	2595 ± 18	774 ± 10	258 ± 6	97 ± 4	40 ± 2	15 ± 1	7 ± 1
$W + \text{jets}$	236 ± 28	82 ± 4	33 ± 3	17 ± 2	8 ± 1	4 ± 1	2 ± 1
Rare	62 ± 4	23 ± 2	9 ± 1	4 ± 1	2 ± 1	0 ± 0	0 ± 0
Total	3009 ± 34	919 ± 11	315 ± 7	123 ± 4	51 ± 3	21 ± 2	10 ± 1
Data	2788	837	288	92	39	19	10
Muon+Electron Combined							
$t\bar{t} \rightarrow \ell\ell$	255 ± 5	86 ± 3	30 ± 2	12 ± 1	5 ± 1	2 ± 1	1 ± 0
$t\bar{t} \rightarrow \ell + \text{jets} \& \text{single top } (1\ell)$	5869 ± 27	1747 ± 15	579 ± 9	209 ± 5	85 ± 3	36 ± 2	15 ± 2
$W + \text{jets}$	529 ± 29	188 ± 6	75 ± 4	36 ± 3	18 ± 2	9 ± 1	4 ± 1
Rare	145 ± 6	58 ± 4	21 ± 2	8 ± 1	3 ± 1	1 ± 0	1 ± 0
Total	6797 ± 40	2079 ± 17	705 ± 10	265 ± 6	111 ± 4	49 ± 3	21 ± 2
Data	6578	1935	646	235	98	43	21

Table 23: MC and data yields in M_T peak region after full selection. The n-jets k-factors have been applied to the $t\bar{t} \rightarrow \ell\ell$. The uncertainties are statistical only. These MC and data yields are used to derive data/MC SFs, the post-veto M_T -SFs, shown in Table 24.

435 The dominant dilepton background is normalized to the pre-veto normalization region. A pre-veto scale
 436 factor (SF_{pre}) is defined as a common scale factors that needs to be applied to the $t\bar{t}$, single-top, and $W+$
 437 jets MC to make the data yield in the pre-veto normalization agree with the MC prediction (the small
 438 rare MC component is held fixed). Then, the dilepton background prediction is obtained by multiplying
 439 the dilepton BG Monte Carlo by SF_{pre} .

440 The $t\bar{t}$ lepton + jet BG is normalized to post-veto normalization region. A post-veto scale factor (SF_{post})
 441 is defined in (almost) the same way as the pre-veto scale factor. The difference here is that this scale factor
 442 applies only to the lepton + jets components and not the dilepton component, since that component is
 443 already rescaled by SF_{pre} . This procedure minimizes the reliance on the understanding of the isolated
 444 track veto.

445 The pre-veto and post-veto SF are shown in Table 24.

Sample	SRA	SRB	SRC	SRD	SRE	SRF	SRG
μ pre-veto M_T -SF	1.02 ± 0.02	0.95 ± 0.03	0.90 ± 0.05	0.98 ± 0.08	0.97 ± 0.13	0.85 ± 0.18	0.92 ± 0.31
μ post-veto M_T -SF	1.00 ± 0.02	0.95 ± 0.03	0.91 ± 0.05	1.00 ± 0.09	0.99 ± 0.13	0.85 ± 0.18	0.96 ± 0.31
μ veto M_T -SF	0.98 ± 0.01	0.99 ± 0.01	1.01 ± 0.02	1.02 ± 0.04	1.02 ± 0.06	1.00 ± 0.09	1.04 ± 0.11
e pre-veto M_T -SF	0.95 ± 0.02	0.95 ± 0.03	0.94 ± 0.06	0.85 ± 0.09	0.84 ± 0.13	1.05 ± 0.23	1.04 ± 0.33
e post-veto M_T -SF	0.92 ± 0.02	0.91 ± 0.03	0.91 ± 0.06	0.74 ± 0.08	0.75 ± 0.13	0.91 ± 0.22	1.01 ± 0.33
e veto M_T -SF	0.97 ± 0.01	0.96 ± 0.02	0.97 ± 0.03	0.87 ± 0.05	0.89 ± 0.08	0.86 ± 0.11	0.97 ± 0.14

Table 24: M_T peak Data/MC scale factors. The pre-veto SFs are applied to the $t\bar{t} \rightarrow \ell\ell$ sample, while the post-veto SFs are applied to the single lepton samples. The veto SF is shown for comparison across channels. The raw MC is used for backgrounds from rare processes. The uncertainties are statistical only.

446 Then the $t\bar{t}$ lepton + jet BG is obtained by taking the number of MC-predicted $t\bar{t}$ lepton + jets in the
 447 post-veto normalization region, scaling it by SF_{post} , and multiplying it by the corrected tail-to-peak ratio
 448 R_{top} of Table 21.

449 The single top background is obtained in exactly the same way as the $t\bar{t}$ lepton + jet BG, using the same
 450 tail-to-peak ratio. The $W+$ jets background is done in a similar way, but using a different tail-to-peak
 451 ratio (R_{wjets} of Table 21).

452 Other (small) backgrounds are taken straight from Monte Carlo, as described in Section 6.

Sample	SRA	SRB	SRC	SRD	SRE	SRF	SRG
Muon							
$t\bar{t} \rightarrow \ell\ell$	326 ± 6	193 ± 5	66 ± 3	23 ± 2	9 ± 1	4 ± 1	2 ± 1
$t\bar{t} \rightarrow \ell + \text{jets} \& \text{single top } (1\ell)$	54 ± 3	38 ± 2	8 ± 1	3 ± 1	1 ± 1	1 ± 0	0 ± 0
$W+\text{jets}$	17 ± 2	8 ± 1	3 ± 1	2 ± 1	0 ± 0	0 ± 0	0 ± 0
Rare	33 ± 2	23 ± 2	9 ± 1	5 ± 1	3 ± 1	1 ± 0	1 ± 0
Total	430 ± 7	262 ± 6	86 ± 3	33 ± 2	14 ± 1	6 ± 1	4 ± 1
Electron							
$t\bar{t} \rightarrow \ell\ell$	261 ± 5	153 ± 4	54 ± 2	19 ± 1	7 ± 1	2 ± 1	1 ± 0
$t\bar{t} \rightarrow \ell + \text{jets} \& \text{single top } (1\ell)$	41 ± 2	28 ± 2	7 ± 1	3 ± 1	1 ± 0	1 ± 0	1 ± 0
$W+\text{jets}$	11 ± 2	7 ± 1	3 ± 1	2 ± 1	0 ± 0	0 ± 0	0 ± 0
Rare	26 ± 2	16 ± 2	7 ± 1	3 ± 1	1 ± 0	0 ± 0	0 ± 0
Total	340 ± 6	204 ± 5	71 ± 3	26 ± 2	8 ± 1	4 ± 1	2 ± 1
Muon+Electron Combined							
$t\bar{t} \rightarrow \ell\ell$	587 ± 8	346 ± 6	120 ± 4	42 ± 2	16 ± 1	7 ± 1	4 ± 1
$t\bar{t} \rightarrow \ell + \text{jets} \& \text{single top } (1\ell)$	95 ± 3	67 ± 3	15 ± 1	6 ± 1	2 ± 1	1 ± 1	1 ± 0
$W+\text{jets}$	29 ± 2	15 ± 2	6 ± 1	3 ± 1	1 ± 0	0 ± 0	0 ± 0
Rare	59 ± 3	38 ± 3	16 ± 2	8 ± 1	4 ± 1	2 ± 0	1 ± 0
Total	770 ± 10	466 ± 7	157 ± 4	59 ± 3	22 ± 2	10 ± 1	6 ± 1

Table 25: MC yields in M_T tail region after full selection. The n-jets k-factors have been applied to the $t\bar{t} \rightarrow \ell\ell$. The uncertainties are statistical only. Note these values are only used for the rare backgrounds prediction.

453 9 Systematic Uncertainties on the Background

454 In this Section we discuss the systematic uncertainty on the BG prediction. This prediction is assembled
455 from the event counts in the peak region of the transverse mass distribution as well as Monte Carlo with
456 a number of correction factors, as described previously. The final uncertainty on the prediction is built
457 up from the uncertainties in these individual components. The calculation is done for each signal region,
458 for electrons and muons separately.

459 The choice to normalize to the peak region of M_T has the advantage that some uncertainties, e.g., luminosity,
460 cancel. It does however introduce complications because it couples some of the uncertainties in
461 non-trivial ways. For example, the primary effect of an uncertainty on the rare MC cross-section is to
462 introduce an uncertainty in the rare MC background estimate which comes entirely from MC. But this
463 uncertainty also affects, for example, the $t\bar{t} \rightarrow$ dilepton BG estimate because it changes the $t\bar{t}$ normaliza-
464 tion to the peak region (because some of the events in the peak region are from rare processes). These
465 effects are carefully accounted for. The contribution to the overall uncertainty from each background
466 source is tabulated in Section 9.9. Here we discuss the uncertainties one-by-one and comment on their
467 impact on the overall result, at least to first order. Second order effects, such as the one described, are
468 also included.

469 9.1 Statistical uncertainties on the event counts in the M_T peak regions

470 These vary between 2% and 20%, depending on the signal region (different signal regions have different
471 E_T^{miss} requirements, thus they also have different M_T regions used as control). Since the major back-
472 grounds, eg, $t\bar{t}$ are normalized to the peak regions, this fractional uncertainty is pretty much carried
473 through all the way to the end. There is also an uncertainty from the finite MC event counts in the M_T
474 peak regions. This is also included, but it is smaller.

475 Normalizing to the M_T peak has the distinct advantages that uncertainties on luminosity, cross-sections,
476 trigger efficiency, lepton ID, cancel out. For the low statistics regions with high E_T^{miss} requirements, the
477 price to pay in terms of event count is that statistical uncertainties start to become significant. In the
478 future we may consider a different normalization strategy in the low statistics regions.

479 9.2 Uncertainty from the choice of M_T peak region

480 This choice affects the scale factors of Table 24. If the M_T peak region is not well modelled, this would
481 introduce an uncertainty.
482 We have tested this possibility by recalculating the post-veto scale factors for a different choice of M_T
483 peak region ($40 < M_T < 100$ GeV instead of the default $50 < M_T < 80$ GeV). This is shown in Table 26.
484 The two results for the scale factors are very compatible. We do not take any systematic uncertainty for
485 this possible effect.

486 9.3 Uncertainty on the W +jets cross-section and the rare MC cross-sections

487 These are taken as 50%, uncorrelated. The primary effect is to introduce a 50% uncertainty on the W +
488 jets and rare BG background predictions, respectively. However they also have an effect on the other BGs
489 via the M_T peak normalization in a way that tends to reduce the uncertainty. This is easy to understand:
490 if the W cross-section is increased by 50%, then the W background goes up. But the number of M_T peak
491 events attributed to $t\bar{t}$ goes down, and since the $t\bar{t}$ BG is scaled to the number of $t\bar{t}$ events in the peak,
492 the $t\bar{t}$ BG goes down.

493 9.4 Tail-to-peak ratios for lepton + jets top and W events

494 The tail-to-peak ratios R_{top} and R_{wjet} are described in Section 7. The data/MC scale factors are studied
495 in CR1 and CR2 (Sections D.3 and 5.2). Only the scale factor for W +jets, SFR_{wjet} , is used, and its
496 uncertainty is given in Table 13. This uncertainty affects both R_{wjet} and R_{top} . The additional systematic
497 uncertainty on R_{top} from the variation between optimistic and pessimistic scenarios is given in Section 7.

Sample	SRA	SRB	SRC	SRD	SRE	SRF	SRG
$50 \leq M_T \leq 80$							
μ pre-veto M_T -SF	1.02 ± 0.02	0.95 ± 0.03	0.90 ± 0.05	0.98 ± 0.08	0.97 ± 0.13	0.85 ± 0.18	0.92 ± 0.31
μ post-veto M_T -SF	1.00 ± 0.02	0.95 ± 0.03	0.91 ± 0.05	1.00 ± 0.09	0.99 ± 0.13	0.85 ± 0.18	0.96 ± 0.31
μ veto M_T -SF	0.98 ± 0.01	0.99 ± 0.01	1.01 ± 0.02	1.02 ± 0.04	1.02 ± 0.06	1.00 ± 0.09	1.04 ± 0.11
e pre-veto M_T -SF	0.95 ± 0.02	0.95 ± 0.03	0.94 ± 0.06	0.85 ± 0.09	0.84 ± 0.13	1.05 ± 0.23	1.04 ± 0.33
e post-veto M_T -SF	0.92 ± 0.02	0.91 ± 0.03	0.91 ± 0.06	0.74 ± 0.08	0.75 ± 0.13	0.91 ± 0.22	1.01 ± 0.33
e veto M_T -SF	0.97 ± 0.01	0.96 ± 0.02	0.97 ± 0.03	0.87 ± 0.05	0.89 ± 0.08	0.86 ± 0.11	0.97 ± 0.14
$40 \leq M_T \leq 100$							
μ pre-veto M_T -SF	1.02 ± 0.01	0.97 ± 0.02	0.91 ± 0.05	0.95 ± 0.06	0.97 ± 0.10	0.80 ± 0.14	0.74 ± 0.22
μ post-veto M_T -SF	1.00 ± 0.01	0.96 ± 0.02	0.90 ± 0.04	0.98 ± 0.07	1.00 ± 0.11	0.80 ± 0.15	0.81 ± 0.24
μ veto M_T -SF	0.98 ± 0.01	0.99 ± 0.01	0.99 ± 0.02	1.03 ± 0.03	1.03 ± 0.05	1.01 ± 0.08	1.09 ± 0.09
e pre-veto M_T -SF	0.97 ± 0.01	0.93 ± 0.02	0.94 ± 0.04	0.81 ± 0.06	0.86 ± 0.10	0.95 ± 0.17	1.06 ± 0.26
e post-veto M_T -SF	0.94 ± 0.01	0.91 ± 0.02	0.91 ± 0.04	0.71 ± 0.06	0.82 ± 0.10	0.93 ± 0.17	1.09 ± 0.27
e veto M_T -SF	0.97 ± 0.01	0.98 ± 0.01	0.97 ± 0.02	0.88 ± 0.04	0.95 ± 0.06	0.98 ± 0.08	1.03 ± 0.09

Table 26: M_T peak Data/MC scale factors. The pre-veto SFs are applied to the $t\bar{t} \rightarrow \ell\ell$ sample, while the post-veto SFs are applied to the single lepton samples. The veto SF is shown for comparison across channels. The raw MC is used for backgrounds from rare processes. The uncertainties are statistical only.

498 9.5 Uncertainty on extra jet radiation for dilepton background

499 As discussed in Section 5.3.1, the jet distribution in $t\bar{t} \rightarrow$ dilepton MC is rescaled by the factors K_3 and
500 K_4 to make it agree with the data. The 3% uncertainties on K_3 and K_4 comes from data/MC statistics.
501 This results directly in a 3% uncertainty on the dilepton background, which is by far the most important
502 one.

503 9.6 Uncertainty from MC statistics

504 This affects mostly the $t\bar{t} \rightarrow \ell\ell$ background estimate, which is taken from Monte Carlo with appropriate
505 correction factors. This uncertainty is negligible in the low E_T^{miss} signal regions, and grows to about 15%
506 in SRG.

507 9.7 Uncertainty on the $t\bar{t} \rightarrow \ell\ell$ Background

508 The $t\bar{t}$ background prediction is obtained from MC, with corrections derived from control samples in data.
509 The uncertainty associated with the $t\bar{t}$ background is derived from the level of closure of the background
510 prediction in CR4 (Table 17) and CR5 (Table 19). The results from these control region checks are shown
511 in Figure 15. The uncertainties assigned to the $t\bar{t} \rightarrow \ell\ell$ background prediction based on these tests are
512 5% (SRA), 10% (SRB), 15% (SRC), 25% (SRD), 40% (SRE-G).

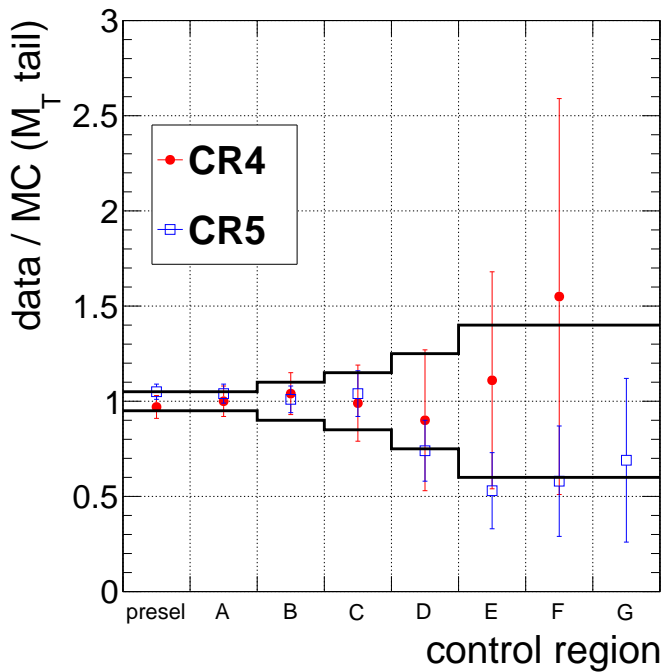


Figure 15: Results of the comparison of yields in the M_T tail comparing the MC prediction (after applying SFs) to data for CR4 and CR5 for all the signal region requirements considered (A-G). The bands indicate the systematic uncertainties assigned based on these tests, ranging from 5% for SRA to 40% for SRE-G.

513 **9.7.1 Check of the impact of Signal Contamination**

514 We examine the contribution of possible signal events in the $t\bar{t} \rightarrow \ell\ell$ control regions (CR4 and CR5).
 515 It should be emphasized that these regions are not used to apply data/MC SFs. They are used only
 516 to quantify the level of data/MC agreement and assign a corresponding uncertainty. As a result, if
 517 signal events were to populate these control regions this would not lead to an increase in the predicted
 518 background.

519 To illustrate how much signal is expected to populate these control regions, we examine signal points
 520 near the edge of the analysis sensitivity ($m(\text{stop}) = 450$ m(χ^0) = 0 for T2tt, $m(\text{stop}) = 450$ m(χ^0) =
 521 0, $x=0.75$ for T2bw) Table 27 compares the expected signal yields and the raw total MC background
 522 prediction in the control regions with the E_T^{miss} and M_T requirements corresponding to SRB, SRC and
 523 SRD (these are the signal regions that dominate the sensitivity). The signal contamination is smaller than
 524 the uncertainty on the dilepton background (10%, 15%, and 25% for SRB, SRC, SRD, respectively) and
 525 smaller than the signal/background in the signal regions. Based on the fact that the CR4 and CR5 are
 526 not used to extract data/MC scale factors and that we do not observe evidence for signal contamination
 527 in these control regions (CR5, the control region with larger statistical precision, actually shows a slight
 528 deficit of data w.r.t. MC), we do not assign a correction for signal contamination in these control regions.

Sample		CR B	CR C	CR D
CR4	Raw MC	168.2 ± 4.5	51.5 ± 2.5	19.6 ± 1.5
	T2tt $m(\text{stop}) = 450$ m(χ^0) = 0	2.6 ± 0.3 (2%)	2.0 ± 0.2 (4%)	1.4 ± 0.2 (7%)
	T2bw $x=0.75$ $m(\text{stop}) = 450$ m(χ^0) = 0	10.5 ± 0.4 (6%)	6.1 ± 0.3 (12%)	3.1 ± 0.2 (16%)
CR5	Raw MC	306.5 ± 6.2	101.8 ± 3.6	38.0 ± 2.2
	T2tt $m(\text{stop}) = 450$ m(χ^0) = 0	10.6 ± 0.6 (3%)	7.8 ± 0.5 (8%)	5.4 ± 0.4 (14%)
	T2bw $x=0.75$ $m(\text{stop}) = 450$ m(χ^0) = 0	17.3 ± 0.5 (6%)	11.3 ± 0.4 (11%)	6.2 ± 0.3 (16%)
SIGNAL	Raw MC	486.3 ± 7.8	164.3 ± 4.5	61.5 ± 2.8
	T2tt $m(\text{stop}) = 450$ m(χ^0) = 0	65.3 ± 1.4 (13%)	48.8 ± 1.2 (30%)	32.9 ± 1.0 (53%)
	T2bw $x=0.75$ $m(\text{stop}) = 450$ m(χ^0) = 0	69.3 ± 1.0 (14%)	47.3 ± 0.8 (29%)	27.3 ± 0.6 (44%)

Table 27: Yields in M_T tail comparing the raw SM MC prediction to the yields for a few signal points on the edge of our sensitivity in the $t\bar{t} \rightarrow \ell\ell$ control regions CR4, CR5 and in the corresponding signal region. The numbers in parenthesis are the expected signal yield divided by the total background. The uncertainties are statistical only.

529 **9.7.2 Check of the uncertainty on the $t\bar{t} \rightarrow \ell\ell$ Background**

530 We check that the systematic uncertainty assigned to the $t\bar{t} \rightarrow \ell\ell$ background prediction covers the
 531 uncertainty associated with the theoretical modeling of the $t\bar{t}$ production and decay by comparing the
 532 background predictions obtained using alternative MC samples. It should be noted that the full analysis
 533 is performed with the alternative samples under consideration, including the derivation of the various
 534 data-to-MC scale factors. The variations considered are

- 535 • Top mass: The alternative values for the top mass differ from the central value by 6 GeV: $m_{\text{top}} =$
 536 178.5 GeV and $m_{\text{top}} = 166.5$ GeV.
- 537 • Jet-parton matching scale: This corresponds to variations in the scale at which the Matrix Element
 538 partons from Madgraph are matched to Parton Shower partons from Pythia. The nominal value is
 539 $x_q > 20$ GeV. The alternative values used are $x_q > 10$ GeV and $x_q > 40$ GeV.
- 540 • Renormalization and factorization scale: The alternative samples correspond to variations in the
 541 scale $\times 2$ and $\times 0.5$. The nominal value for the scale used is $Q^2 = m_{\text{top}}^2 + \sum_{\text{jets}} p_T^2$.
- 542 • Alternative generators: Samples produced with different generators, Powheg (our default) and
 543 Madgraph.
- 544 • Modeling of taus: The alternative sample does not include Tauola and is otherwise identical to the
 545 Powheg sample. This effect was studied earlier using 7 TeV samples and found to be negligible.

- 546 • The PDF uncertainty is estimated following the PDF4LHC recommendations. The events are
 547 reweighted using alternative PDF sets for CT10 and MSTW2008 and the uncertainties for each are
 548 derived using the alternative eigenvector variations and the “master equation”. The NNPDF2.1 set
 549 with 100 replicas is also used. The central value is determined from the mean and the uncertainty
 550 is derived from the 1σ range. The overall uncertainty is derived from the envelope of the alternative
 551 predictions and their uncertainties. This effect was studied earlier using 7 TeV samples and found
 552 to be negligible.

$\Delta/N [\%]$	Madgraph	Mass Up	Mass Down	Scale Up	Scale Down	Match Up	Match Down
SRA	2	2	5	12	7	0	2
SRB	6	0	6	5	12	5	6

Table 28: Relative difference in $t\bar{t} \rightarrow \ell\ell$ predictions for alternative MC samples in the higher statistics regions SRA and SRB. These differences are based on the central values of the predictions. For a fuller picture of the situation, including statistical uncertainties, see Fig. 16.

553 In Fig. 16 we compare the alternate MC $t\bar{t} \rightarrow \ell\ell$ background predictions for regions A through E. We
 554 can make the following observations based on this Figure.

- 555 • In the tighter signal regions we are running out of statistics.
 556 • Within the limited statistics, there is no evidence that the situation changes as we go from signal
 557 region A to signal region E.
 558 • In signal regions B and above, the uncertainties assigned in Section 9.7 fully cover the alternative
 559 MC variations.
 560 • In order to fully (as opposed as 1σ) cover the alternative MC variations in region A we would
 561 have to take a systematic uncertainty of $\approx 10\%$ instead of 5%. This would be driven by the scale
 562 up/scale down variations, see Table 28.

Sample	K3	K4
Powheg	1.01 ± 0.03	0.93 ± 0.04
Madgraph	1.01 ± 0.04	0.92 ± 0.04
Mass Up	1.00 ± 0.04	0.92 ± 0.04
Mass Down	1.06 ± 0.04	0.99 ± 0.05
Scale Up	1.14 ± 0.04	1.23 ± 0.06
Scale Down	0.89 ± 0.03	0.74 ± 0.03
Match Up	1.02 ± 0.04	0.97 ± 0.04
Match Down	1.02 ± 0.04	0.91 ± 0.04

Table 29: $E_T^{\text{miss}} > 100$ GeV: Data/MC scale factors used to account for differences in the fraction of events with additional hard jets from radiation in $t\bar{t} \rightarrow \ell\ell$ events.

- 563 However, we have two pieces of information indicating that the scale up/scale down variations are incon-
 564 sistent with the data. These are described below.
 565 The first piece of information is that the jet multiplicity in the scale up/scale down sample is the most
 566 inconsistent with the data. This is shown in Table 29, where we tabulate the K_3 and K_4 factors of
 567 Section 5.3.1 for different $t\bar{t}$ MC samples. The data/MC disagreement in the N_{jets} distribution for the
 568 scale up/scale down samples is also shown in Fig. 17 and 18. This should be compared with the equivalent
 569 N_{jets} plots for the default Powheg MC, see Fig. 9, which agrees much better with data.

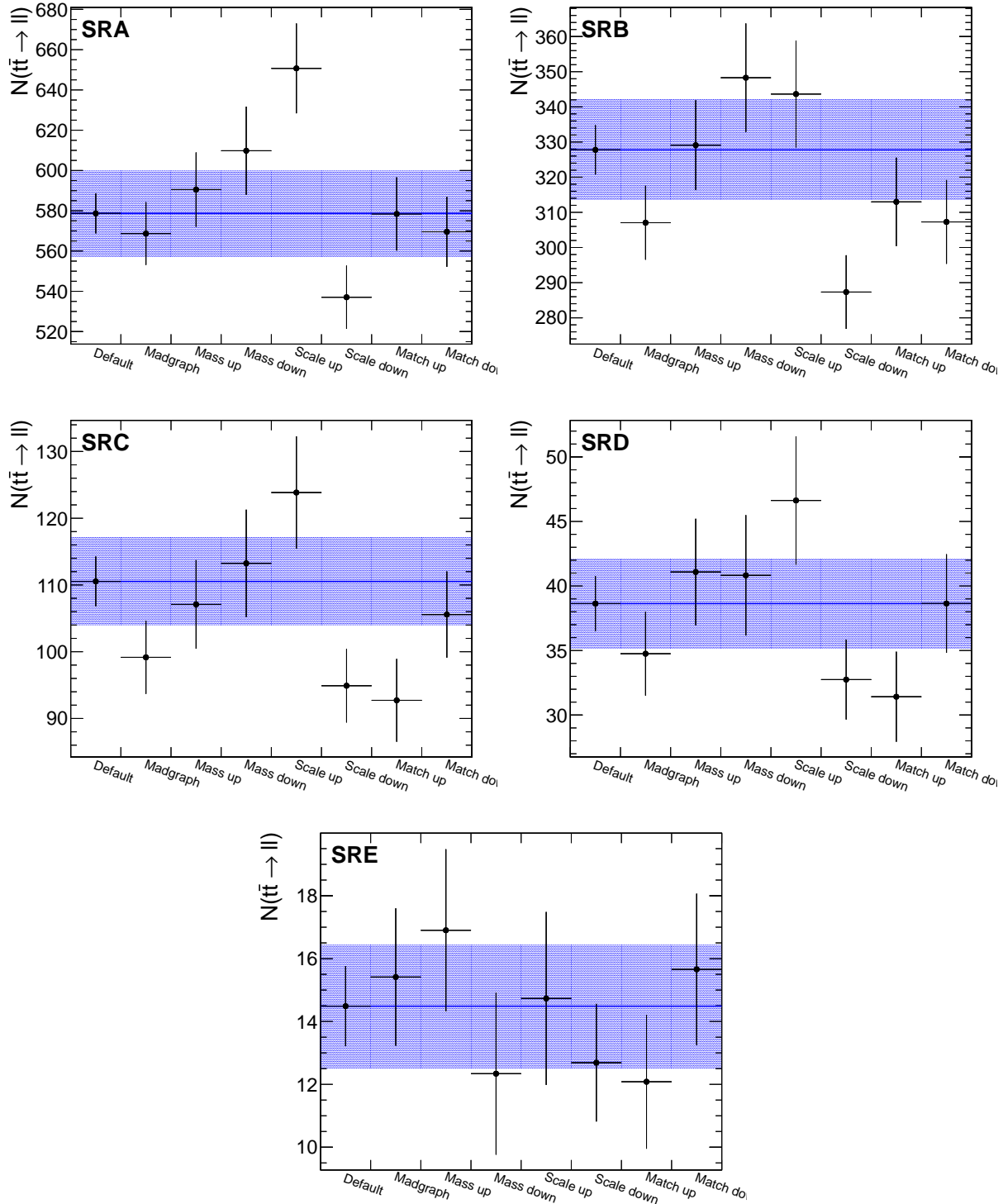


Figure 16: Comparison of the $t\bar{t} \rightarrow \ell\ell$ central prediction with those using alternative MC samples. The blue band corresponds to the total statistical error for all data and MC samples. The alternative sample predictions are indicated by the datapoints. The uncertainties on the alternative predictions correspond to the uncorrelated statistical uncertainty from the size of the alternative sample only. Note the suppressed vertical scales.

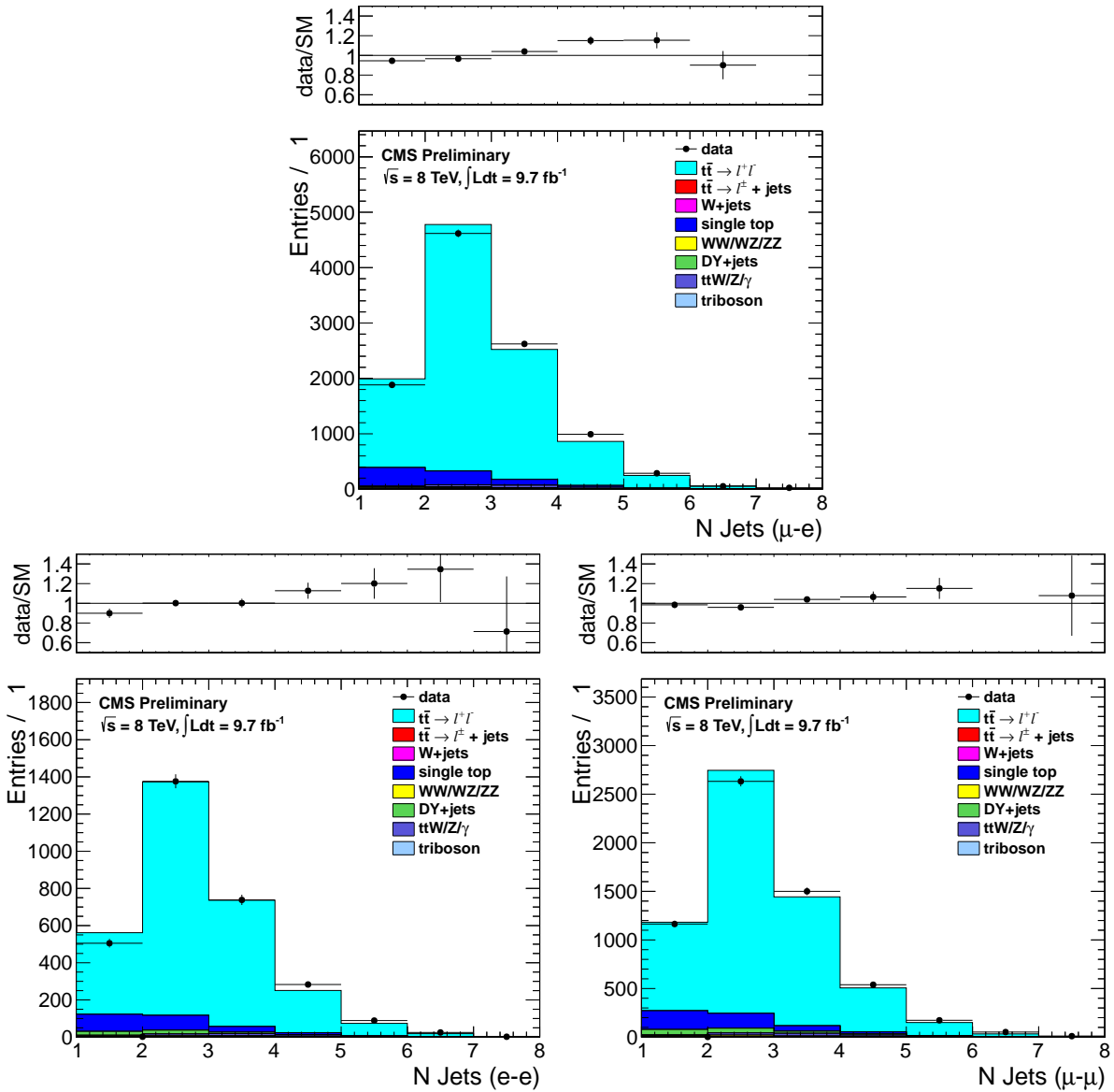


Figure 17: SCALE UP: Comparison of the jet multiplicity distribution in data and MC for dilepton events in the $e\text{-}\mu$ (top), $e\text{-}e$ (bottom left) and $\mu\text{-}\mu$ (bottom right) channels.

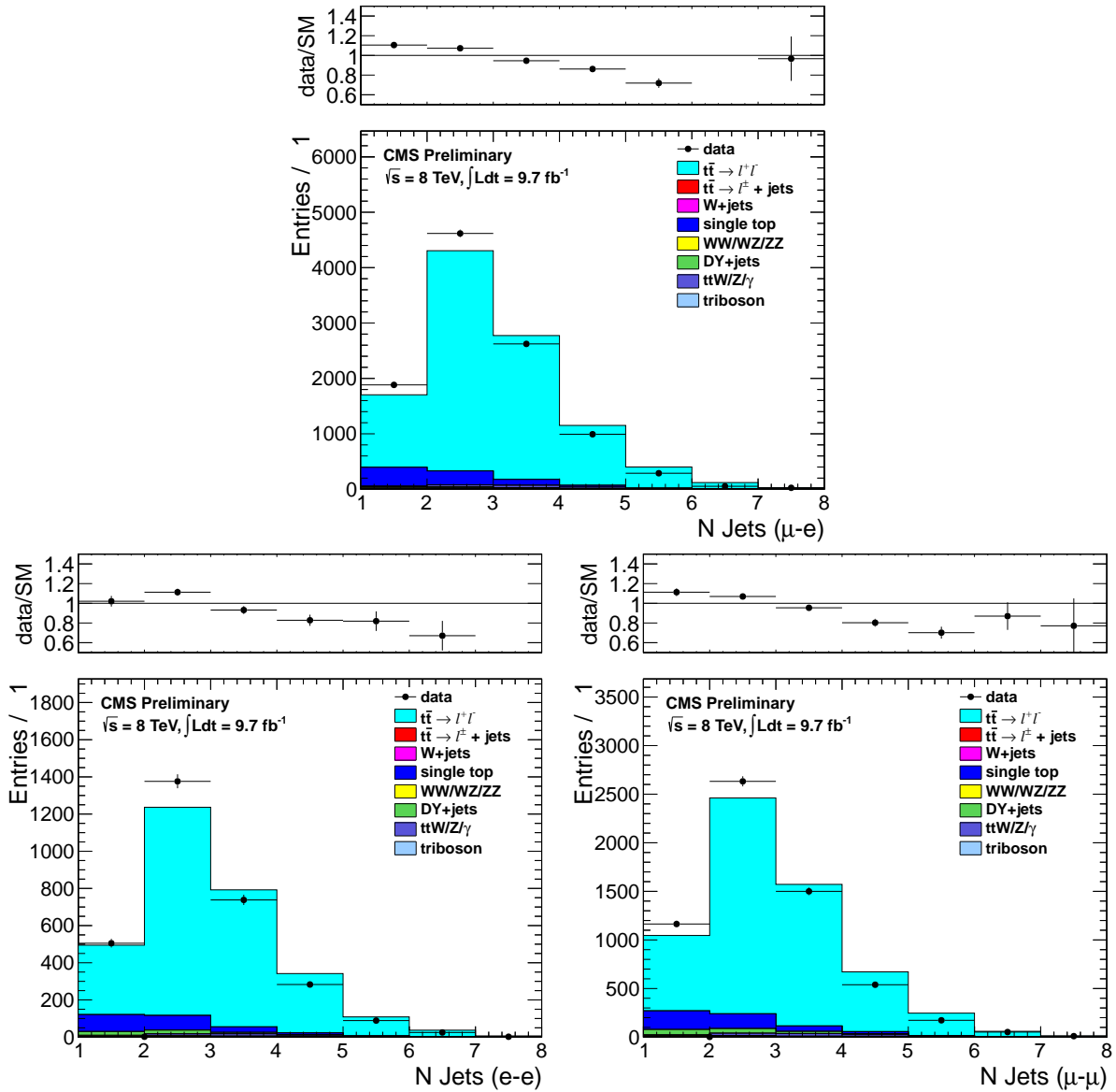


Figure 18: SCALE DOWN: Comparison of the jet multiplicity distribution in data and MC for dilepton events in the $e\text{-}\mu$ (top), $e\text{-}e$ (bottom left) and $\mu\text{-}\mu$ (bottom right) channels.

570 The second piece of information is that we have performed closure tests in CR5 using the alternative MC
 571 samples. These are exactly the same tests as the one performed in Section D.2 on the Powheg sample.
 572 As we argued previously, this is a very powerful test of the background calculation. The results of this
 573 test are summarized in Table 30. Concentrating on the relatively high statistics CR5A region, we see
 574 for all $t\bar{t}$ MC samples except scale up/scale down we obtain closure within 1σ . The scale up/scale down
 575 tests closes worse, only within 2σ . This again is evidence that the scale up/scale down variations are in
 576 disagreement with the data.

Sample	CR5PRESEL	CR5A	CR5B	CR5C	CR5D	CR5E
POWHEG						
μ Data/MC SF	1.05 ± 0.05	1.04 ± 0.06	1.08 ± 0.09	1.17 ± 0.17	0.64 ± 0.20	0.54 ± 0.29
e Data/MC SF	1.06 ± 0.06	1.04 ± 0.07	0.93 ± 0.09	0.89 ± 0.16	0.86 ± 0.25	0.52 ± 0.28
$\mu+e$ Data/MC SF	1.05 ± 0.04	1.04 ± 0.05	1.01 ± 0.07	1.04 ± 0.12	0.74 ± 0.16	0.53 ± 0.20
MADGRAPH						
μ Data/MC SF	1.05 ± 0.05	1.06 ± 0.07	1.08 ± 0.10	1.21 ± 0.19	0.64 ± 0.21	0.43 ± 0.24
e Data/MC SF	1.06 ± 0.06	1.04 ± 0.08	0.97 ± 0.10	0.97 ± 0.18	1.10 ± 0.34	0.68 ± 0.38
$\mu+e$ Data/MC SF	1.06 ± 0.04	1.05 ± 0.05	1.03 ± 0.07	1.10 ± 0.13	0.83 ± 0.18	0.53 ± 0.21
MASS UP						
μ Data/MC SF	1.04 ± 0.06	1.04 ± 0.07	1.07 ± 0.10	1.20 ± 0.19	0.57 ± 0.18	0.56 ± 0.31
e Data/MC SF	1.04 ± 0.06	1.05 ± 0.08	1.01 ± 0.11	1.12 ± 0.22	1.02 ± 0.33	0.61 ± 0.34
$\mu+e$ Data/MC SF	1.04 ± 0.04	1.04 ± 0.05	1.04 ± 0.07	1.17 ± 0.15	0.74 ± 0.17	0.58 ± 0.23
MASS DOWN						
μ Data/MC SF	1.02 ± 0.06	1.02 ± 0.07	1.04 ± 0.10	1.25 ± 0.21	0.82 ± 0.28	0.94 ± 0.56
e Data/MC SF	1.06 ± 0.06	1.02 ± 0.08	0.95 ± 0.11	0.91 ± 0.18	1.07 ± 0.35	0.59 ± 0.33
$\mu+e$ Data/MC SF	1.04 ± 0.04	1.02 ± 0.05	1.00 ± 0.07	1.09 ± 0.14	0.94 ± 0.22	0.72 ± 0.30
SCALE UP						
μ Data/MC SF	0.94 ± 0.05	0.94 ± 0.07	0.99 ± 0.10	1.24 ± 0.21	0.71 ± 0.24	0.69 ± 0.39
e Data/MC SF	0.94 ± 0.06	0.89 ± 0.07	0.81 ± 0.09	0.77 ± 0.15	0.84 ± 0.27	0.49 ± 0.28
$\mu+e$ Data/MC SF	0.94 ± 0.04	0.91 ± 0.05	0.91 ± 0.07	1.00 ± 0.13	0.77 ± 0.18	0.57 ± 0.23
SCALE DOWN						
μ Data/MC SF	1.11 ± 0.06	1.10 ± 0.07	1.24 ± 0.12	1.26 ± 0.20	0.64 ± 0.21	0.70 ± 0.39
e Data/MC SF	1.16 ± 0.07	1.20 ± 0.09	1.00 ± 0.11	1.02 ± 0.19	1.02 ± 0.32	0.53 ± 0.29
$\mu+e$ Data/MC SF	1.13 ± 0.04	1.14 ± 0.06	1.13 ± 0.08	1.15 ± 0.14	0.80 ± 0.18	0.60 ± 0.23
MATCH UP						
μ Data/MC SF	1.06 ± 0.06	1.06 ± 0.07	1.20 ± 0.11	1.42 ± 0.23	0.70 ± 0.23	0.63 ± 0.35
e Data/MC SF	1.06 ± 0.06	1.04 ± 0.08	0.97 ± 0.11	0.93 ± 0.18	1.25 ± 0.41	0.63 ± 0.36
$\mu+e$ Data/MC SF	1.06 ± 0.04	1.06 ± 0.05	1.09 ± 0.08	1.18 ± 0.15	0.92 ± 0.21	0.63 ± 0.25
MATCH DOWN						
μ Data/MC SF	1.08 ± 0.06	1.06 ± 0.07	1.14 ± 0.11	1.17 ± 0.19	0.59 ± 0.19	0.45 ± 0.25
e Data/MC SF	1.05 ± 0.06	0.99 ± 0.08	0.86 ± 0.09	0.78 ± 0.15	0.79 ± 0.25	0.50 ± 0.28
$\mu+e$ Data/MC SF	1.07 ± 0.04	1.03 ± 0.05	1.00 ± 0.07	0.98 ± 0.12	0.68 ± 0.15	0.48 ± 0.18

Table 30: Ratio of yields in M_T tail comparing the MC prediction (after applying SFs) to data. The uncertainties are statistical only.

577 Based on the two observations above, we argue that the MC scale up/scale down variations are too
 578 extreme. We feel that a reasonable choice would be to take one-half of the scale up/scale down variations
 579 in our MC. This factor of $1/2$ would then bring the discrepancy in the closure test of Table 30 for the
 580 scale up/scale down variations from about 2σ to about 1σ .
 581 Then, going back to Table 28, and reducing the scale up/scale down variations by a factor 2, we can see
 582 that a systematic uncertainty of 5% covers the range of reasonable variations from different MC models
 583 in SRA and SRB. Note that this 5% is also consistent with the level at which we are able to test the
 584 closure of the method with alternative samples in CR5 for the high statistics regions (Table 30). The
 585 range of reasonable variations obtained with the alternative samples are consistent with the uncertainties
 586 assigned for the $t\bar{t} \rightarrow \ell\ell$ background based on the closure of the background predictions and data in CR4
 587 and CR5.

588 9.8 Uncertainty from the isolated track veto

589 This is the uncertainty associated with how well the isolated track veto performance is modeled by the
 590 Monte Carlo. This uncertainty only applies to the fraction of dilepton BG events that have a second e/μ
 591 or a one prong $\tau \rightarrow h$, with $P_T > 10$ GeV in $|\eta| < 2.4$. This fraction is about 1/3, see Table 31. The
 592 uncertainty for these events is 6% and is obtained from tag-and-probe studies, see Section 9.8.1.

Sample	SRA	SRB	SRC	SRD	SRE	SRF	SRG
μ Frac. $t\bar{t} \rightarrow \ell\ell$ with true iso. trk.	0.32 ± 0.03	0.30 ± 0.03	0.32 ± 0.06	0.34 ± 0.10	0.35 ± 0.16	0.40 ± 0.24	0.50 ± 0.32
e Frac. $t\bar{t} \rightarrow \ell\ell$ with true iso. trk.	0.32 ± 0.03	0.31 ± 0.04	0.33 ± 0.06	0.38 ± 0.11	0.38 ± 0.19	0.60 ± 0.31	0.61 ± 0.45

Table 31: Fraction of $t\bar{t} \rightarrow \ell\ell$ events with a true isolated track.

593 9.8.1 Isolated Track Veto: Tag and Probe Studies

594 In this section we compare the performance of the isolated track veto in data and MC using tag-and-
 595 probe studies with samples of $Z \rightarrow ee$ and $Z \rightarrow \mu\mu$. The purpose of these studies is to demonstrate that the
 596 efficiency to satisfy the isolated track veto requirements is well-reproduced in the MC, since if this were
 597 not the case we would need to apply a data-to-MC scale factor in order to correctly predict the $t\bar{t} \rightarrow \ell\ell$
 598 background.

599 This study addresses possible data vs. MC discrepancies for the **efficiency** to identify (and reject)
 600 events with a second **genuine** lepton (e, μ , or $\tau \rightarrow 1$ -prong). It does not address possible data vs.
 601 MC discrepancies in the fake rate for rejecting events without a second genuine lepton; this is handled
 602 separately in the top normalization procedure by scaling the $t\bar{t} \rightarrow \ell + \text{jets}$ contribution to match the data
 603 in the M_T peak after applying the isolated track veto.

604 Furthermore, we test the data and MC isolated track veto efficiencies for electrons and muons since we are
 605 using a Z tag-and-probe technique, but we do not directly test the performance for hadronic tracks from
 606 τ decays. The performance for hadronic τ decay products may differ from that of electrons and muons
 607 for two reasons. First, the τ may decay to a hadronic track plus one or two π^0 's, which may decay to
 608 $\gamma\gamma$ followed by a photon conversion. As shown in Figure 33, the isolation distribution for charged tracks
 609 from τ decays that are not produced in association with π^0 's are consistent with that from es and μ s.
 610 Since events from single prong τ decays produced in association with π^0 's comprise a small fraction of the
 611 total sample, and since the kinematics of τ , π^0 and $\gamma \rightarrow e^+e^-$ decays are well-understood, we currently
 612 demonstrate that the isolation is well-reproduced for electrons and muons only. Second, hadronic tracks
 613 may undergo nuclear interactions and hence their tracks may not be reconstructed. As discussed above,
 614 independent studies show that the MC reproduces the hadronic tracking efficiency within 4%, leading
 615 to a total background uncertainty of less than 0.5% (after taking into account the fraction of the total
 616 background due to hadronic τ decays with $p_T > 10$ GeV tracks), and we hence regard this effect as
 617 negligible.

618 The tag-and-probe studies are performed in the full data sample, and compared with the DYJets mad-
 619 graph sample. All events must contain a tag-probe pair (details below) with opposite-sign and satisfying
 620 the Z mass requirement 76–106 GeV. We compare the distributions of absolute track isolation for probe
 621 electrons/muons in data vs. MC. The contributions to this isolation sum are from ambient energy in the
 622 event from underlying event, pile-up and jet activity, and hence do not depend on the p_T of the probe
 623 lepton. We therefore restrict the probe p_T to be > 30 GeV in order to suppress fake backgrounds with
 624 steeply-falling p_T spectra. To suppress non-Z backgrounds (in particular $t\bar{t}$) we require $E_T^{\text{miss}} < 30$ GeV
 625 and 0 b-tagged events. The specific criteria for tags and probes for electrons and muons are:

- 626 • Electrons
 - 627 – Tag criteria
 - * Electron passes full analysis ID/iso selection
 - * $p_T > 30$ GeV, $|\eta| < 2.1$
 - * Matched to the single electron trigger HLT_Ele27_WP80_v*
 - 631 – Probe criteria

- * Electron passes full analysis ID selection
- * $p_T > 30 \text{ GeV}$
- Muons
 - Tag criteria
 - * Muon passes full analysis ID/iso selection
 - * $p_T > 30 \text{ GeV}, |\eta| < 2.1$
 - * Matched to 1 of the 2 single muon triggers
 - HLT_IsoMu30_v*
 - HLT_IsoMu30_eta2p1_v*
 - Probe criteria
 - * Muon passes full analysis ID selection
 - * $p_T > 30 \text{ GeV}$

The absolute track isolation distributions for passing probes are displayed in Fig. 19. In general we observe good agreement between data and MC. To be more quantitative, we compare the data vs. MC efficiencies to satisfy absolute track isolation requirements varying from $> 1 \text{ GeV}$ to $> 5 \text{ GeV}$, as summarized in Table 32. In the ≥ 0 and ≥ 1 jet bins where the efficiencies can be tested with statistical precision, the data and MC efficiencies agree within 6%, and we apply this as a systematic uncertainty on the isolated track veto efficiency. For the higher jet multiplicity bins the statistical precision decreases, but we do not observe any evidence for a data vs. MC discrepancy in the isolated track veto efficiency.

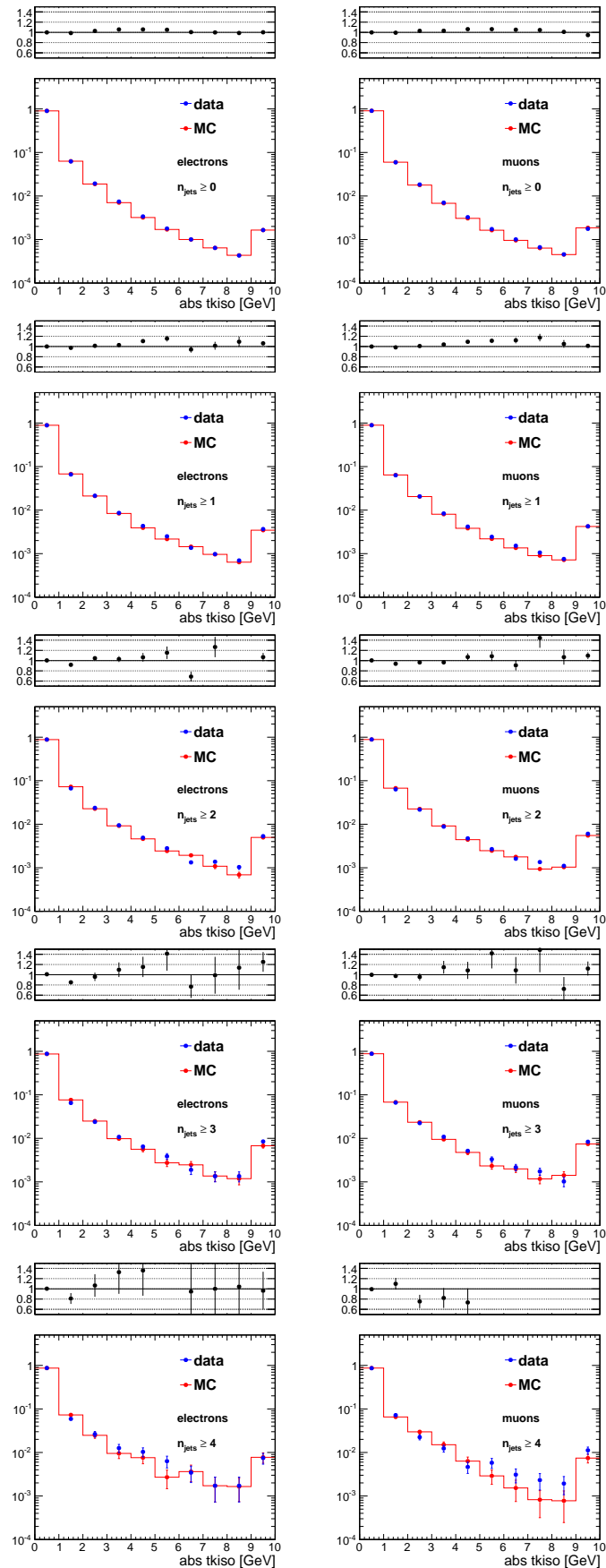


Figure 19: Comparison of the absolute track isolation in data vs. MC for electrons (left) and muons (right) for events with the N_{jets} requirement varied from $N_{\text{jets}} \geq 0$ to $N_{\text{jets}} \geq 4$.

$e + \geq 0$ jets	> 1 GeV	> 2 GeV	> 3 GeV	> 4 GeV	> 5 GeV
data	0.098 ± 0.0002	0.036 ± 0.0001	0.016 ± 0.0001	0.009 ± 0.0001	0.006 ± 0.0000
mc	0.097 ± 0.0002	0.034 ± 0.0001	0.016 ± 0.0001	0.009 ± 0.0001	0.005 ± 0.0000
data/mc	1.00 ± 0.00	1.04 ± 0.00	1.04 ± 0.01	1.03 ± 0.01	1.02 ± 0.01
$\mu + \geq 0$ jets	> 1 GeV	> 2 GeV	> 3 GeV	> 4 GeV	> 5 GeV
data	0.094 ± 0.0001	0.034 ± 0.0001	0.016 ± 0.0001	0.009 ± 0.0000	0.006 ± 0.0000
mc	0.093 ± 0.0001	0.033 ± 0.0001	0.015 ± 0.0001	0.009 ± 0.0000	0.006 ± 0.0000
data/mc	1.01 ± 0.00	1.03 ± 0.00	1.03 ± 0.01	1.03 ± 0.01	1.02 ± 0.01
$e + \geq 1$ jets	> 1 GeV	> 2 GeV	> 3 GeV	> 4 GeV	> 5 GeV
data	0.110 ± 0.0005	0.044 ± 0.0003	0.022 ± 0.0002	0.014 ± 0.0002	0.009 ± 0.0002
mc	0.110 ± 0.0005	0.042 ± 0.0003	0.021 ± 0.0002	0.013 ± 0.0002	0.009 ± 0.0001
data/mc	1.00 ± 0.01	1.04 ± 0.01	1.06 ± 0.02	1.08 ± 0.02	1.06 ± 0.03
$\mu + \geq 1$ jets	> 1 GeV	> 2 GeV	> 3 GeV	> 4 GeV	> 5 GeV
data	0.106 ± 0.0004	0.043 ± 0.0003	0.023 ± 0.0002	0.014 ± 0.0002	0.010 ± 0.0001
mc	0.106 ± 0.0004	0.042 ± 0.0003	0.021 ± 0.0002	0.013 ± 0.0002	0.009 ± 0.0001
data/mc	1.00 ± 0.01	1.04 ± 0.01	1.06 ± 0.01	1.08 ± 0.02	1.07 ± 0.02
$e + \geq 2$ jets	> 1 GeV	> 2 GeV	> 3 GeV	> 4 GeV	> 5 GeV
data	0.117 ± 0.0012	0.050 ± 0.0008	0.026 ± 0.0006	0.017 ± 0.0005	0.012 ± 0.0004
mc	0.120 ± 0.0012	0.048 ± 0.0008	0.025 ± 0.0006	0.016 ± 0.0005	0.011 ± 0.0004
data/mc	0.97 ± 0.01	1.05 ± 0.02	1.05 ± 0.03	1.07 ± 0.04	1.07 ± 0.05
$\mu + \geq 2$ jets	> 1 GeV	> 2 GeV	> 3 GeV	> 4 GeV	> 5 GeV
data	0.111 ± 0.0010	0.048 ± 0.0007	0.026 ± 0.0005	0.018 ± 0.0004	0.013 ± 0.0004
mc	0.115 ± 0.0010	0.048 ± 0.0006	0.025 ± 0.0005	0.016 ± 0.0004	0.012 ± 0.0003
data/mc	0.97 ± 0.01	1.01 ± 0.02	1.04 ± 0.03	1.09 ± 0.04	1.09 ± 0.04
$e + \geq 3$ jets	> 1 GeV	> 2 GeV	> 3 GeV	> 4 GeV	> 5 GeV
data	0.123 ± 0.0031	0.058 ± 0.0022	0.034 ± 0.0017	0.023 ± 0.0014	0.017 ± 0.0012
mc	0.131 ± 0.0030	0.055 ± 0.0020	0.030 ± 0.0015	0.020 ± 0.0013	0.015 ± 0.0011
data/mc	0.94 ± 0.03	1.06 ± 0.06	1.14 ± 0.08	1.16 ± 0.10	1.17 ± 0.12
$\mu + \geq 3$ jets	> 1 GeV	> 2 GeV	> 3 GeV	> 4 GeV	> 5 GeV
data	0.121 ± 0.0025	0.055 ± 0.0018	0.033 ± 0.0014	0.022 ± 0.0011	0.017 ± 0.0010
mc	0.120 ± 0.0024	0.052 ± 0.0016	0.029 ± 0.0012	0.019 ± 0.0010	0.014 ± 0.0009
data/mc	1.01 ± 0.03	1.06 ± 0.05	1.14 ± 0.07	1.14 ± 0.08	1.16 ± 0.10
$e + \geq 4$ jets	> 1 GeV	> 2 GeV	> 3 GeV	> 4 GeV	> 5 GeV
data	0.129 ± 0.0080	0.070 ± 0.0061	0.044 ± 0.0049	0.031 ± 0.0042	0.021 ± 0.0034
mc	0.132 ± 0.0075	0.059 ± 0.0053	0.035 ± 0.0041	0.025 ± 0.0035	0.017 ± 0.0029
data/mc	0.98 ± 0.08	1.18 ± 0.15	1.26 ± 0.20	1.24 ± 0.24	1.18 ± 0.28
$\mu + \geq 4$ jets	> 1 GeV	> 2 GeV	> 3 GeV	> 4 GeV	> 5 GeV
data	0.136 ± 0.0067	0.064 ± 0.0048	0.041 ± 0.0039	0.029 ± 0.0033	0.024 ± 0.0030
mc	0.130 ± 0.0063	0.065 ± 0.0046	0.035 ± 0.0034	0.020 ± 0.0026	0.013 ± 0.0022
data/mc	1.04 ± 0.07	0.99 ± 0.10	1.19 ± 0.16	1.47 ± 0.25	1.81 ± 0.37

Table 32: Comparison of the data vs. MC efficiencies to satisfy the indicated requirements on the absolute track isolation, and the ratio of these two efficiencies. Results are indicated separately for electrons and muons and for various jet multiplicity requirements.

651 9.9 Summary of uncertainties

652 The contribution from each source to the total uncertainty on the background yield is given in Tables 33
 653 and 34 for the relative and absolute uncertainties, respectively. In the low- E_T^{miss} regions the dominant
 654 uncertainty comes from the top tail-to-peak ratio, R_{top} (Section 7), while in the high- E_T^{miss} regions the
 655 $t\bar{t} \rightarrow \ell\ell$ systematic uncertainty dominates (Section 9.7).

Sample	SRA	SRB	SRC	SRD	SRE	SRF	SRG
Muon							
$W + \text{jets}$ cross-section	1.7%	2.3%	3.0%	3.7%	4.2%	4.2%	5.3%
rare cross-sections	2.0%	2.3%	3.4%	5.6%	8.8%	8.0%	10.4%
top tail-to-peak ratio	12.6%	8.7%	8.6%	6.7%	7.1%	8.6%	4.6%
$W + \text{jets}$ tail-to-peak ratio	6.5%	5.3%	5.8%	6.9%	8.9%	12.0%	13.6%
$t\bar{t} \rightarrow \ell\ell$ (stat)	1.1%	1.5%	2.8%	4.7%	6.7%	9.7%	12.2%
K_3 and K_4	1.9%	1.9%	2.0%	2.0%	1.9%	1.8%	1.8%
2nd lepton veto	1.2%	1.3%	1.3%	1.3%	1.2%	1.2%	1.2%
$t\bar{t} \rightarrow \ell\ell$ (CR4 and CR5 closure tests)	3.1%	6.5%	10.2%	16.9%	25.1%	23.8%	23.4%
M_T peak data and MC (stat)	1.1%	2.1%	3.8%	6.0%	8.6%	13.1%	20.0%
total	15.0%	13.0%	16.1%	22.1%	31.3%	33.7%	37.9%
Electron							
$W + \text{jets}$ cross-section	1.7%	2.3%	2.9%	4.2%	4.4%	4.5%	4.6%
rare cross-sections	2.1%	2.1%	2.9%	3.7%	1.9%	3.2%	1.9%
top tail-to-peak ratio	12.4%	8.6%	8.3%	6.1%	8.7%	11.0%	8.8%
$W + \text{jets}$ tail-to-peak ratio	6.4%	5.2%	5.5%	6.3%	10.8%	15.4%	25.7%
$t\bar{t} \rightarrow \ell\ell$ (stat)	1.3%	1.8%	3.2%	5.6%	8.7%	13.6%	16.6%
K_3 and K_4	1.9%	2.0%	2.1%	2.1%	2.1%	2.0%	2.0%
2nd lepton veto	1.2%	1.3%	1.4%	1.4%	1.4%	1.3%	1.3%
$t\bar{t} \rightarrow \ell\ell$ (CR4 and CR5 closure tests)	3.1%	6.6%	10.4%	17.7%	28.1%	26.1%	26.6%
M_T peak data and MC (stat)	1.4%	2.5%	4.3%	7.4%	11.5%	15.2%	22.5%
total	14.8%	13.0%	16.1%	22.7%	34.9%	38.7%	47.5%
Muon+Electron Combined							
$W + \text{jets}$ cross-section	1.7%	2.3%	3.0%	3.9%	4.3%	4.3%	5.1%
rare cross-sections	2.0%	2.2%	3.2%	4.9%	6.4%	6.2%	7.6%
top tail-to-peak ratio	12.5%	8.7%	8.5%	6.5%	7.7%	9.5%	6.0%
$W + \text{jets}$ tail-to-peak ratio	6.4%	5.2%	5.7%	6.6%	9.6%	13.3%	17.6%
$t\bar{t} \rightarrow \ell\ell$ (stat)	1.2%	1.6%	3.0%	5.1%	7.4%	11.1%	13.6%
K_3 and K_4	1.9%	2.0%	2.1%	2.1%	2.0%	1.9%	1.8%
2nd lepton veto	1.2%	1.3%	1.4%	1.4%	1.3%	1.2%	1.2%
$t\bar{t} \rightarrow \ell\ell$ (CR4 and CR5 closure tests)	3.1%	6.5%	10.3%	17.3%	26.1%	24.7%	24.5%
M_T peak data and MC (stat)	0.9%	1.7%	2.9%	4.7%	7.0%	10.1%	15.4%
total	14.9%	12.9%	15.9%	21.8%	31.7%	34.2%	38.2%

Table 33: Contributions to the total relative uncertainties.

Sample	SRA	SRB	SRC	SRD	SRE	SRF	SRG
Muon							
W +jets cross-section	9.0	6.5	2.6	1.2	0.6	0.3	0.2
rare cross-sections	10.4	6.6	3.0	1.9	1.3	0.5	0.4
top tail-to-peak ratio	67.1	24.8	7.6	2.2	1.0	0.5	0.2
W +jets tail-to-peak ratio	34.5	14.9	5.1	2.3	1.3	0.7	0.5
$t\bar{t} \rightarrow \ell\ell$ (stat)	6.0	4.4	2.4	1.6	1.0	0.6	0.5
K_3 and K_4	9.9	5.5	1.8	0.7	0.3	0.1	0.1
2nd lepton veto	6.5	3.6	1.2	0.4	0.2	0.1	0.0
$t\bar{t} \rightarrow \ell\ell$ (CR4 and CR5 closure tests)	16.5	18.3	8.9	5.6	3.6	1.5	0.9
M_T peak data and MC (stat)	6.0	6.1	3.4	2.0	1.2	0.8	0.8
total	79.8	36.8	14.2	7.3	4.5	2.1	1.4
Electron							
W +jets cross-section	6.8	5.0	2.2	1.0	0.3	0.2	0.1
rare cross-sections	8.1	4.6	2.2	0.9	0.1	0.1	0.0
top tail-to-peak ratio	49.2	18.9	6.1	1.4	0.7	0.4	0.2
W +jets tail-to-peak ratio	25.3	11.4	4.1	1.4	0.8	0.6	0.5
$t\bar{t} \rightarrow \ell\ell$ (stat)	5.2	3.9	2.4	1.3	0.7	0.5	0.3
K_3 and K_4	7.4	4.3	1.5	0.5	0.2	0.1	0.0
2nd lepton veto	4.9	2.9	1.0	0.3	0.1	0.0	0.0
$t\bar{t} \rightarrow \ell\ell$ (CR4 and CR5 closure tests)	12.4	14.4	7.7	4.0	2.2	1.0	0.5
M_T peak data and MC (stat)	5.7	5.4	3.2	1.7	0.9	0.6	0.4
total	58.8	28.5	11.9	5.2	2.7	1.5	0.9
Muon+Electron Combined							
W +jets cross-section	15.9	11.5	4.8	2.2	0.9	0.4	0.3
rare cross-sections	18.5	11.1	5.1	2.7	1.4	0.6	0.4
top tail-to-peak ratio	116.3	43.6	13.7	3.6	1.7	1.0	0.3
W +jets tail-to-peak ratio	59.8	26.3	9.1	3.7	2.1	1.3	1.0
$t\bar{t} \rightarrow \ell\ell$ (stat)	11.2	8.3	4.8	2.9	1.7	1.1	0.8
K_3 and K_4	17.4	9.8	3.3	1.2	0.4	0.2	0.1
2nd lepton veto	11.5	6.5	2.2	0.8	0.3	0.1	0.1
$t\bar{t} \rightarrow \ell\ell$ (CR4 and CR5 closure tests)	28.9	32.8	16.6	9.7	5.8	2.5	1.4
M_T peak data and MC (stat)	8.7	8.4	4.7	2.6	1.5	1.0	0.9
total	138.4	64.8	25.6	12.2	7.0	3.4	2.2

Table 34: Contributions to the total uncertainties.

656 10 Results

657 The results of the search are shown in Table 35, including both statistical and systematic uncertainties.
 658 Agreement is observed between the data and the predicted background for all signal regions. The pre-
 659 dicted and observed E_T^{miss} distribution for $E_T^{\text{miss}} > 150 \text{ GeV}$ and $M_T > 120 \text{ GeV}$ are shown in Figure 20,
 660 obtained from the yields for SRB to SRG. Two signal points are shown for comparison, corresponding
 661 to the low and high stop mass sensitivity boundaries for this search. This shows that the lower E_T^{miss}
 662 region is more sensitive to lighter stop signals, while the higher E_T^{miss} region is more sensitive to heavier
 663 stops, for the T2tt signal model shown. The M_T distributions for increasing values of E_T^{miss} are shown
 664 in Fig 21 and 22.

Sample	SRA	SRB	SRC	SRD	SRE	SRF	SRG
Muon							
$t\bar{t} \rightarrow \ell\ell$	331 ± 22	183 ± 21	59.5 ± 10.0	23 ± 6	9.0 ± 3.9	3.7 ± 1.8	2.2 ± 1.2
$t\bar{t} \rightarrow \ell + \text{jets \& single top } (1\ell)$	148 ± 75	67.9 ± 28.9	16.1 ± 9.1	4.7 ± 3.2	1.8 ± 1.6	0.9 ± 0.9	0.4 ± 0.5
$W + \text{jets}$	19.2 ± 4.5	10.0 ± 2.2	3.11 ± 0.98	1.2 ± 0.6	0.6 ± 0.4	0.4 ± 0.3	0.2 ± 0.2
Rare	33.2 ± 16.6	22.7 ± 11.4	9.00 ± 4.50	4.8 ± 2.4	2.9 ± 1.5	1.2 ± 0.6	1.0 ± 0.5
Total	531 ± 80	284 ± 37	87.7 ± 14.2	33 ± 7	14 ± 5	6.1 ± 2.1	3.8 ± 1.4
Data	494	254	76	31	8	2	1
Electron							
$t\bar{t} \rightarrow \ell\ell$	248 ± 17	144 ± 17	51.1 ± 8.8	16 ± 5	5.5 ± 2.5	2.5 ± 1.3	1.3 ± 0.7
$t\bar{t} \rightarrow \ell + \text{jets \& single top } (1\ell)$	108 ± 55	51.8 ± 22.1	12.9 ± 7.3	3.0 ± 2.0	1.2 ± 1.1	0.7 ± 0.7	0.4 ± 0.5
$W + \text{jets}$	14.3 ± 3.3	7.50 ± 1.66	2.43 ± 0.77	0.8 ± 0.4	0.4 ± 0.3	0.3 ± 0.2	0.1 ± 0.2
Rare	25.8 ± 12.9	15.8 ± 7.9	7.10 ± 3.55	2.9 ± 1.5	0.7 ± 0.4	0.3 ± 0.2	0.1 ± 0.1
Total	396 ± 59	219 ± 29	73.5 ± 11.9	23 ± 5	7.8 ± 2.7	3.9 ± 1.5	1.9 ± 0.9
Data	367	202	74	30	15	7	2
Muon+Electron Combined							
$t\bar{t} \rightarrow \ell\ell$	579 ± 38	328 ± 37	111 ± 18	39 ± 10	14 ± 6	6.2 ± 2.9	3.5 ± 1.8
$t\bar{t} \rightarrow \ell + \text{jets \& single top } (1\ell)$	256 ± 131	120 ± 51	29.0 ± 16.4	7.7 ± 5.1	3.1 ± 2.7	1.7 ± 1.6	0.8 ± 1.0
$W + \text{jets}$	33.5 ± 8.2	17.5 ± 4.5	5.54 ± 1.98	2.0 ± 1.0	1.0 ± 0.7	0.7 ± 0.6	0.3 ± 0.4
Rare	59.0 ± 29.5	38.5 ± 19.3	16.1 ± 8.1	7.7 ± 3.9	3.6 ± 1.8	1.5 ± 0.8	1.1 ± 0.6
Total	927 ± 138	504 ± 65	161 ± 26	56 ± 12	22 ± 7	10 ± 3	5.7 ± 2.2
Data	861	456	150	61	23	9	3

Table 35: The result of the search.

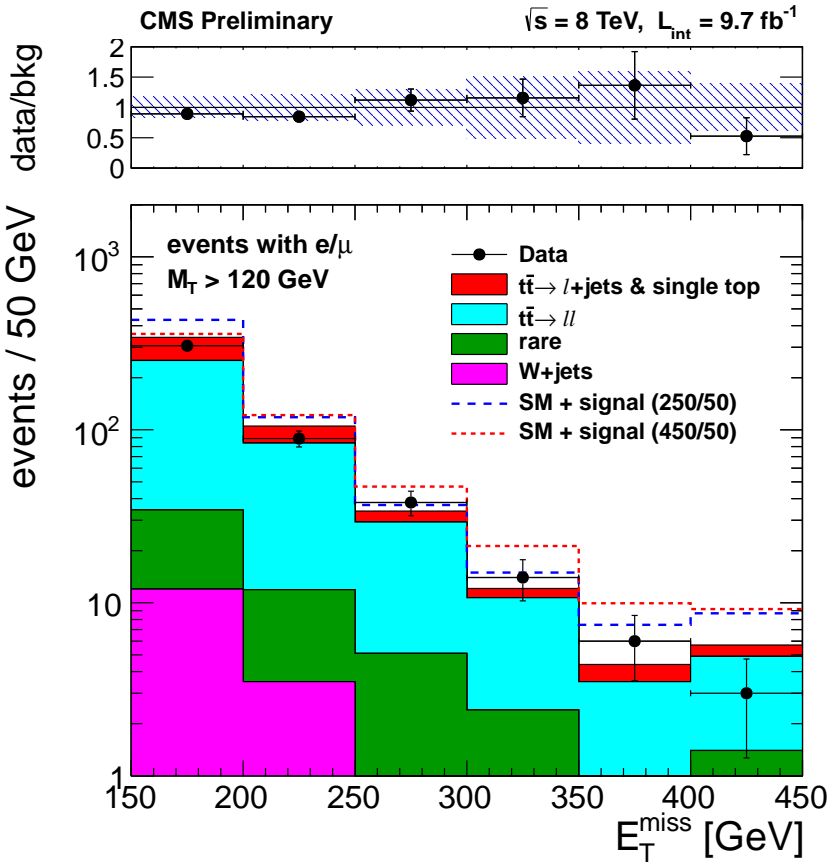


Figure 20: Predicted and observed E_T^{miss} for $M_T > 120$ GeV, obtained from the yields for SRB to SRG. Note SRB corresponds to the integral of the distribution, while subsequent signal regions SRC to SRG correspond to integrals from subsequent bins. The band on the ratio (above) corresponds to the full relative background uncertainty.

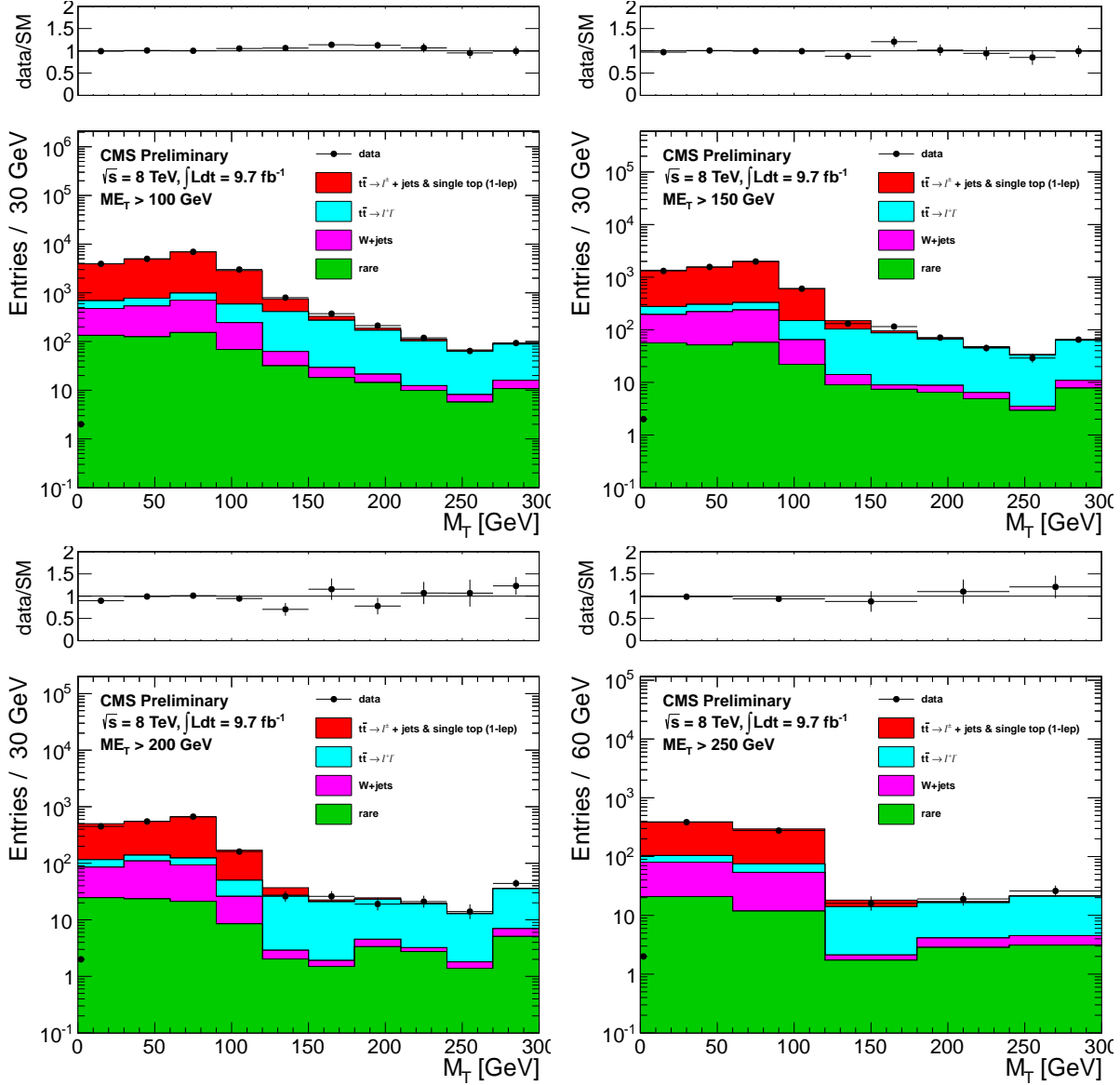


Figure 21: M_T in the data compared to SM Monte Carlo, for increasing values of E_T^{miss} . Only statistical uncertainties are shown. Note that the MC tails have not been rescaled at this point.

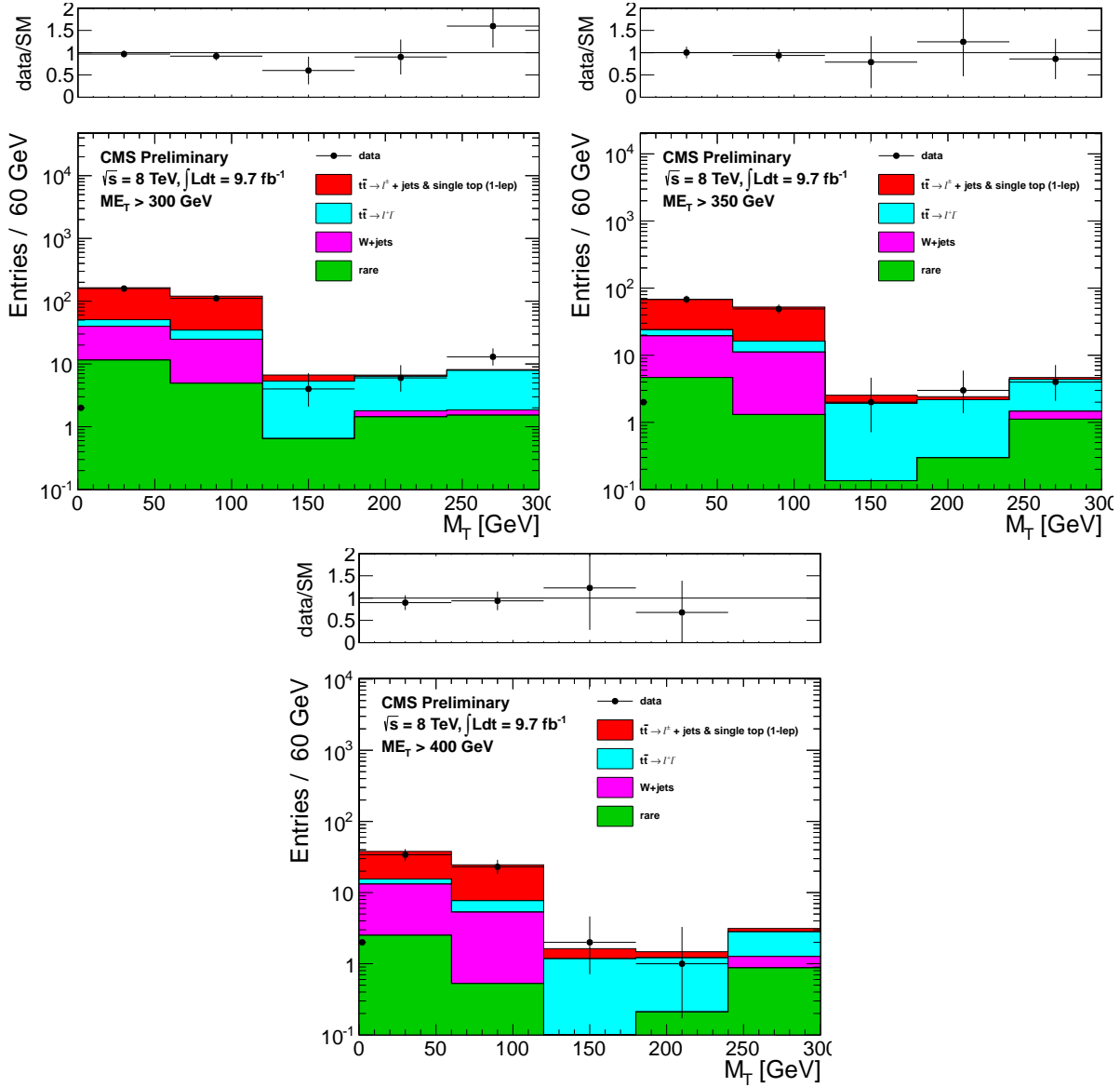


Figure 22: M_T in the data compared to SM Monte Carlo, for increasing values of E_T^{miss} . Only statistical uncertainties are shown. Note that the MC tails have not been rescaled at this point.

665 11 Limits

666 In this Section, we interpret the results of this search in terms of the T2tt and T2bw simplified models,
 667 see Figure 23. The branching fractions for the stop decay are assumed to be 100% for each model. The
 668 signal samples are normalized to cross sections calculated at NLO in α_S , including the resummation of
 669 soft gluon emission at next-to-leading-logarithmic accuracy (NLO+NLL).

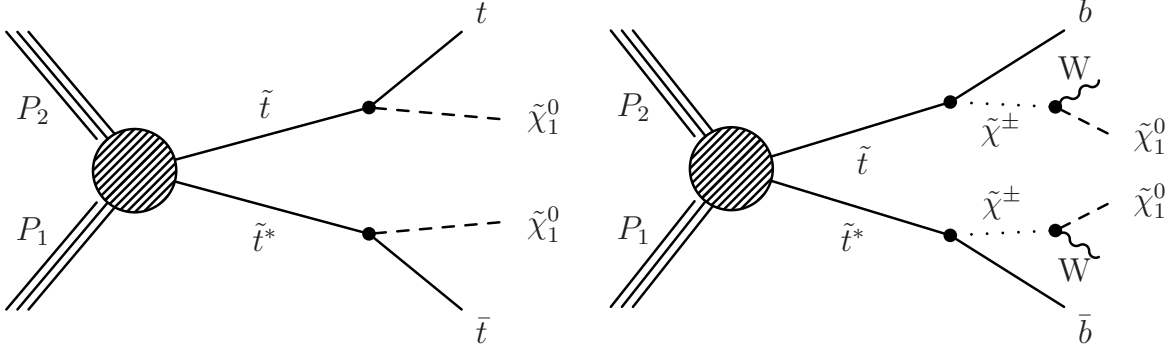


Figure 23: Diagram for the T2tt (left) and T2bw (right) simplified models.

670 The exclusion is performed using the results from the counting experiments in the signal regions defined
 671 by E_T^{miss} and M_T and listed in Table 4. The cross section upper limit calculation is performed with the
 672 LandS software using the LHC-type CLs criterion.

673 The signal efficiency uncertainties include the luminosity (4.4%), lepton ID and isolation efficiency (2%),
 674 and trigger efficiency (3%). The uncertainty from JES is assessed for each scan point following the POG-
 675 recommended procedure, by varying the jet energies by the p_T - and η - dependent uncertainties, and
 676 propagating this to the jet multiplicity, E_T^{miss} and M_T . The official b-tagging scale-factors for CSVm are
 677 used to compute scale factors for the signal. The results are nearly constant across the model parameter
 678 space, and an overall scale factor of $(98 \pm 2)\%$ is used.

679 The signal efficiency in the stop vs LSP mass plane for T2tt is shown for each signal region in Figures 24,
 680 25 and 26 (left). The corresponding distributions for T2bw are shown in Figures 27 and 28 (left) for
 681 $x=0.75$ and in Figure 29 (left) for $x=0.5$. The current analysis is not sensitive to the $x=0.25$ scenario
 682 (Figure 31, bottom).

683 These distributions show how challenging it is to have sensitivity near the kinematical boundaries. The
 684 cross section upper limits, along with the observed and expected exclusion contours, are also shown in
 685 Figures 24, 25 and 26 for T2tt, in Figures 27 and 28 for T2bw with $x=0.75$, and in Figure 29 for T2bw with
 686 $x=0.5$ (right). The complementarity of the different signal regions is readily apparent. The sensitivity to
 687 low (high) stop masses comes from the low (high) E_T^{miss} signal regions.

688 A combined result is obtained using the observed limit from the signal region with the best expected limit
 689 for each scan point. The combined cross section upper limits, with the observed and expected exclusion
 690 contours, are shown in Figure 30 for T2tt and Figure 31 for T2bw (left). The signal region with the best
 691 expected limit for each scan point is also shown in Figure 30 for T2tt and Figure 31 for T2bw (right).
 692 For the T2tt scenario, these results exclude stops with masses in the range of approximately 230 – 460
 693 GeV, for LSP masses up to about 120 GeV. In the T2bw scenario with $x=0.75$, this search excludes stops
 694 with masses in the range of approximately 150 – 430 GeV, for LSP masses up to about 140 GeV. The
 695 sensitivity is reduced in the $x=0.5$ scenario, where the results exclude stops with masses in the range of
 696 approximately 250 – 360 GeV, for LSP masses less than approximately 100 GeV.

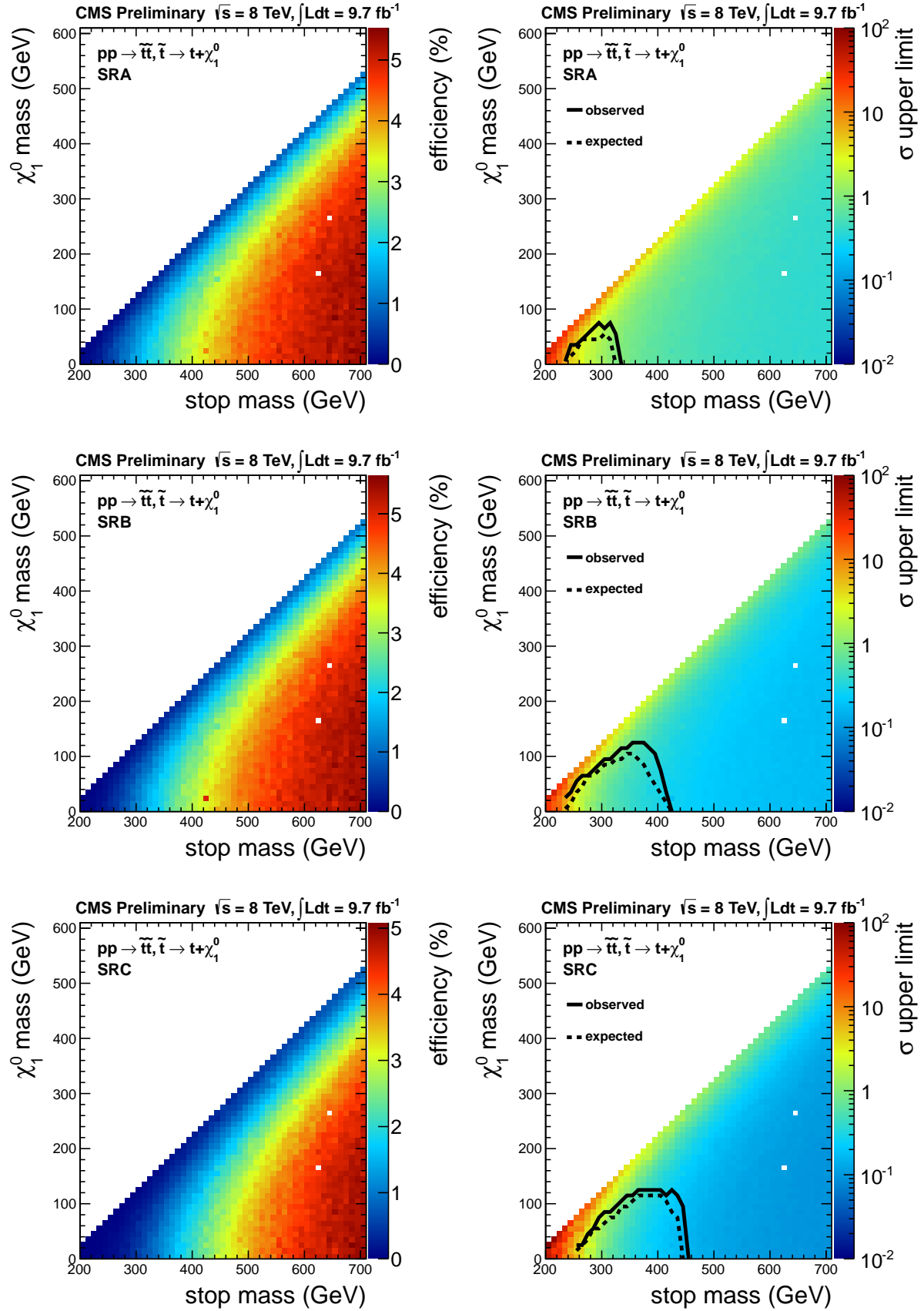


Figure 24: Signal efficiency (left) and cross section upper limit (right) for the T2tt model, showing both the expected and observed exclusion contours. The results for signal regions SRA (top), SRB (middle) and SRC (bottom) are shown separately.

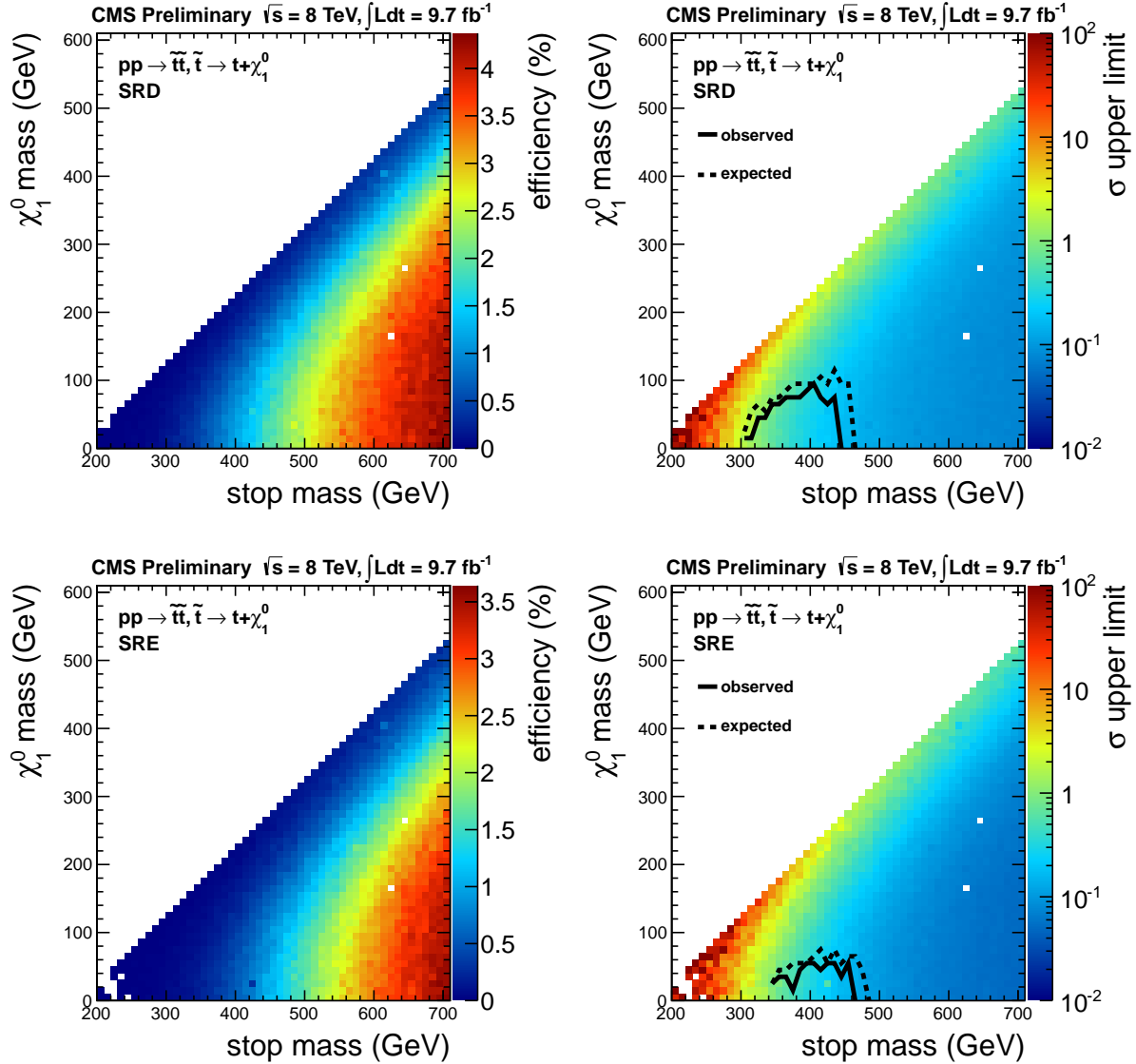


Figure 25: Signal efficiency (left) and cross section upper limit (right) for the T2tt model, showing both the expected and observed exclusion contours. The results for signal regions SRD (top), and SRE (bottom) are shown separately.

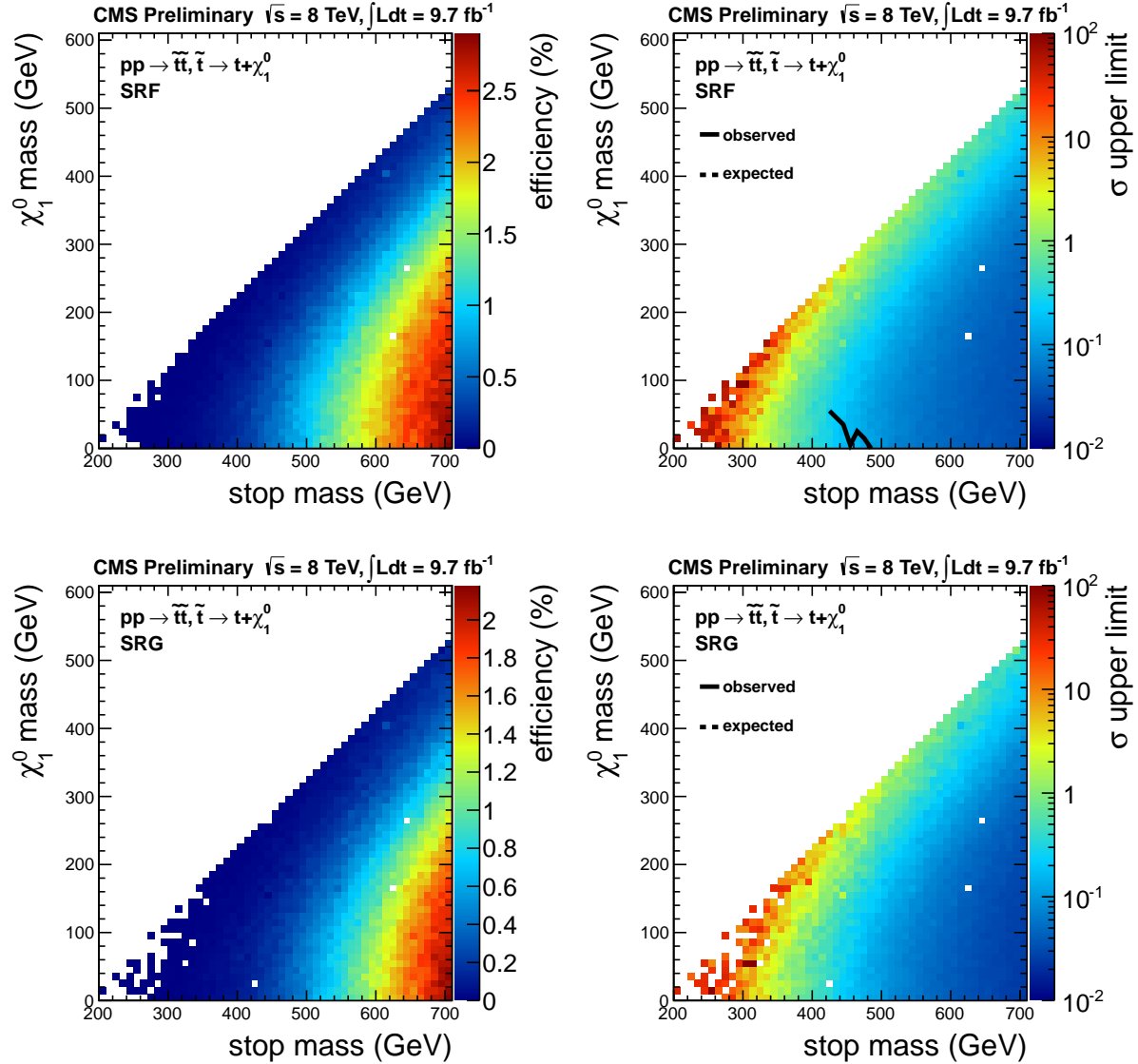


Figure 26: Signal efficiency (left) and cross section upper limit (right) for the T2tt model, showing both the expected and observed exclusion contours. The results for signal regions SRF (top) and SRG (bottom) are shown separately.

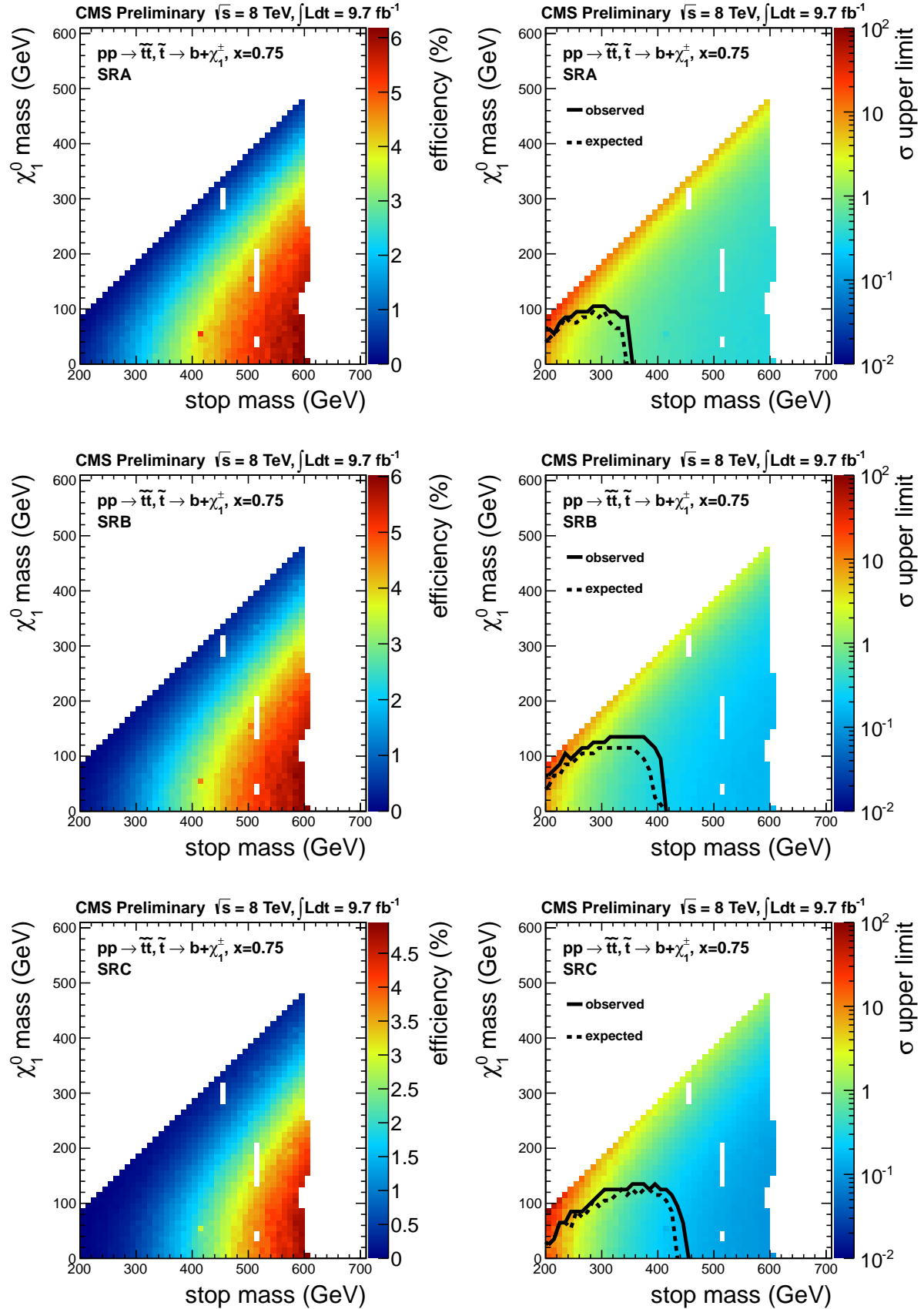


Figure 27: Signal efficiency (left) and cross section upper limit (right) for the T2bw model with $x=0.75$, showing both the expected and observed exclusion contours. The results for signal regions SRA (top), SRB (middle) and SRC (bottom) are shown separately.

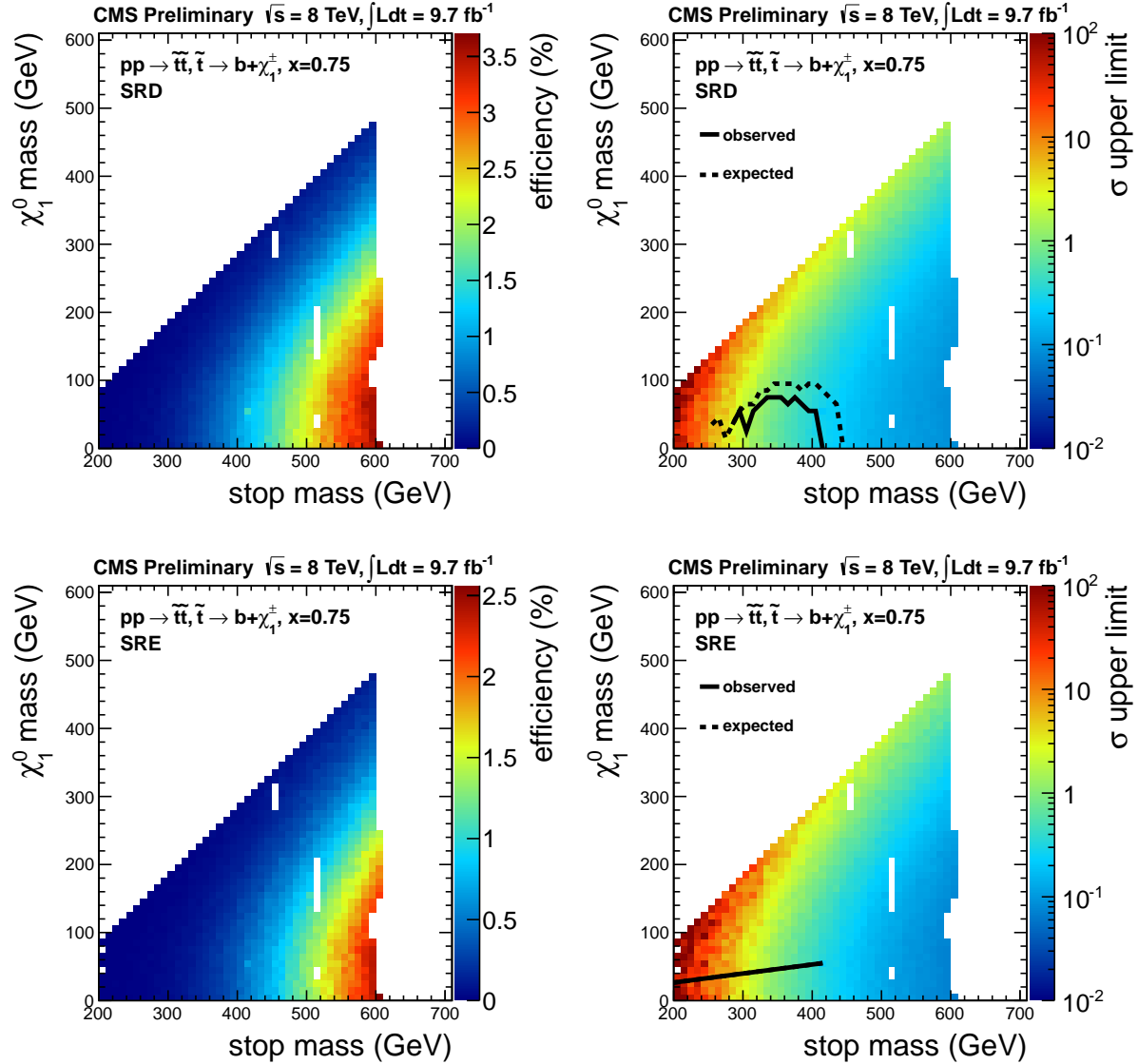


Figure 28: Signal efficiency (left) and cross section upper limit (right) for the T2bw model with $x=0.75$, showing both the expected and observed exclusion contours. The results for signal regions SRD (top), and SRE (bottom) are shown separately.

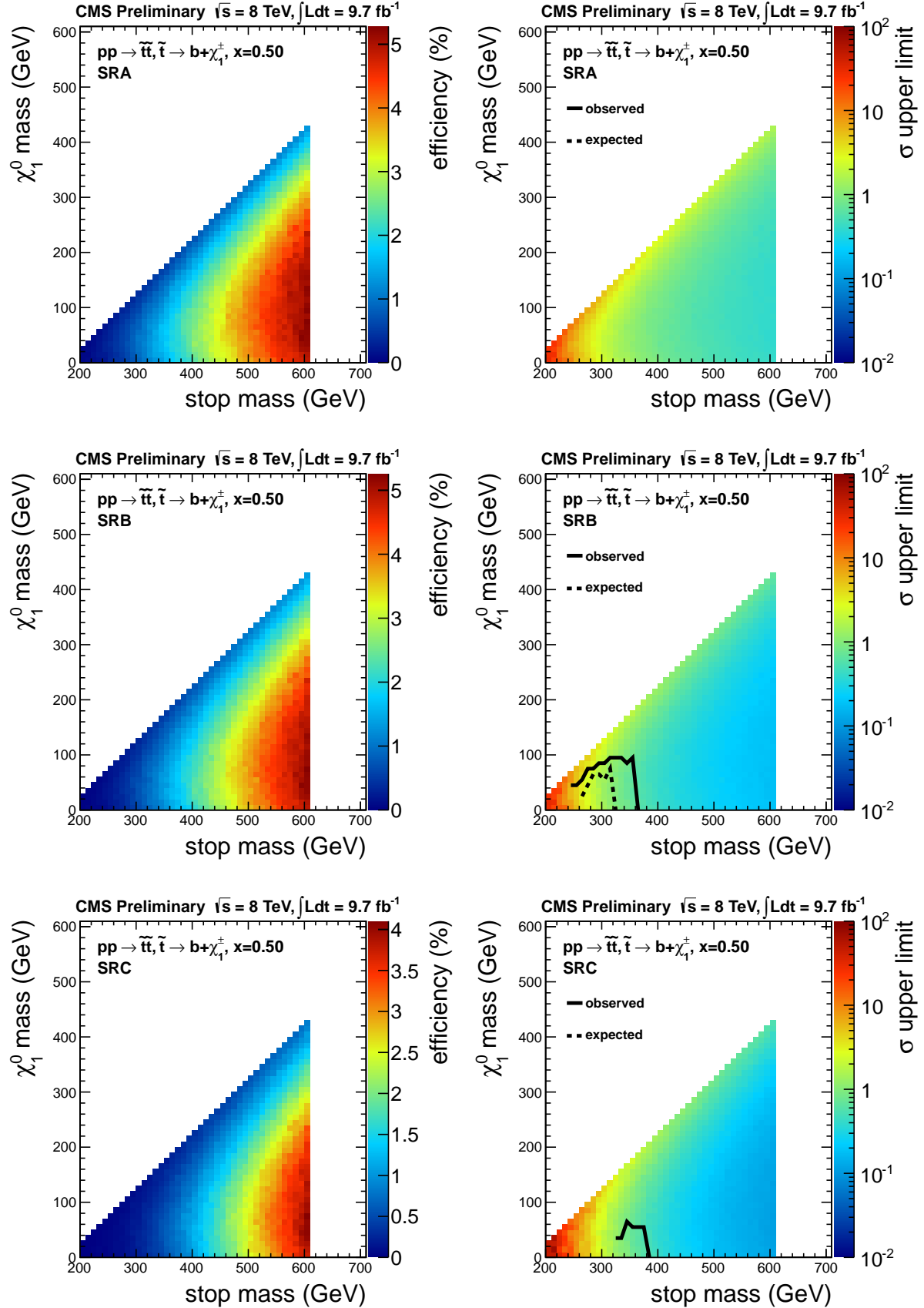


Figure 29: Signal efficiency (left) and cross section upper limit (right) for the T2bw model with $x=0.5$, showing both the expected and observed exclusion contours. The results for signal regions SRA (top), SRB (middle) and SRC (bottom) are shown separately.

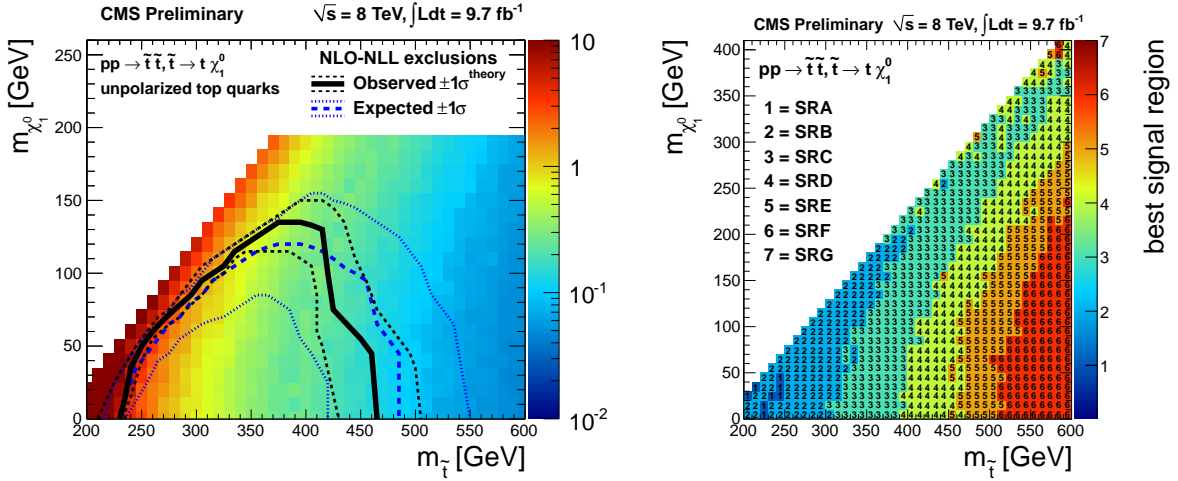


Figure 30: Upper limit on the cross section for the T2tt model in the plane of stop vs. LSP mass, showing both the expected (dashed) and observed (solid curve) exclusion contours (left). The observed limit is selected from the signal region with the best expected limit (shown on right). All uncertainties are included and the dotted contours around the dashed expected limit correspond to the $\pm 1\sigma$ result.

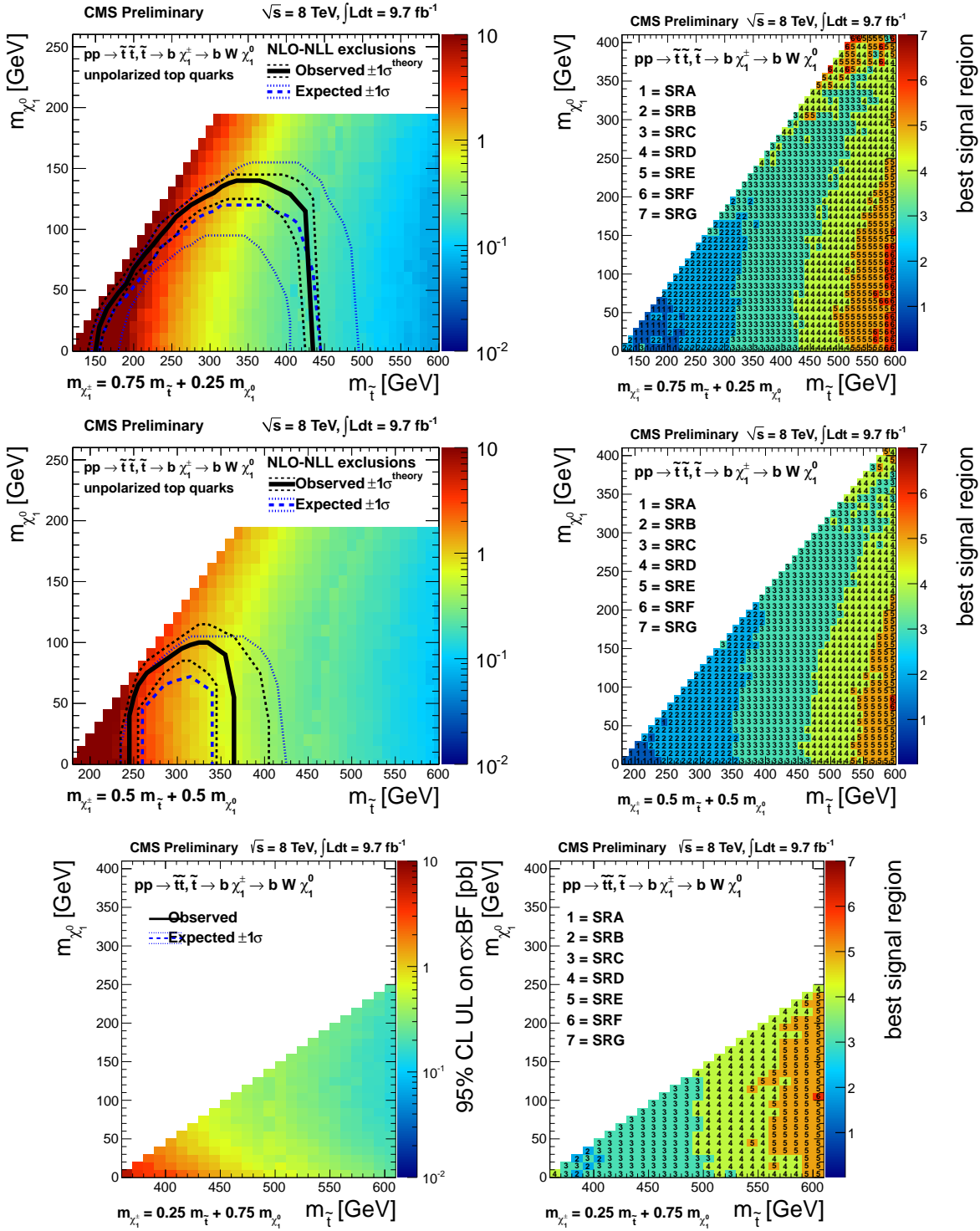


Figure 31: Upper limit on the cross section for the T2bw model for $x=0.7$ (top), $x=0.5$ (middle) and $x=0.25$ (bottom) in the plane of stop vs. LSP mass, showing both the expected (dashed) and observed (solid curve) exclusion contours (left). The observed limit is selected from the signal region with the best expected limit (shown on right). All uncertainties are included and the dotted contours around the dashed expected limit correspond to the $\pm 1\sigma$ result.

697 12 Conclusion

698 This note presents a search for the production of stop quark pairs in events with a single isolated lepton,
699 several jets, missing transverse energy, and large transverse mass. The dataset used corresponds to an
700 integrated luminosity of 9.7 fb^{-1} at center-of-mass energy of 8 TeV. Seven signal regions are defined, based
701 on E_T^{miss} and M_T requirements. Agreement is observed between the data and the predicted backgrounds
702 for all signal regions. The results are interpreted in the context of simplified SUSY models where the
703 stops decay to top-neutralino or b-chargino and are used to place constraints on the stop mass.

704 References

- 705 [1] <https://twiki.cern.ch/twiki/bin/view/LHCPhysics/SUSYCrossSections8TeVstopsbottom>
- 706 [2] T. Plenh *et al.*, JHEP 1208(2012) 091.
- 707 [3] These are measured by the Florida group in the context of the same sign and ewk-ino analyses.
- 708 [4] M. Perelstein, A. Weiler, arXiv:0811.1024v2 [hep-ph]

709 A Performance of the Isolation Requirement

710 The last requirement used in the analysis is an isolated track veto. This selection criteria rejects events
 711 containing a track of $p_T > 10$ GeV with relative track isolation $\sum p_T/p_T(\text{trk})$ in a cone of size $R = 0.3 <$
 712 0.1. It may be noted that only tracks consistent with the vertex with highest $\sum p_T^2$ are considered in
 713 order to reduce the impact of spurious tracks, for example from pileup interactions. This requirement
 714 has very good performance. Figure 32 shows the efficiency for rejecting dilepton events compared to the
 715 efficiency for selecting single lepton events for various cone sizes and cut values. The chosen working
 716 point provides a signal efficiency of $\epsilon(\text{sig}) = 92\%$ for a background rejection of $\epsilon(\text{bkg}) = 53\%$ in MC.
 717 With "signal" ("background") we are referring to $t\bar{t} \rightarrow \ell + \text{jets}$ ($t\bar{t} \rightarrow \ell\ell$).

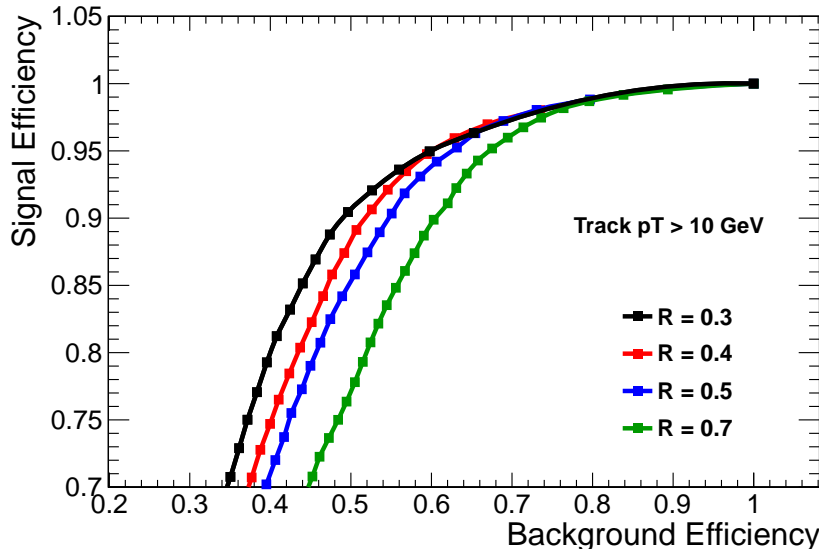


Figure 32: Comparison of the performance in terms of signal (single lepton events) efficiency and background (dilepton events) rejection for various cone sizes and cut values. The current isolation requirement uses a cone of size $\Delta R = 0.3$ and a cut value of 0.1, corresponding to $\epsilon(\text{sig}) = 92\%$ for $\epsilon(\text{bkg}) = 53\%$.

718 It should be emphasized that the isolated track veto has a different impact on the samples with a single
 719 lepton (mainly $t\bar{t} \rightarrow \ell + \text{jets}$ and $W + \text{jets}$) and that with two leptons (mainly $t\bar{t} \rightarrow \ell\ell$). For the dilepton
 720 background, the veto rejects events which have a genuine second lepton. Thus the performance may
 721 be understood as an efficiency $\epsilon_{iso, trk}$ to identify the isolated track. In the case of the single lepton
 722 background, the veto rejects events which do not have a genuine second lepton, but rather which contain
 723 a "fake" isolated track. The isolated track veto thus effectively scales the single lepton sample by $(1 -$
 724 $\epsilon_{fake})$, where ϵ_{fake} is the probability to identify an isolated track with $p_T > 10$ GeV in events which contain
 725 no genuine second lepton. It is thus necessary to study the isolated track efficiency $\epsilon(trk)$ and ϵ_{fake} in
 726 order to fully characterize the veto performance.

727 The veto efficiency for dilepton events is calculated using the tag and probe method in Z events. A good
 728 lepton satisfying the full ID and isolation criteria and matched to a trigger object serves as the tag. The
 729 probe is defined as a track with $p_T > 10$ GeV that has opposite charge to the tag and has an invariant
 730 mass with the probe consistent with the Z mass.

731 The variable used to study the performance of the veto is the absolute track isolation, since it removes
 732 the dependence of the isolation variable on the p_T of the object under consideration. This is particularly
 733 useful because the underlying p_T distribution is different for second leptons in $t\bar{t} \rightarrow \ell\ell$ events compared to
 734 Z events, particularly due to the presence of τ s that have softer decay products. As shown in Figure 33,
 735 the absolute isolation is consistent between Z + 4 jet events and $t\bar{t} \rightarrow \ell\ell$ events, including leptons from W
 736 and τ decays. This supports the notion that the isolation, defined as the energy surrounding the object
 737 under consideration, depends only on the environment of the object and not on the object itself. The
 738 isolation is thus sensitive to the ambient pileup and jet activity in the event, which is uncorrelated with
 739 the lepton p_T . It is thus justified to use tag and probe in Z + 4 jet events, where the jet activity is similar
 740 to $t\bar{t} \rightarrow \ell\ell$ events in our $N_{\text{jets}} > 4$ signal region, in order to estimate the performance of the isolation
 741 requirement for the various leptonic categories of $t\bar{t} \rightarrow \ell\ell$ events.

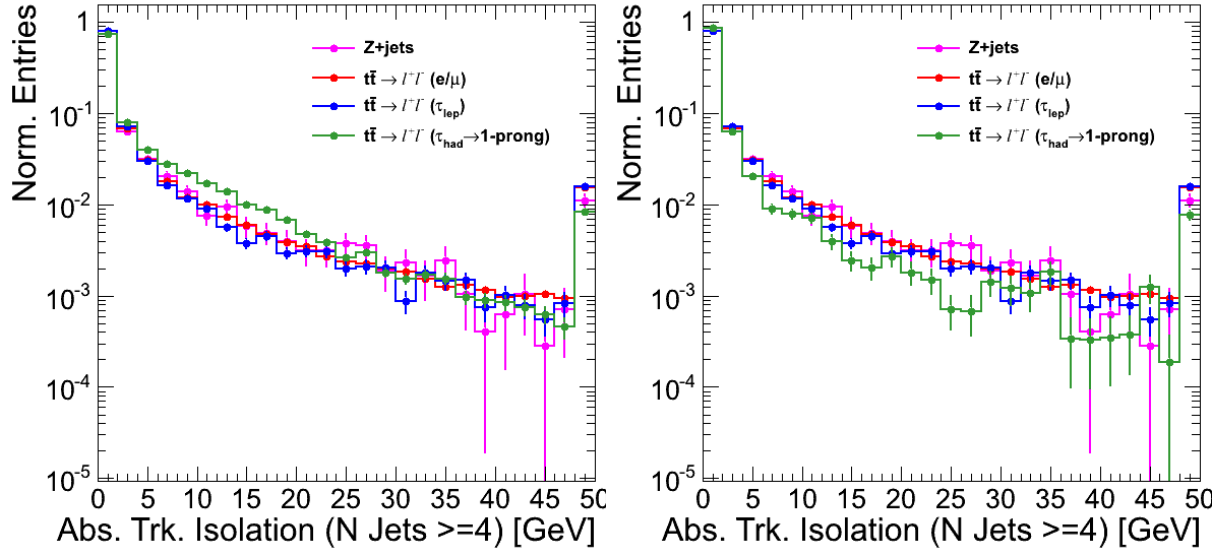


Figure 33: Comparison of absolute track isolation for track probes in Z + 4 jet and $t\bar{t} \rightarrow \ell\ell$ events for different lepton types. The isolation variables agree across samples, except for single prong τ s, that tend to be slightly less isolated (left). The agreement across isolation distributions is recovered after removing single prong τ events produced in association with π^0 s from the sample (right).

742 B Example BG prediction calculation

743 The calculation of the background prediction is a bit complicated. Here we walk the reader through a
 744 concrete example.

745 **NB: the numbers in this section corresponded to the numbers in V3 of the analysis note.**
 746 **They will not be updated, because this is meant as an illustration only..**

747 The main background is $t\bar{t}$. The main idea is to normalize to the M_T peak region ($50 < M_T < 80$ GeV).
 748 This eliminates dependence on $t\bar{t}$ cross-section, luminosity, trigger efficiency, JES, lepton ID, etc. This
 749 gets a bit complicated because the M_T peak region, while dominantly $t\bar{t}$ lepton + jets, also includes some
 750 $W+jets$, $t\bar{t} \rightarrow \ell\ell$, rare processes, etc. Also, we want to minimize our need to understand the effect of the
 751 isolated track veto on $t\bar{t} \rightarrow \ell + jets$. As a result we actually define two M_T peak regions: one before and
 752 one after applying the isolated track veto. Then the $t\bar{t} \rightarrow \ell\ell$ background is normalized the the “before
 753 veto” region, and the $t\bar{t} \rightarrow \ell + jets$ and $W+jets$ background are normalized to the “post veto” region.

754 This complex procedure is important for the high statistics signal regions with relatively low E_T^{miss}
 755 requirements, eg, SRA. For these SRs we want to keep the systematics low in order to be sensitive to low
 756 mass stop; for the signal regions with hard cuts on E_T^{miss} this is less important. However, we apply the
 757 same procedure to all SRs.

758 For concreteness, we show the calculation for SRA, electron channel. The MC and data event counts used
 759 in the background calculation are collected in Table 36. Note that the background uncertainties have
 760 already been described in Section 9. The one tricky point to keep in mind is that when the $W+jets$ and
 761 rare cross-sections are changed by their assumed uncertainties (50% each), the whole calculation describe
 762 below is repeated in order to take care of all the correlations properly.

Sample	M_T peak, before trk veto	M_T peak, after trk veto	Signal Region A
$t\bar{t} \rightarrow \ell\ell$	290 ± 6	116 ± 4	261 ± 6
$t\bar{t} \rightarrow \ell + jets$ (1ℓ)	2899 ± 19	2595 ± 18	not used
$W+jets$	252 ± 28	236 ± 28	not used
Rare	89 ± 5	62 ± 4	26 ± 2
Total	3530 ± 35	3009 ± 34	not used
Data	3358	2787	not used

Table 36: Data and MC event counts used to predict the background in SRA, for electron events. Uncertainties are statistical only. The trigger efficiency has been applied to the MC samples. In the case of $t\bar{t} \rightarrow \ell\ell$ the K_3 and K_4 factors of Section 5.3.1 have also been applied.

763 B.1 Central value of dilepton background

764 A “before veto” scale factor is defined from the second column in Table 36 as the factor by which all MC
 765 except the “rare” need to be scaled up in order to have data/MC agreement. This is

$$766 SF_{\text{pre}} = (3358 - 89) / (2899 + 252 + 290) = 0.950.$$

767 Then the $t\bar{t} \rightarrow \ell\ell$ background prediction is the number of events predicted by the MC in SRA (261 from
 768 the last column of SRA), rescaled by SF_{pre} . The result for the central value is 248 events.

769 B.2 Central value of the $t\bar{t} \rightarrow \ell + jets$ background

770 A “post veto” scale factor is defined from the third column in Table 36 as the factor by which the
 771 $t\bar{t} \rightarrow \ell + jets$ and the $W+jets$ backgrounds need to be scaled to have data/MC agreement.

$$772 SF_{\text{post}} = (2787 - 62 - SF_{\text{pre}} \cdot 116) / (2595 + 236) = 0.924.$$

773 Then the $t\bar{t} \rightarrow \ell + jets$ background is obtained as the product of the following three factors

- 774 • $SF_{\text{post}} = 0.924$ as obtained above
- 775 • 2595, from the third column of Table 36

776 • The tail-to-peak ratio $R_{top} = 0.045$ from Table 21

777 The result for the central value is 108 events.

778 B.3 Central value for the W +jets background

779 It is calculated as the product of

780 • $SF_{post} = 0.924$ from Section B.2

781 • 236, from the third column of Table 36

782 • The tail-to-peak ratio $R_{wjet} = 0.066$ from Table 21

783 The result for the central value is 14.3 events.

784 B.4 Central value for the rare backgrounds

785 This is 26 events from Table 36

786 C Additional CR Data and MC Comparisons

787 This appendix shows some additional comparisons of the data and MC background samples for various
 788 CRs. Figure 34 shows some additional components of the M_T , the lepton p_T and the azimuthal angle
 789 between the lepton and the E_T^{miss} for CR1 (Section D.3). Figure 35 shows the equivalent distributions
 790 for CR2 (Section 5.2), the positive lepton p_T and the angle between this lepton and the pseudo- E_T^{miss} .
 791 Similarly, figure 38 shows the lepton p_T and the azimuthal angle between the lepton and the E_T^{miss}
 792 for CR5 (Section D.2). Figures 36 and 37 provide some data and MC comparisons of the $t\bar{t} \rightarrow \ell\ell$ control
 793 sample CR4 (Section 5.3) for various kinematic distributions: leading lepton p_T and eta, as well as the
 794 angles between the two leptons and between the leading lepton and the E_T^{miss} . These distributions show
 795 quite good agreement between data and MC. More quantitative information is included in the section
 796 discussing each control region.

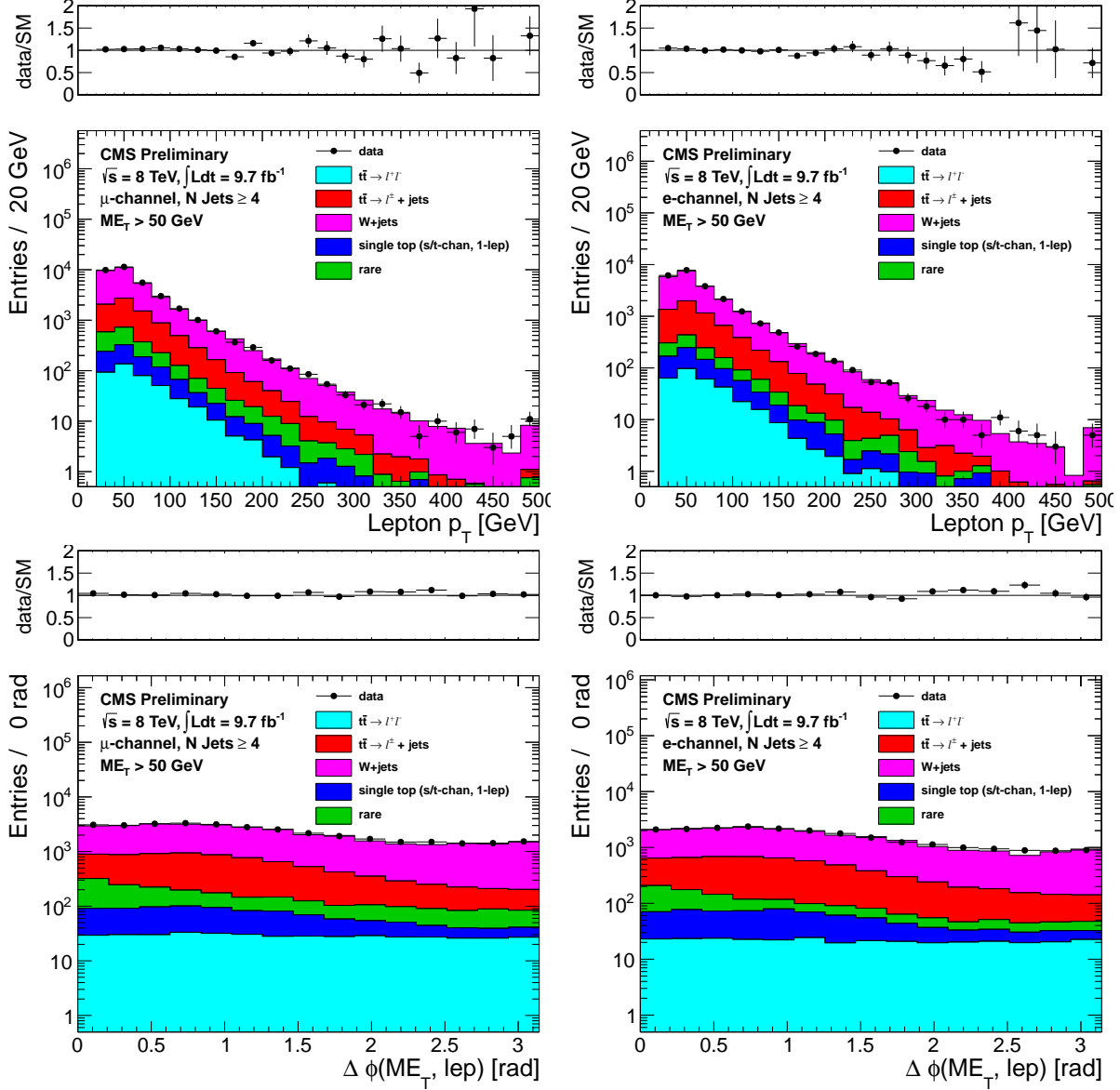


Figure 34: Comparison of the lepton p_T (top) and azimuthal angle between the E_T^{miss} and the lepton (bottom) for data vs. MC for events with a leading muon (left) and leading electron (right) satisfying the requirements of CR1.

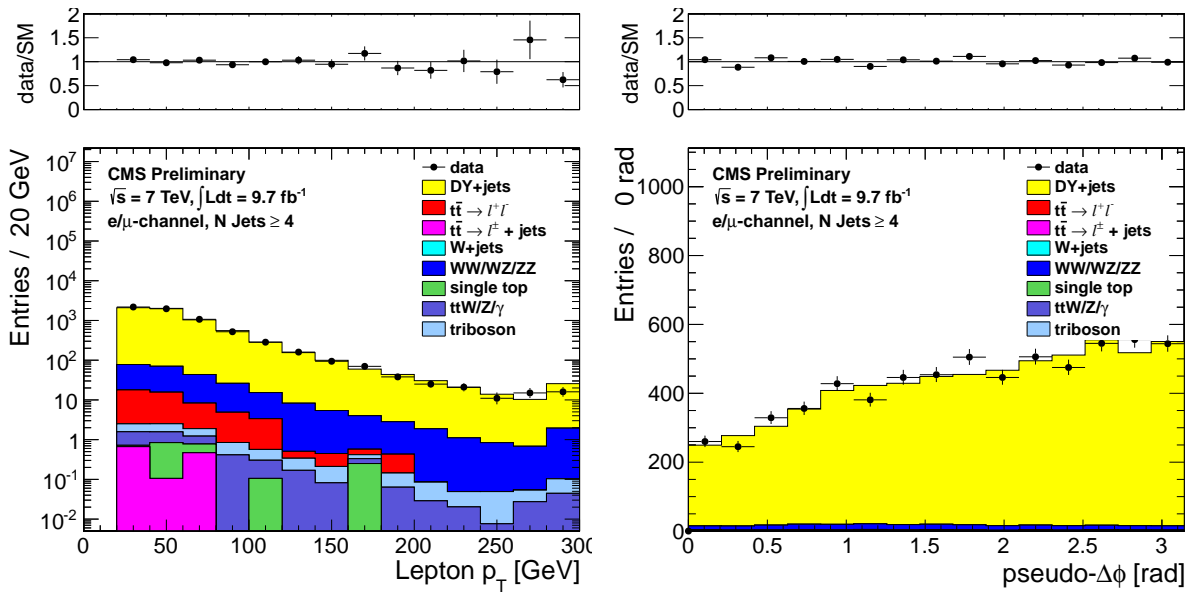


Figure 35: Comparison of the positive lepton p_T (left) and the azimuthal angle between this lepton and the pseudo- E_T^{miss} (right) distributions in data vs. MC for events satisfying the requirements of CR2, combining both the muon and electron channels.

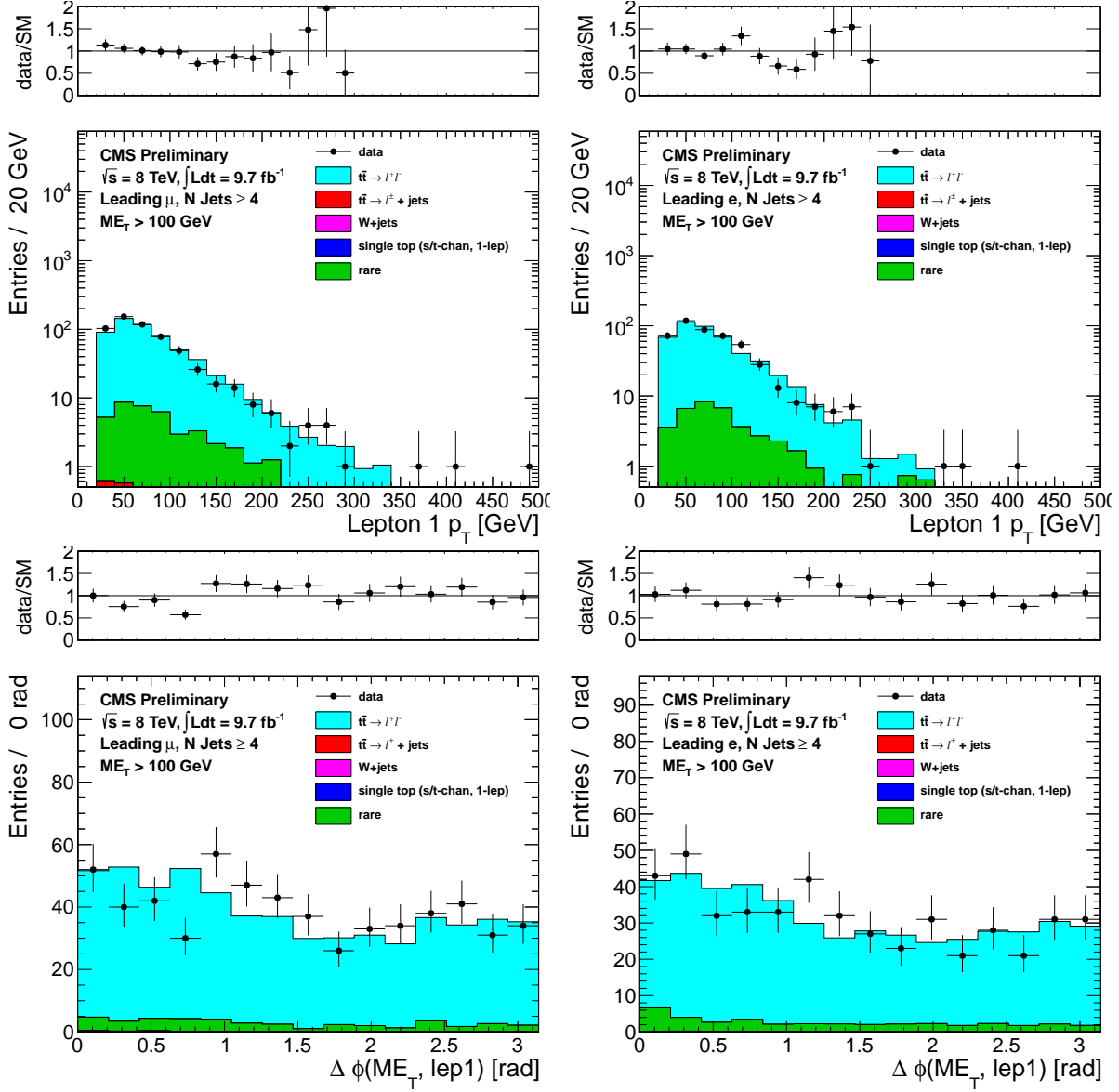


Figure 36: Comparison of the leading lepton p_T (top) and azimuthal angle between the leading lepton and the E_T^{miss} for $E_T^{\text{miss}} > 100$ GeV distributions in data vs. MC for events with a leading muon (left) and leading electron (right) satisfying the requirements of CR4.

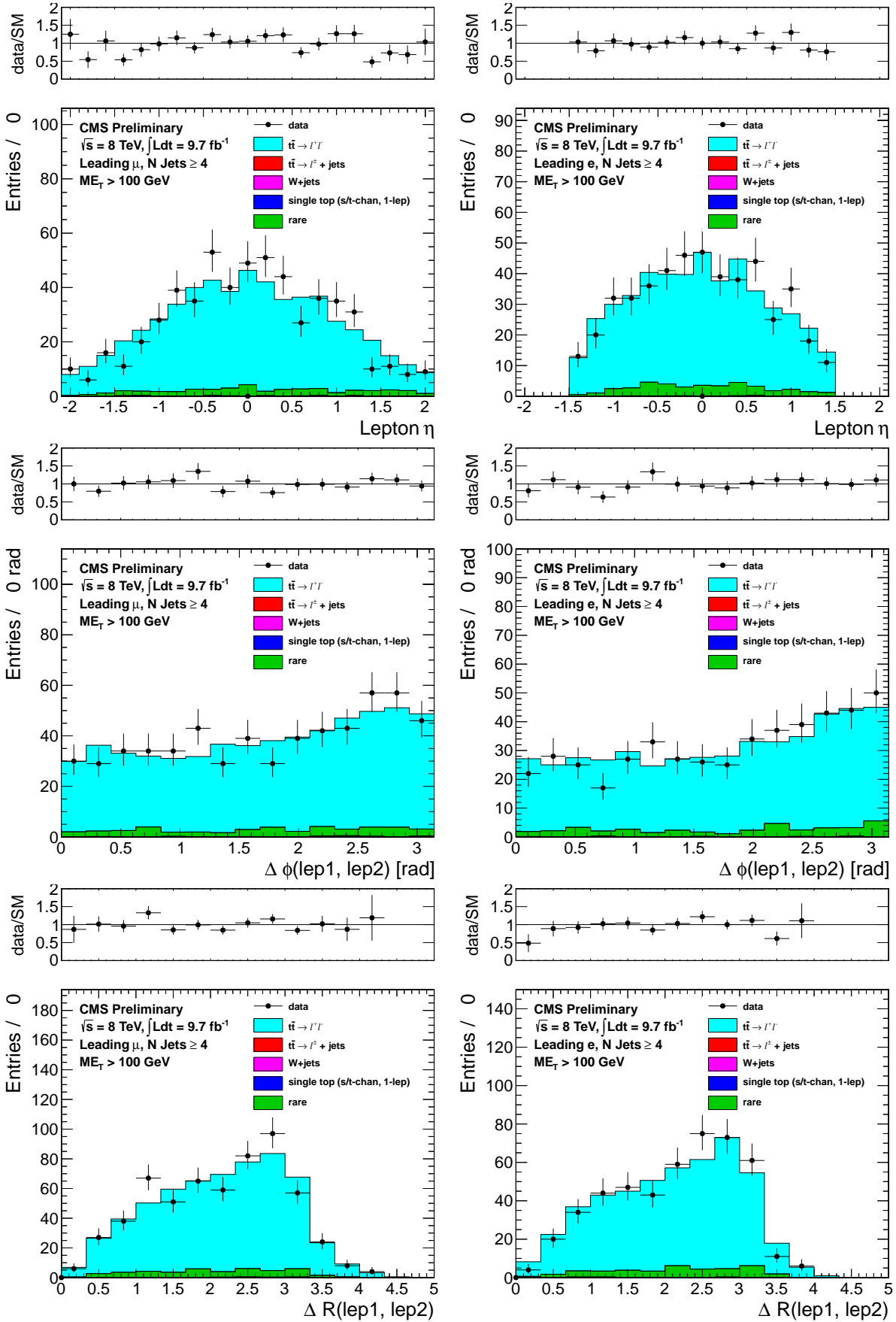


Figure 37: Comparison of the leading lepton eta (top), difference in the azimuthal angle (center) and ΔR separation (bottom) between the two leptons for $E_T^{\text{miss}} > 100 \text{ GeV}$ distributions in data vs. MC for events with a leading muon (left) and leading electron (right) satisfying the requirements of CR4.

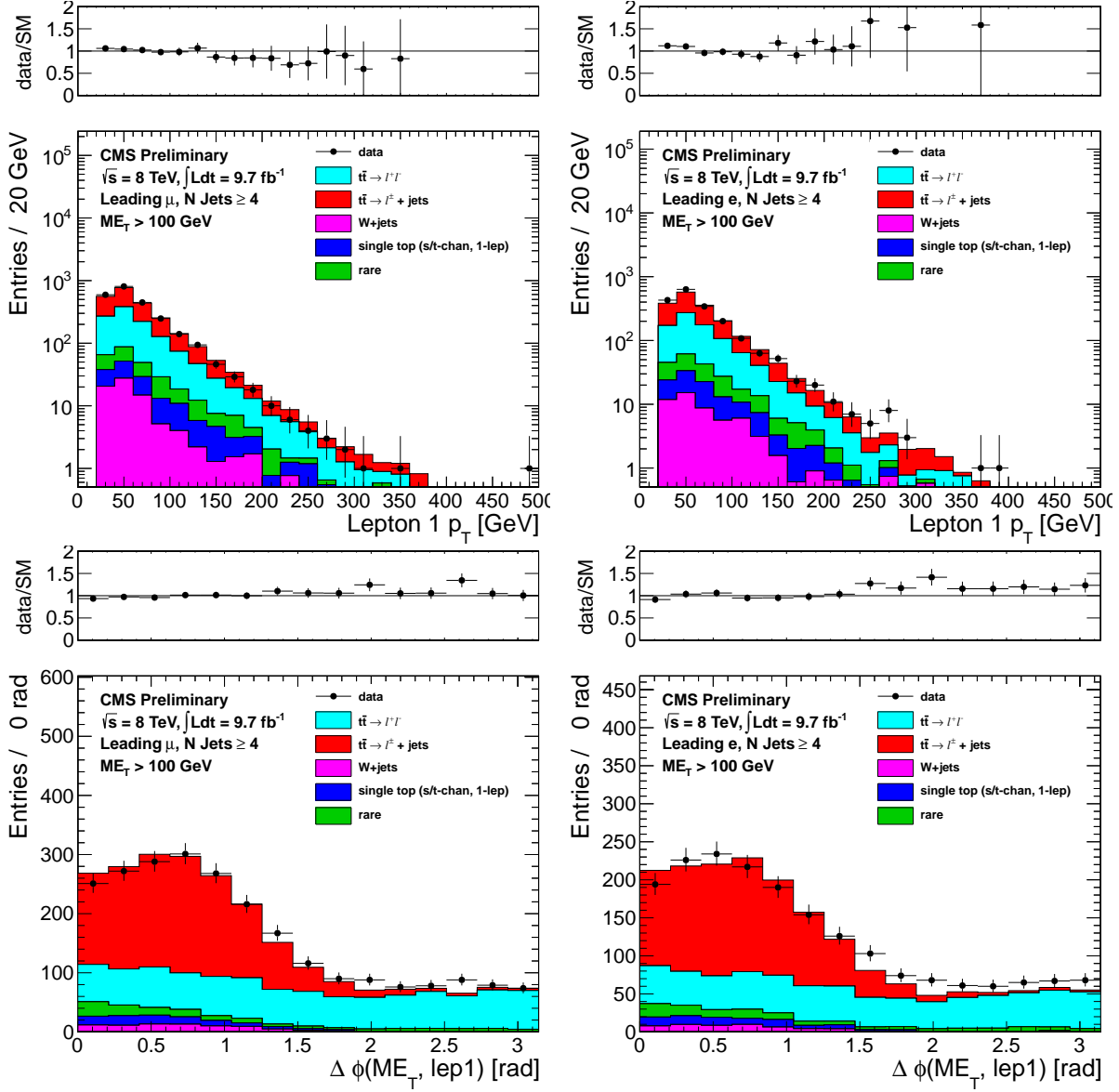


Figure 38: Comparison of the lepton p_T (top) and azimuthal angle between the E_T^{miss} and the lepton (bottom) for data vs. MC for $E_T^{\text{miss}} > 100 \text{ GeV}$ for events with a leading muon (left) and leading electron (right) satisfying the requirements of CR5.

797 D Control Region Plots Summary

798 This appendix includes distributions from the various control regions used in the analysis used to validate
 799 the MC modeling of the E_T^{miss} and M_T distributions in data and derive systematic uncertainties on the
 800 background predictions. The distributions are shown in both log and linear scale.

801 D.1 CR4: ≥ 1 b-tag, exactly 2 leptons

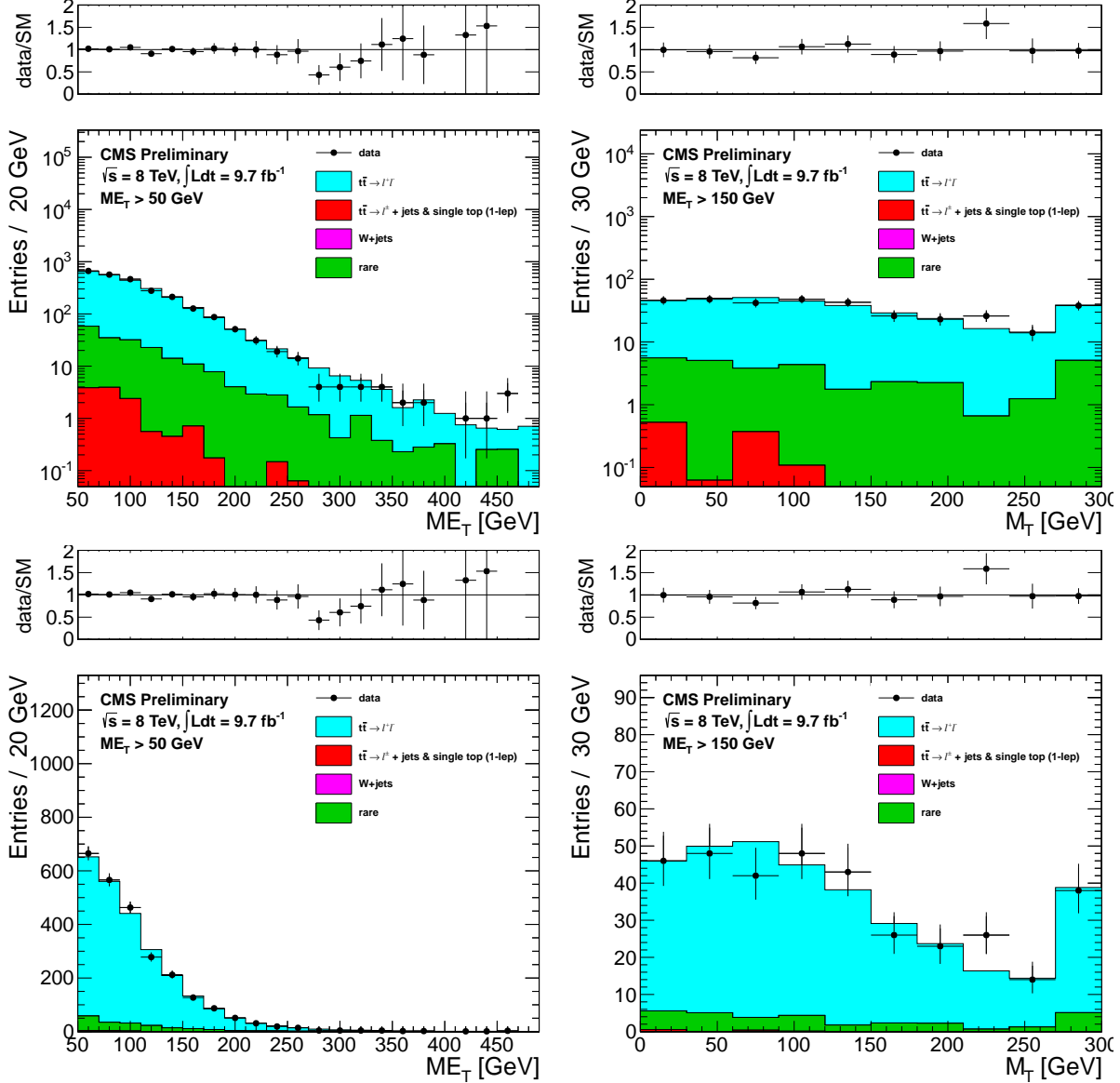


Figure 39: Comparison of the E_T^{miss} distribution (left) and M_T distribution for events satisfying $E_T^{\text{miss}} > 150 \text{ GeV}$ (right) in data vs. MC for CR4.

802 D.2 CR5: ≥ 1 b-tag, 1 lepton + 1 isolated track

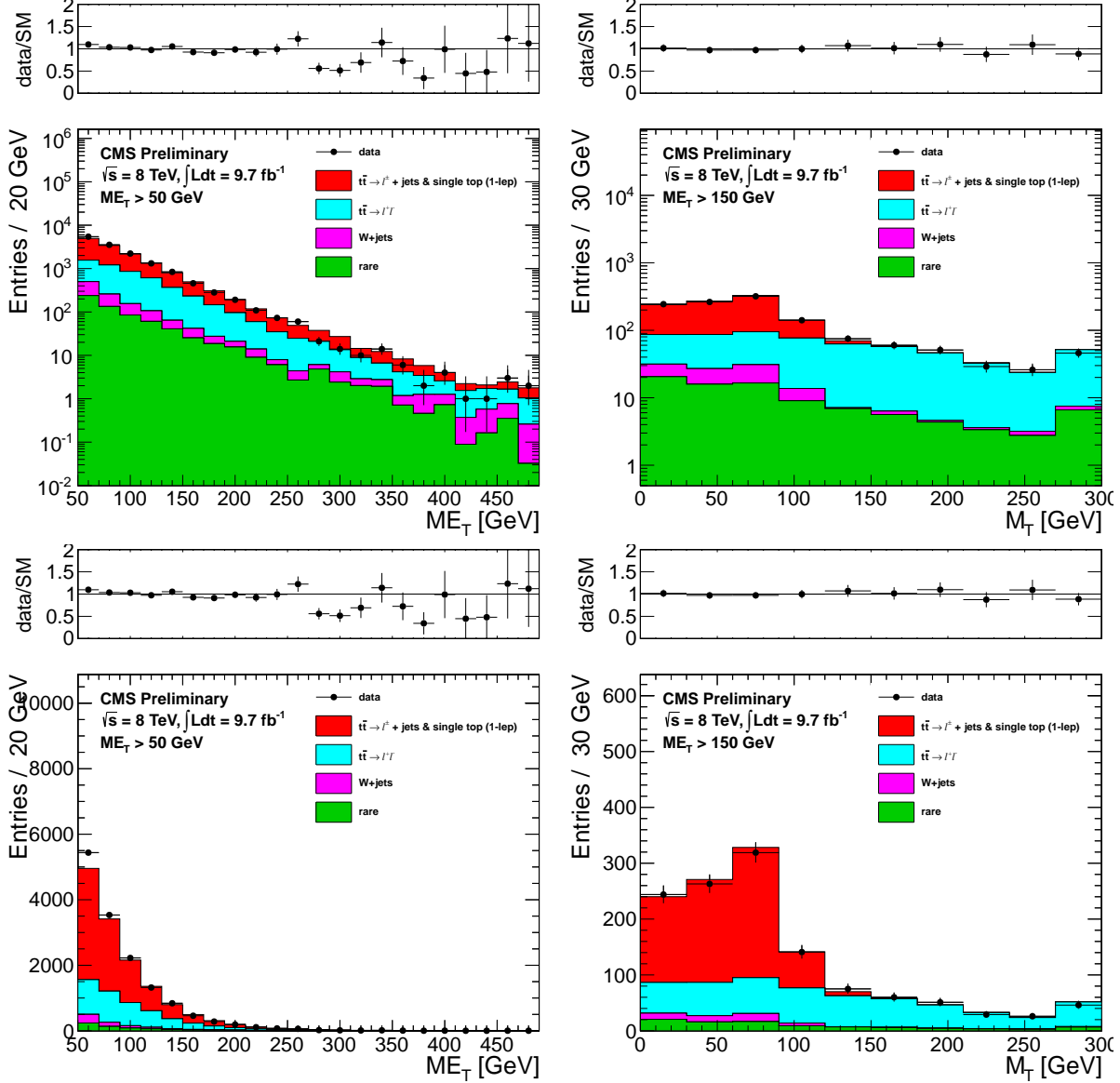


Figure 40: Comparison of the E_T^{miss} distribution (left) and M_T distribution for events satisfying $E_T^{\text{miss}} > 150 \text{ GeV}$ in data vs. MC for CR5.

803 D.3 CR1: 0 b-tags, exactly 1 lepton

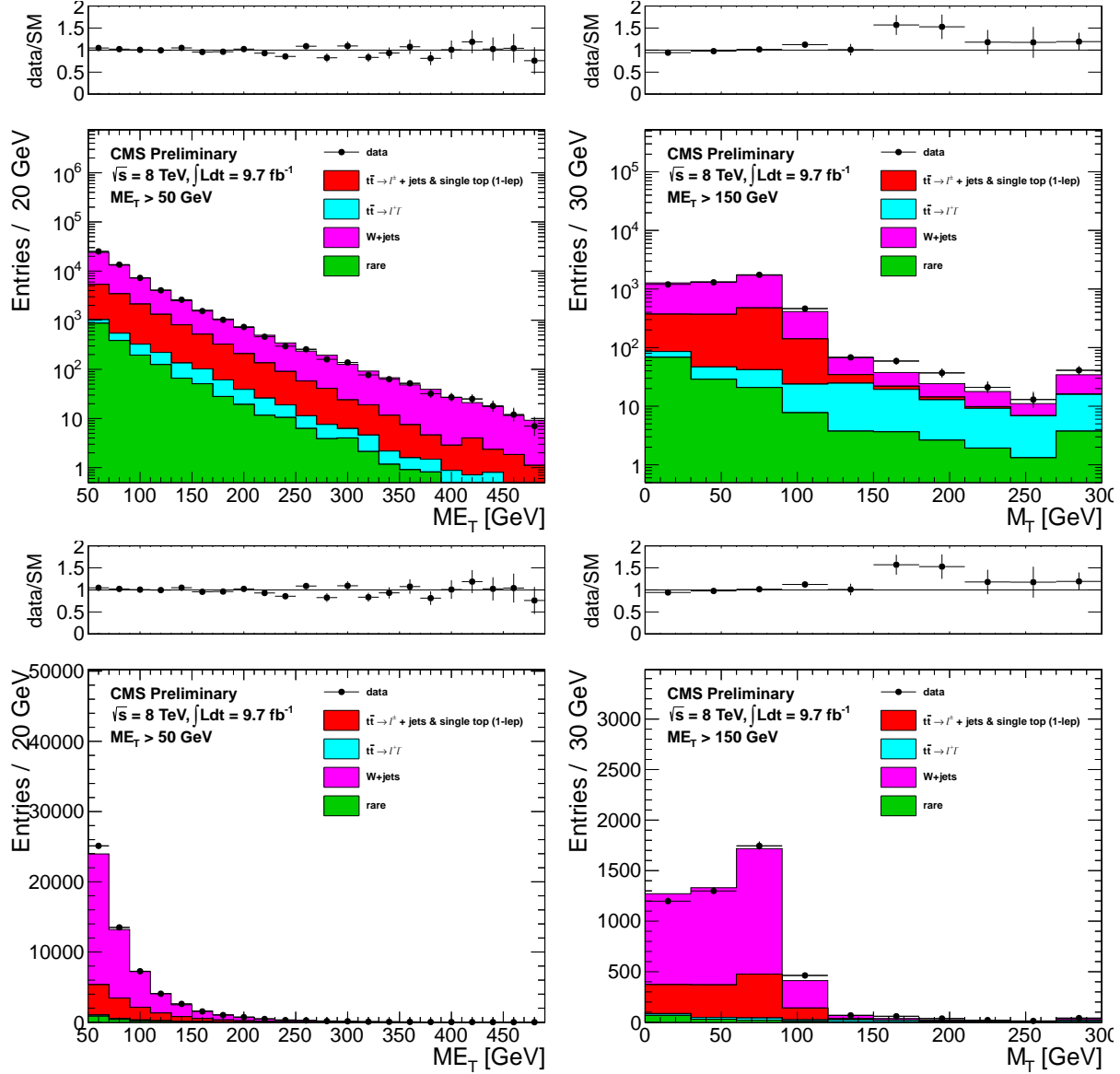


Figure 41: Comparison of the E_T^{miss} distribution (left) and the M_T distribution after a $E_T^{\text{miss}} > 150 \text{ GeV}$ requirement (right) in data vs. MC for events satisfying the requirements of CR1.

804 D.4 CR2: 0 b-tags, exactly 2 leptons

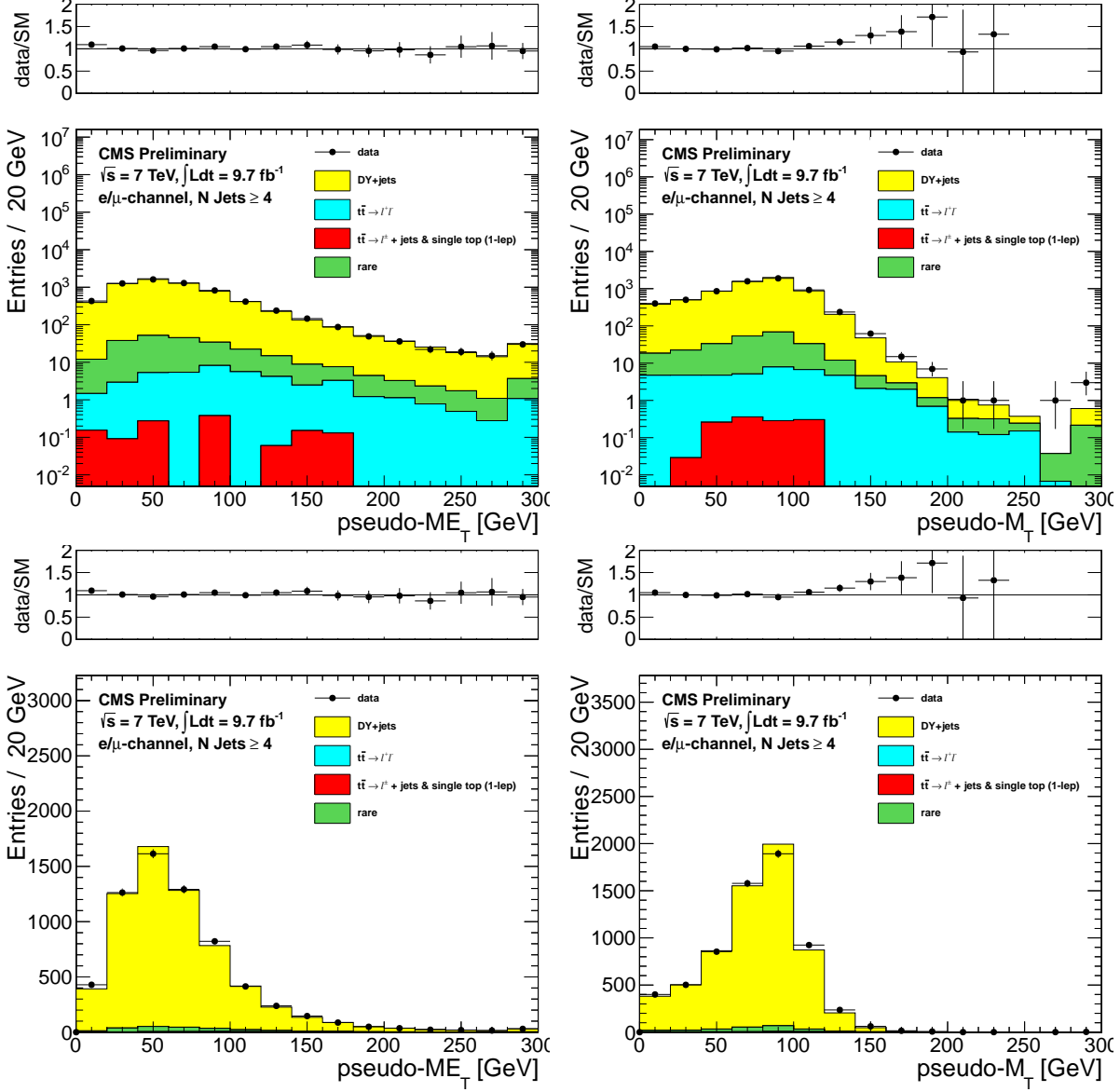


Figure 42: Comparison of the pseudo- E_T^{miss} distribution (left) and the pseudo- M_T distribution (right) in data vs. MC for CR2.

805 E Signal Kinematics

806 This appendix includes some kinematic distributions for a few signal points in the T2tt (Figure 43) and
 807 T2bw (Figure 44) models. The parameter values shown correspond to the edge of the sensitivity of the
 808 analysis and reflect the range of kinematics of the signal. The lower $M(\tilde{t})$ samples have softer E_T^{miss} and
 809 M_T distributions and are thus better targeted by the signal regions with looser requirements. The higher
 810 $M(\tilde{t})$ samples are harder in E_T^{miss} and M_T and the signal regions with tighter requirements provide higher
 811 sensitivity to these models.

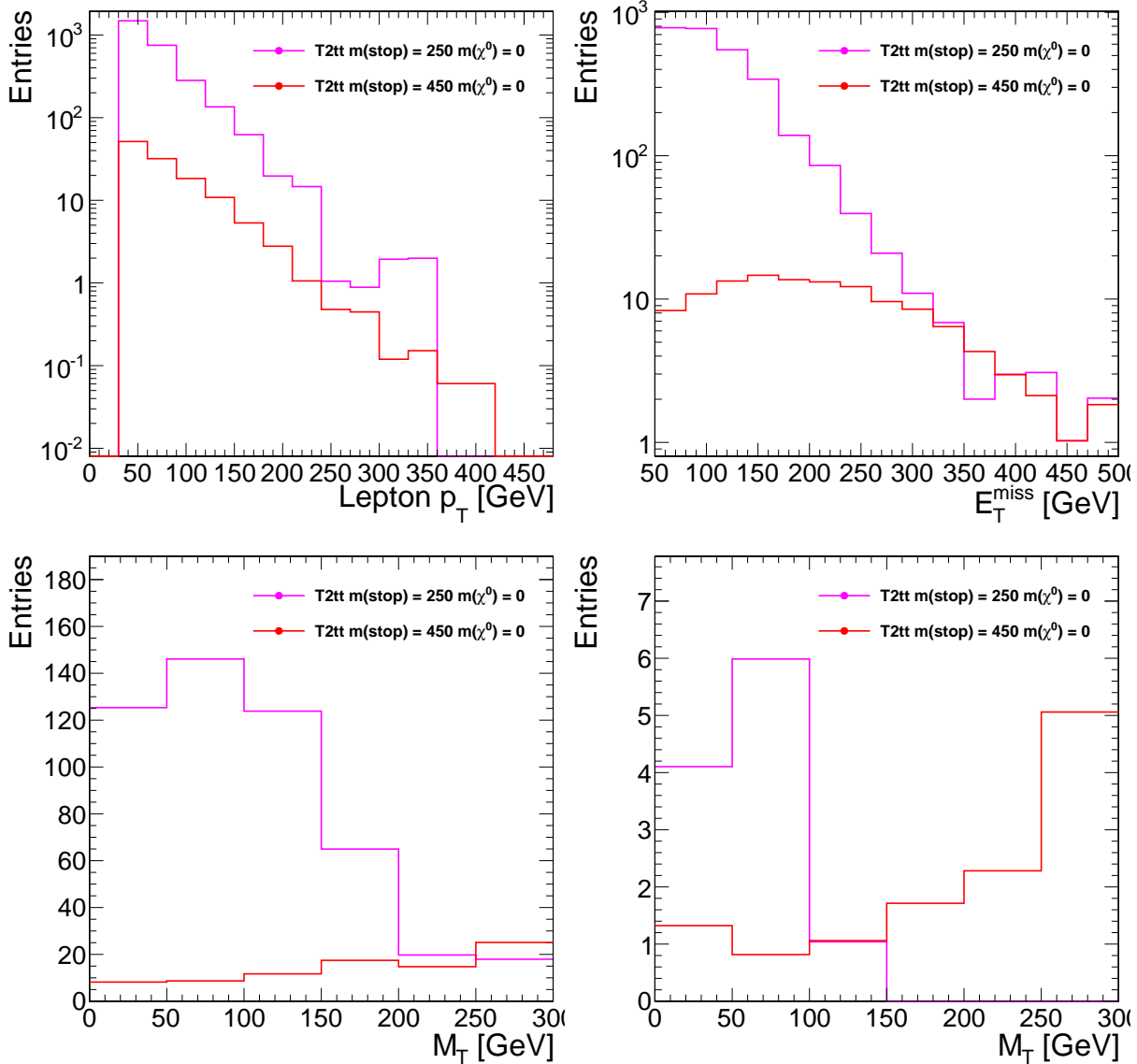


Figure 43: Signal kinematics for two signal points in the T2tt model: the lepton p_T (top, left), the E_T^{miss} (top, right) and the M_T for two values of the E_T^{miss} requirement, $E_T^{\text{miss}} > 150 \text{ GeV}$ (bottom, left) and $E_T^{\text{miss}} > 350 \text{ GeV}$ (bottom, right).

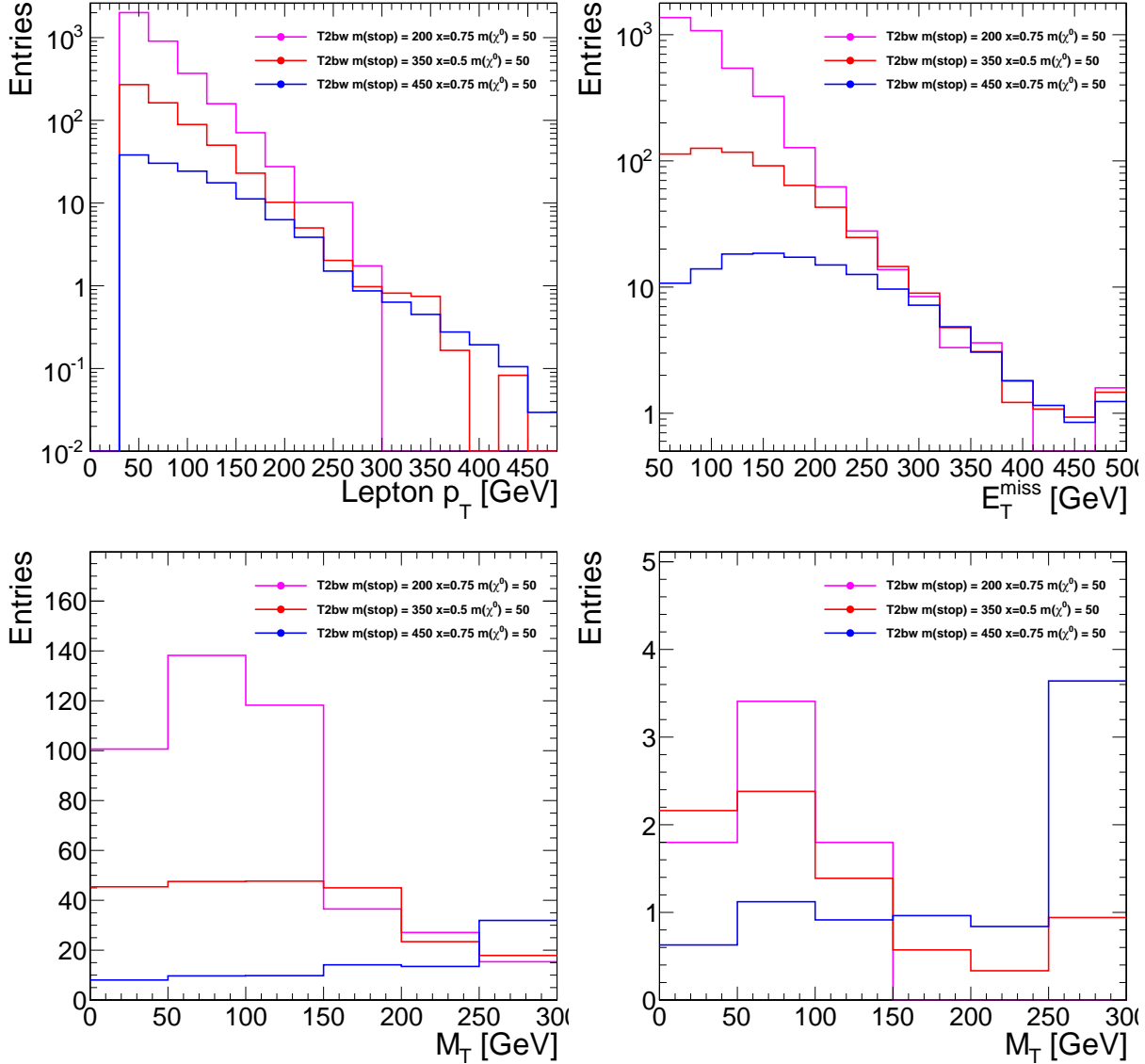


Figure 44: Signal kinematics for three signal points in the T2bw model: the lepton p_T (top, left), the E_T^{miss} (top, right) and the M_T for two values of the E_T^{miss} requirement, $E_T^{\text{miss}} > 150$ GeV (bottom, left) and $E_T^{\text{miss}} > 350$ GeV (bottom, right).

812 F Model dependence of the signal acceptance

813 The signal acceptance for T2tt events has a significant dependence on the model parameters, particularly
 814 the mixing angle of left- and right-handed stops. Depending on the choice of mixing angle, the top quarks
 815 produced in the decay can have a polarization anywhere between $+p_{\chi_1^0}/E_{\chi_1^0}$ and $-p_{\chi_1^0}/E_{\chi_1^0}$ [4], which for
 816 a massless χ_1^0 becomes ± 1 . For right-handed top quarks, the charged lepton is emitted preferentially in
 817 the direction parallel to the top velocity, resulting in larger lepton p_T and M_T .

818 The default signal MC used in this analysis has unpolarized top quarks. We estimate the impact of the
 819 top polarization on our signal acceptance by reweighting our signal MC events to match the expected
 820 distribution of the charged lepton decay angle (θ^*) corresponding to the choice of top polarizations of
 821 ± 1 . The default and reweighted $\cos \theta^*$ distributions are shown in Figure 45. Note that this is only an
 822 approximate study, because the angular distribution is in fact triply differential. We attempt to account
 823 for the dominant effect.

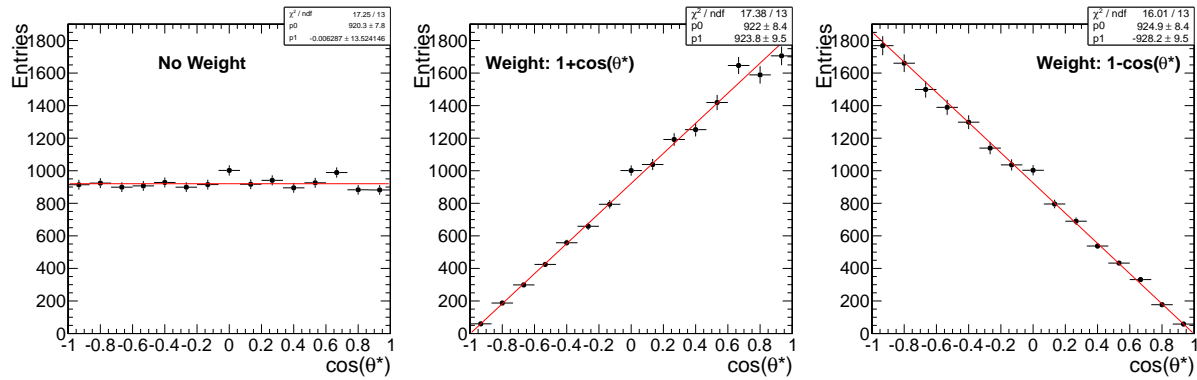


Figure 45: The default and reweighted $\cos \theta^*$ distributions. The $1 \pm \cos \theta^*$ weightings correspond to top polarizations of ± 1 .

824 We find that reweighting to resemble a top polarization of $+1$ increases the signal acceptance by ap-
 825 proximately 20-25% relative to the default MC, while using a top polarization of -1 decreases the signal
 826 acceptance by a similar amount.

827 G Glossary of abbreviations

828 R_{wjet}^{MC}, R_{wjet}

829 Monte Carlo and corrected ratios of $W+jets$ events in the M_T tail to the M_T peak.

830 R_{top}^{MC}, R_{top}

831 Monte Carlo and corrected ratios of $t\bar{t}$ or single-top $\ell+jets$ events in the M_T tail to the M_T peak.

832 SFR_{wjet}

833 Data/MC scale factor for R_{wjet}^{MC}

834

835 SFR_{top}

836 Data/MC scale factor for R_{top}^{MC} (not used)

837

838 K_3 and K_4

839 Scale factors for $t\bar{t} \rightarrow \ell\ell$ events with one or two extra jets from radiation

840

841 SF_{pre} and SF_{post}

842 Scale factors to be applied to MC to normalize to the yields in the M_T control region before and after
 843 the application of the isolated track veto.